Università degli Studi di Roma "La Sapienza"

Tesi di Dottorato in Scienza dei Materiali

XVIII Ciclo

"Energy Dispersive X-ray Reflectometry studies of the morphological response of Metal-Phthalocyanine sensing films upon exposure to NO_2 molecules."

di

Amanda Generosi

Relatore	Candidato
Prof. R. Caminiti Dr. V. Rossi Albertini	Dr. Amanda Generosi

"Where shell I begin, please, jour majesty?"
he asked.
“Begin at the beginning,”
the King said, gravely,
“and go on till you come to the end: than stop.”

Lewis Carroll
Alice’s Adventures in Wonderland

Preface

This thesis is devoted to the main results of a three years long research work in the field of nitrogen dioxide sensing metallo-phthalocyanines (MPc).

The experimental methodology chosen for the study of gas sensing device's is quite unconventional being completely different from the electro-chemical techniques, to investigate their properties. In fact the relevance of this research lies both in the contribution given to deepen the knowledge about the gas- phthalocyanine interaction mechanisms and in the use of a completely different experimental approach, the Energy Dispersive X-ray Reflectometry. It was used as a probe to evaluate the efficiency of the morphological response of MPc thin films and, then, compared with the information in the literature on the conduction mechanisms inside these films.

An Italian patented MPc device, the titanium bis-phthalocyanine $TiPc_2$, was chosen to test the possibility of such new experimental approach. Besides, a newly synthesised phthalocyanine, the ruthenium phthalocyanine $(RuPc)_2$, was systematically investigated, in the same way, for its possible use as a nitrogen dioxide sensing device.

The second chapter of this thesis is mainly devoted to the theoretical aspects of X-ray Reflectometry, since the energy dispersive mode requires a different formalism with respect to the traditional Reflectometry technique (angular dispersive). Another chapter is devoted to the experimental apparatus. Indeed, the energy dispersive X-ray Reflectometer is a non commercial machine, designed and patented by the research group collaborating to this thesis. The description of the apparatus, and the theoretical section, are meant to make the reader more familiar to the experimental methodology.

In the subsequent chapters, the experimental results are discussed. However, in order to explain the scientific contents of this work in a more homogeneous way, the data reported are not listed in chronological order, as the experiments really were carried out following the logic evolution of the research. Indeed, since the $TiPc_2$ was used as an internal test to allow a comparison with $(RuPc)_2$, the same experimental procedures were applied to both, so that the study oscillated constantly between the two materials. This was a convenient way to proceed into the experimental investigation, but it didn’t seem to be the best way to show the results.

Therefore, two distinct chapters are devoted to the two phthalocyanine molecules. These sections are divided into the same paragraphs, since the study was always carried out in parallel; In this way the probability to easily make a comparison between the two phthalocyanines was preserved. However, the fact that the chapter devoted to titanium is reported before that devoted to ruthenium, has no temporal significance and has to be regarded as a convenient way to organize a large amount of information.

Each section contains the conclusions regarding the set of experiments discussed in it, giving the possibility of reading, if necessary, each paragraph separately. Only the last part of this thesis, devoted to the general conclusions regarding both the scientific contribution given to the phthalocyanine gas sensing community, and the technical improvements obtained in the energy dispersive X-ray Reflectometry and its potentialities, contains data on both molecules.

Introduction

In developed and rapidly industrialising countries, the major historic air pollution problem has typically been high levels of smoke and SO_2 arising from the combustion of sulphur-containing fossil fuels such as coal for domestic and industrial purposes. However, this problem has progressively diminished over recent decades as the result of changing fuel-use patterns: the increasing use of cleaner fuels such as natural gas, and the implementation of effective smoke and emission control policies.

At present, the major threat to clean air is posed by traffic emissions. Petrol- and diesel-engined motor vehicles emit a wide variety of pollutants, principally carbon monoxide (CO), nitrogen oxides (NO_x), volatile organic compounds (VOCs) and particulates, which have an increasing impact on urban air quality. In addition, photochemical reactions resulting from the action of sunlight on NO_2 from vehicles, leads to the formation of ozone, a secondary long-range pollutant, which impacts in rural areas often far from the original emission site. Acid rain is another long-range pollutant influenced by vehicle NO_x emissions.

While, industrial and domestic pollutant sources, together with their impact on air quality, tend to be steady-state or improving over time, traffic pollution problems are worsening world-wide. The problem may be particularly acute in developing countries with dramatically increasing vehicle fleets, infrastructural limitations, poor engine/emission control technologies and limited provision for maintenance or vehicle regulation.

Health risks from nitrogen oxides may potentially result from NO_2 itself or its reaction products including O_3 and secondary particles. Nevertheless, studies of exposures to NO_2 from outdoor air are unable in distinguishing these effects. Additionally, NO_2 concentrations closely follow vehicle emissions in many situations so that NO_2 levels are generally a reasonable marker of exposure to traffic related emissions.

Given these complex relationships, findings of multivariate models that include NO_2 and other pollutants need careful interpretation. Statistical models considering interactions must be based on strong a priori hypothesis about the nature of these interactions to allow an interpretation. While multi-pollutant models have been routinely applied to various forms of observational data, they may miss-specify underlying relationships. Even models that include only NO_2 and PM, NO_2 and O_3, or NO_2, PM and O_3 do not reflect the interrelationships among these pollutants.

With these constraints in mind, much research is nowadays devoted to the development of devices able to, discriminate NO_2 among other bi-products of the polluting emissions. In particular, Phthalocyanines (Pc), their metalloderivates (MPc) and related compounds, have shown the architectural flexibility and environmental stability suitable for technological applications. Moreover, their electrical properties change upon exposure to oxidizing gases like NO_2, and the interest in developing gas detectors having Pc derivates as the chemically sensitive component of chemical/conductometric transduction systems is steadly increasing.

In this work, two differently doped phthalocyanines will be studied, Titanium and Ruthenium being the insertion metals respectively. The first system, $TiPc_2$, is a patented NO_2 detector which has been deeply investigated from an optical/conductometric point of view. The latter, $(RuPc)_2$, is a newly synthesized bis-phthalocyanine, with unconventional semiconducting properties, but whose behaviour versus oxidising gases, such as NO_2, is still unknown.

The primary aim of this research is to investigate the possibility of developing a novel NO_2 sensing device based on ruthenium phthalocyanines. In order to classify this material as a sensor it must satisfy and possess several qualities. They can be collected in two categories:

- Sensitivity, Selectivity and Reversibility are the fundamental properties to classify a material as sensing device.

- Recovery rates, time response, durability, are the complementary ones, on which the sensor quality depends.

Moreover, in order to evaluate the potentialities of $(RuPc)_2$ as device, the physical-chemical interaction occurring between the material and NO_2 must be investigated. The morphologic effects on the sensor induced by such physical-chemical interactions, represents the scientific goals of this work.

Gas sensors are traditionally studied by optical/conductometric techniques because a result of the interaction with gas is usually a change in the absorbance spectra or in conductivity. However, neither the gas-sensing process has never been studied in real time, nor the kinetics ruling such process.

Since MPcs are processed as thin films when have to act as sensitive elements of a gas sensing electro resistive device, it has been demonstrated their structural/morphological arrangement, plays a major role in their properties as sensors (recovery rates, reversibility, etc.). The study of titanium and ruthenium phthalocyanine thin films will be approached from this point of view. Energy Dispersive X-ray Reflectometry is a technique able to study morphological characteristics of layered samples, at the A resolution. This will be the main tool to investigate the sensing potential of the $(RuPc)_2$ and to deepen the knowledge of the basic interactions occurring inside the films matrix when they come in contact with the NO_2 gas. This unconventional approach aims to establish a novel experimental protocol, namely a “morphological monitoring” of gas sensing devices.

The energy dispersive mode combined with X-ray Reflectometry is able to enhance the performances of a technique usually regarded as auxiliary. Indeed, time resolved in-situ measurements can be used to monitor the morphological time evolution of systems that undergo specific treatments. In our case the aim is monitor the evolution of Phthalocyanine thin films while exposed to the NO_2 gas and verify if there is some kind of morphological response. In this case, the correlations between such modifications and the electro-chemical responses induced by the polluting gas, will be investigated.

Chapter 1

1.1 Phthalocyanines and Metallo-Phthalocyanines

1.1.1 Properties

Phthalocynines (Pcs) and metallo-phythalocyanines (Mpcs) [1-3] have been investigated form many years especially with regard to their properties as dyestuffs, paints and colours.

A metal-free phthalocyanine was found for the first time in 1907 [4] as a by product during the preparation of 2-cyanobenzaminde. However, not much importance was attributed to the discovery at that time. Later, in 1927, a copper phthalocyanine was prepared in 23% yield by reacting 1,2-dibrombenzene with copper (I) cyanide in pyridine [5]. The structure was investigated meticulously by Linstead and he was the first to use the term phthalocyanine [6], deriving the name from the Greek words *naphtha* (rock oil) and *cyanine* (blue). In the subsequent years he elucidated the structure of phthalocyanines as well as procedures for obtaining several metal phthalocyanines and the metal free Pc's. [9-15].

In the last 20 years phthalocyanine chemistry is undergoing a renaissance, because phthalocyanines and many of their derivatives exhibit singular and unconventional physical properties useful for application in materials science. Thus, the interest of phthalocyanines, in addition to basic research, has been recently expanding also into applied fields such as photovoltaics, electrochromism, optical data storage, laser dyes, liquid crystals and chemical sensors, among others.

Indeed, it is well known that substances which show semiconducting or conducting properties or high linear and nonlinear optical responses are currently of great scientific and technological interest for designing electronic or optoelectronic devices [16].

In general, the phthalocyanine molecule has a two-dimensional π–electron conjugated system (an aromatic system with 18 π–electrons) and a number of modifications can be made either in the macrocycle by incorporating more than 70 different metal atoms or by substituting side groups at the peripheral sites of the macrocycle, see figure 1.

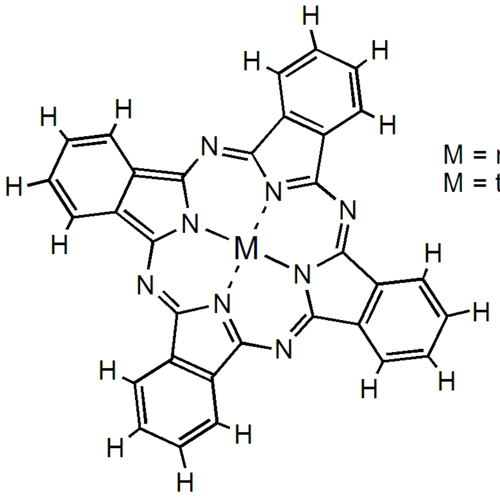

M = metal(s), metalloid(s) => metallophthalocyanine
M = two hydrogens => metal-free phthalocyanine

Figure 1. *Schematic drawing of a phthalocyanine molecule. In the central cavity a metal (M) can be allocated.*

Moreover, the formal substitution of one or more isoindole units by another heterocyclic affords the phthalocyanine analogues. Phthalocynines can also be polymerized in one- or two-dimensional arrays. These changes facilitate the tailoring of electro physical parameters of MPcs over a broad range and, consequently, allow to modulate the electrical and optical behaviour of the compounds.

On the other hand, phthalocyanines can present several kinds of condensed phases such as single crystals, polycrystalline films, dichotic liquid crystals and Langmuir Blodgett films, among others. This fact is extremely important:

- In order to organize the phthalocyanines in a supramolecular architecture to achieve supramolecular properties.
- To improve the processability of the compounds for their incorporation in molecular devices.

Electrically semiconducting molecular materials have important advantages over conventional inorganic semiconductors such as lower weight, tunability, versatility, etc. therefore, they have attracted much interest for their potential technical applications [17,18]. However, any members of the current generation of substances, like polyacetylenes and related conducting polymers, exhibit severe limitations with regard to chemical-structural control at the molecular level. Moreover, oxidative doping in these products usually leads to unstable compounds, which can not be easily processed. For these reasons, research on molecular semiconductors have concentrated recently on a special topic, namely the possibility to develop systems which exhibit intrinsic semiconducting properties, without external doping.

Up to now, few intrinsic molecular and polymeric semiconductors based on metallo macrocycles have been reported [19-21]. Macrocyclic (Ma) transition metal (M) complexes which are linked by linear bridging ligands (L), containing delocalizable π–electrons to form polymeric stacked arrangements $[MacML]_n$ have been synthesized. The electrical properties of this kind of bridges coordination compounds, are determined by three building blocks Mac, M and L. The bridged systems can be ox datively doped with iodine resulting in the formation of stoichiometric compounds $[MacM(L)I_y]_n$, which are stable up to 120°C with semiconducting properties (up to $\sigma_{RT} = 10^{-2} - 10^{-1}$ S/cm). However, if the bridging ligand L in the systems is e.g. *s*-tetrazine (tz), then the bridges macrocyclic compound $[MacFe(tz)]_n$ (Mac = phthalocyanine, 2.3- naphthalocyanine, etc.) shows semiconductive properties (0.1 S/cm) without additional external oxidative doping.

On the other hand, in most molecular or macromolecular phthalocyanine systems, the difference between the oxidation and reduction potentials is equal or greater than 1.5 eV. [22] This yields consequently insulators. Undoped phthalocyanine radicals behave differently:

- Lutetium bis-phththalocyanine (Pc_2Lu) and lithium mono-phthalocyanine (PcLi) have been shown to be the first two members of the class of *intrinsic molecular semiconductors.*

The radical phthalocyanines may therefore be used as bricks for making molecular semiconductors, being it still necessary to obtain a proper organization.

Moreover the physical properties of the phthalocyanines may be significantly altered by modification of their molecular subunits. The chemical versatility in the preparation of hemiporphirazines, closely related to phthalocyanines [23] provides a unique opportunity to vary the electronic structure through ligand and metal modifications, thus allowing a systematic correlation between the modifications and the changes induced in the physical and physico-chemical properties of the molecules, such as polarity, solubility, redox behaviour, etc.

Metallophythalocyanines (Mpcs, figure 1) [24] are multipurpose synthetic electroactive materials with particular electronic and structural characteristics which show semiconducting and nonlinear optical properties. The term “Synthetic Electroactive materials” includes synthetic organic molecules or macromolecules which have a particular activity under either static electric field or electromagnetic field of optical radiation. Charge transfer complexes, polymers, fullerenes, metallomacrocycles and ferroelectric liquid-crystals are examples of this kind of materials [25, 26].

1.1.2 General Synthesis of phthalocyanines

In general, the synthesis of phthalocyanines proceeds from a single step reaction, normally denominated cyclotetramerization of benzoic acid or its derivatives, e.g. phthalic anhydride, phthalimidee, *o*-cyanobenzamide, phthalonitrile or isoindolinediimine [1,27] (see figure 2).

The most used precursor for substituted phthalocyanine synthesis is the substituted phthalonitrile, or in some cases, when the low reactivity of the precursor inhibits the macrocycle formation, isoindolnediimnes can be used as well.

Nucleophilic hindered bases like, 1,8-diazabicyclo-(5,4,0)-undec-7-ene (DBU) can be used as powerful catalysts for the cyclotetramerization of phthalonitriles in solution (e.g. pentanol, octanol), with the metal ion as template for the formation of metal phthalocyanines [27].

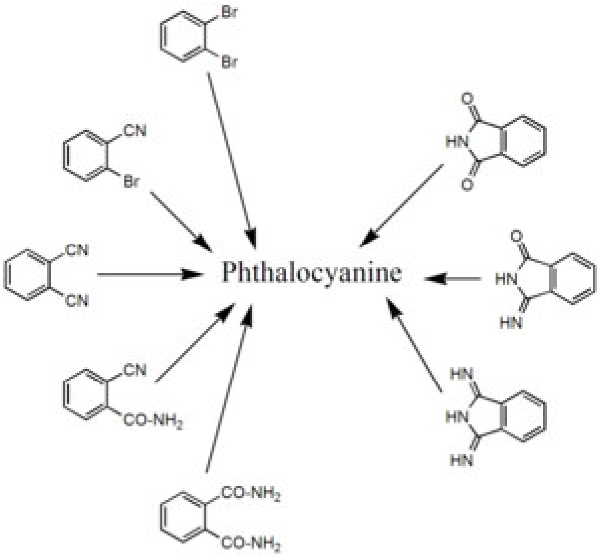

Figure 2. Phthalocyanine general synthesis scheme.

1.2 Gas sensors based on phthalocyanine thin films

1.2.1 Introduction

The electrical properties of phthalocyanines are modulated upon exposure to gases such as NO_2 or ammonia [28,29], and this phenomenon has led to an interest in developing gas detectors using Pc derivatives as the chemically sensitive component [30,31]. Current drawbacks which have prevented the development of practical Pcs conductometric gas sensors are the lack of selectivity, low sensitivity, long response times, slow recovery rates and particularly poor behaviour at room temperature.

Indeed, it has been shown that a number of amphiphilic Pcs, deposited as films, show excellent sensitivity and, more importantly, selectivity in their response to exposure to particular gases, e.g. NO_2 [32-34].

Phthalocyanines posses other properties that are also favourable for the sensing application:

- Manipulation as microelectronic device compatible thin films
- Good chemical and thermal stability toward many environments
- Good potential for development of gas specificity

In its simplest form a phthalocyanine sensor consists of a planar interdigital electrode with a thin phthalocyanine film: microelectronics technology has influenced the Pcs sensor development. In fact, since phthalocyanines are generally weakly conducting materials (e.g., 10^{-12} S/cm), voltages of 10-700V are necessary to measure conductivity changes with conventional electrodes. In addition, such high voltages could cause an electrochemical degradation at the phthalocyanine-electrode interface. However, with microelectronic substrates having an electrode spacing ranging from 1 to 25 μm, it is possible to make these measurements with potentials less than 1V.

1.2.2 Phthalocyanine - gas interaction

The function of the phthalocyanine thin film, coating the microelectronic substrate, is to absorb or form a weak bond with a particular gas and to undergo a large change in conductivity as a result of this interaction. This is due to the formation of a donor-acceptor complex with the equilibrium driven by the partial pressure of the gaseous component.

It has been observed that acceptor gases such as oxygen, nitric oxide, and nitrogen dioxide cause an increase in phthalocyanine conductivities, a decrease in the activation energies, and the appearance of charge transfer bands in the visible spectra [35]. On the other hand, a donor gas such as ammonia causes a conductivity decrease in most phthalocyanine and reverses the effects of the acceptor gases. On this basic responses, phthalocyanines have been classified as p-type semiconductors [36].

1.2.3 Phthalocyanine - NO_2 gas interaction

Nitrogen oxides are formed during high temperature combustion processes [37] from the oxidation of nitrogen in the air or fuel. The principal source of nitrogen oxides - nitric oxide (NO) and nitrogen dioxide (NO_2), collectively known as NO_x - is road traffic, which is responsible for approximately half the emissions in Europe. NO and NO_2 concentrations are therefore greatest in urban areas where traffic is heaviest. Other important sources are power stations, heating plants and industrial processes. Nitrogen oxides are released into the atmosphere mainly in the form of NO, which is then readily oxidised to NO_2 by reaction with ozone. Elevated levels of NO_2 occur in urban environments under stable meteorological conditions, when the air mass is unable to disperse. Nitrogen dioxide has a variety of environmental and health impacts. It is a respiratory irritant, may exacerbate asthma and possibly increase susceptibility to infections. In the presence of sunlight, it reacts with hydrocarbons to produce photochemical pollutants such as ozone (see below). In addition, nitrogen oxides have a lifetime of approximately 1 day with respect to conversion to nitric acid. This nitric acid is in turn removed from the atmosphere by direct deposition to the ground, or transfer to aqueous droplets (e.g. cloud or rainwater), thereby contributing to acid deposition.

These are the reasons why the detection of nitrogen dioxide (NO_2) is of extreme importance for environmental protection. EPA's health-based national air quality standard for NO_2 is 0.053 ppm (measured as an annual arithmetic mean concentration). Prolonged exposure to higher concentrations are statistically related to acute respiratory illnesses. Nitrogen dioxide itself is a somewhat complicated gas in that two species, monomeric NO_2 and dimeric N_2O_4, exist in a strongly temperature dependent equilibrium.

However, the interaction of nitrogen dioxide gas with phthalocyanine crystals and films has one of the largest effects on conductivity (6 to 8 orders of magnitude) and has received more study than other gas interactions [38]. Indeed, most studies have been performed on the crystalline precursor phthalocyanine powders and many interesting results give useful insight into the phthalocyanine-gas interaction mechanism.

Among these, it is worth noticing that the conduction mechanism is due to the formation of a charge-transfer complex formed between a phthalocyanine donor and an NO_2 acceptor and the charge carriers are the holes produced in the phthalocyanine matrix [39, 40].

Moreover, the nature of the acceptor is important for the conductivity enhancing effect. Nitrogen dioxide is a π–electron acceptor, and the accepted electron would be delocalized over the planar NO_2 and N_2O_4 structure. Since the hole is also delocalized over the phthalocyanine structure, the columbic force between the opposite charges is weakened and charge carrier movement is facilitated. On the contrary, this effect is contrasted with the effect induced by the exposure to a strong σ–electron acceptor, e.g. boron trifluirde.

However, when the same studies are performed upon the sensor device precursors, i.e. the phthalocyanine thin films, the results are not as convincing as those referred to the crystalline powders.

Among others:

- ➢ The conductivity response of sublimated films to NO_2 appears to be, unfortunately, somewhat different than that of single crystals.
- ➢ Different phthalocyanine films display different conductivity dependences on the concentrations of NO_2 exposure.
- ➢ Evacuation at room temperature does not completely reverse the exposure effect in all films, nor is it completely reversed by exposure to donor gases.

These evidences suggests that the film deposition process strongly affects the phthalocyanine properties and this influence differs from MPcs to MPcs depending on the chemical nature of the precursor and of the film texture deriving from the evaporation process.

Moreover many thin Pc films still acts as very good NO_2 sensing materials, but their response differs depending on various factors. In fact, sublimated films may have an amorphous or polycrystalline character: defects and disordering affects gas absorption sites as well as charge carrier transport. Indeed, simple annealing of a sublimated film in the α crystalline form to the β crystalline form changes its electrical conduction and gas response characteristics [41].

This observations, among others, indicate that the phthalocyanine film morphology plays a fundamental role in the film’s electrical response to gas exposure. Indeed, the morphology must accommodate both the charge transfer interaction and charge carrier transport. While these mechanisms are not well understood, it is believed that the charge transfer interaction is easier if the face of a phthalocyanine ring rather than an edge is available (the smoothest film surface as possible) for an electron transfer complex formation. On the other hand, charge carrier transport is facilitated by a long-range stacking of co-facially oriented phthalocyanine rings.

These are among the main reasons why this work approach the metal phthalocyanines - NO_2 gas interaction, from a morphological point of view:

- In order to study the behaviour of the gas sensing MPcs when processed as sensing thin films, rather than original materials (crystalline powders).
- In order to study the influence of morphological parameters on the sensing devices properties: sensitivity, recovery times, reversibility, stability, etc.
- In order to understand the gas-film interaction mechanisms that affect the electrical behaviour of the devices.
- In order to discriminate the sensors performances in different experimental conditions (gas concentration, device temperature, etc.) depending on the film morphology.

In the next chapter a brief description of the experimental techniques chosen to perform these studies, is presented. Moreover a deeper insight into the structure and morphology of sublimated Phthalocyanine films is necessary and follows in the next section.

1.2.4. Phthalocyanine Film structure and morphology

The morphology of the phthalocyanine films is variable and strongly dependent on the sublimation conditions. It ranges from amorphous to highly crystalline. Amorphous films are prepared by vacuum sublimation (10^{-6} Torr) onto liquid-nitrogen-cooled (100°K) substrates [42].

These films are stable at room temperature but crystallize to the an α phase on annealing over the temperature range 60-140°C followed by an α to β phase transition at 210°C.

Since the structure of a generic sublimated Mpc film consists of columnar stacks with the ring orientation inclined relative to the axis of the stack, the α and β form differs because of the different tilt angle (depending on the Metal) between the axis and the stack, see figure 3.

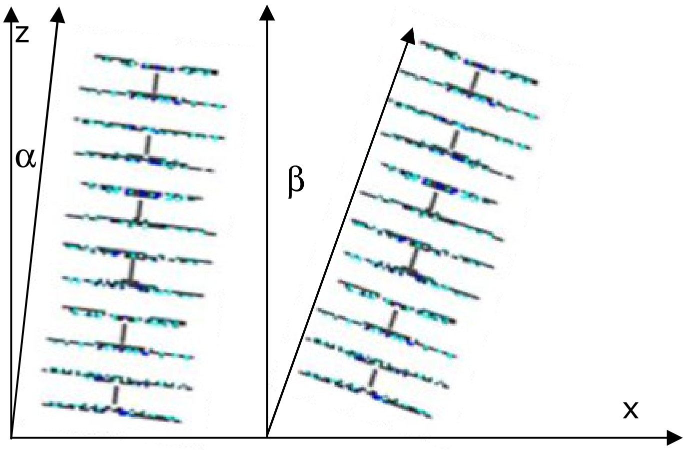

Figure 3. Schematic sketch of the packing of a generic MPc processed as thin film. The columnar stacks are characterized by two different tilt angles with respect to the normal of the film surface/substrate, corresponding to two different phases: the α-phase, being the less tilted and the β–phase, being the more tilted.

In particular the α phase is less tilted than the β one and its axial position is more open. These structures in sublimated films are important since they determinate how vapours may enter the lattice and interact with the phthalocyanine units. A more detailed description of the structural arrangement of the MPcs studied in this thesis, follows in the related chapters.

The morphology changes, passing from one structure to the other, is very important since it affects the response of the thin film towards the gas. In fact, the α phase is much more sensitive to some particular gas, e.g. oxygen [1], while the intrinsic conductivities of the two phases are identical.

If the substrate is held at room temperature, the α phase is obtained by sublimation at pressures less than 50 Torr. At higher pressures or at substrate temperatures above 210°C, the β phase is obtained [43]. Moreover, to avoid decomposition, phthalocyanine should never be heated above 400°C.

References

[1] C. C. Leznoff, A. B. Lever, *Phthalocyanines. Properties and Applications;* VCH Pubblishers, Cambridge, U.K., 1989, 1993 and **1996**; Vols. 1-4.

[2] R. Dagani, *Chemical & Engineering News* **1996**, 22.

[3] N. B. Mckeown, *Phthalocinines Materials, Synethesis, Structure and Function;* Cambridge University Press, Cambridge, **1998**.

[4] A. Braun, J. Therniac, *Ber. Dtsch. Chem. Ges.*, 40, **1907**, 2709.

[5] H. de Diesbach, E. von der Weid*, Helv. Chim. Acta*, 10, **1927**, 886.

[6] R. P. Linstead, *Br. Ass. Adv. Sci. Rep.* **1933**, 465.

[7] R. P. Linstead, *J. Chem. Soc.*, **1934**, 1016.

[8] G. T. Byrne, R. P. Linstead, A. R. Lowe, *J. Chem. Soc.*, **1934**, 1017.

[9] R. P. Linstead, A. R. Lowe, *J. Chem. Soc.*, **1934**, 1022.

[10] C. E. Dent, R. P. Linstead, *J. Chem. Soc.*, **1934**, 1027.

[11] C. E. Dent, R. P. Linstead, R. Lowe, *J. Chem. Soc.*, **1934**, 1033.

[12] P. A. Barret, C. E. Dent, R. P. Linstead, *J. Chem. Soc.*, **1936**, 1719.

[13] P. A. Barret, D. A. Frye, R. P. Linstead, *J. Chem. Soc.*, **1938**, 1157.

[14] J. S. Anderson, E. F. Bradbrook, A. H. Cook, R. P. Linstead, *J. Chem. Soc.*, **1938**, 1151.

[15] R. P. Linstead, *Ber. Dtsch. Chem. Ges. A*, 72, **1939**, 93.

[16] J. Simon and T.Toupance, “Intrinsic Molecular Semiconductors: Electronics and Ioni-lectronics Finalities”, in *Comprehensive Supramolecular Chemistry*, Vol. 10 (Eds. D. N. reinhoudt), Pergamon, Exeter, **1996**.

[17] T.J.Marks, *Ang. Chem. Int. Ed. Engl.*, 29, **1990**, 857.

[18] D.F. Eaton, G. R. Meredith, S.J. Miller, *Adv. Mater.*, 3, **1991**, 564.

[19] H. Schultz, H. Lehmann, M. Rein, M. Hnack, *Structure and Bonding* 74, Springer-Verlag, Hidelberg, p. 41, **1991**.

[20] J. Simon, J.-J. André, *Molecular Semconductors*, Springer Verlag, Berlin, **1985**.

[21] D. P. Jiang, A. D. Lu, Y.J. Li, X. M. Pang, Y. L. Hua, *Thin Solid Films,* 199, **1991**, 173.

[22] J. Simon, J.-J. André, M. Maitrot, in *Molecular Electronics, (*Ed. M. Borissov), World Scient. Pub., Singapore, **1987**.

[23] F. Fernàndez-Làzaro, T. Torres, B. Hauschel, M. Hanack, *Chem. Rev.*, 98, **1998**, 563-575

[24] F.H.Moser, A.L. Thomas, *The Phthalocynines*, Vols. 1-2, C.R.S. Press, Bocaaton, Florida, **1983**.

[25] J.S. Miller, *Adv. Mater.,* 5, **1993**, 671.

[26] P. Bauerle, *Adv. Mater.*, 5, **1993**, 879.

[27] M. Hanack, H. Heckmann, R. Polley, in *Methoden der Organischen Chemie (Houben–Weyl), vol. E9d; 4th Ed.*; Thieme Verlag:Stuttgart, **1997.**

[28] C.Hamann, A. Mrwa, M. Müller, W. Göpel, M. Rager, *Sensors and Actuators B,* 4, **1991**, 73-78.

[29] J. Souto, R. De Aroca, J. A. Saja, *J. Phys. Chem.,* 98, **1994**, 8998.

[30] A. Capobianchi, A. M. Paoletti, G. Pennesi, G. Rossi, S. Panero, *Synth. Met.,* 75, **1995**, 37-42.

[31] F. Baldini, A. Capobianchi, A. Falai, G. Pennesi, *Sens. Actuators B,* 51, **1998**, 176-180.

[32] S. Mukhopadhyay, C. A. Hogart, *Adv. Mater.,* 6, **1994**, 162.

[33] T. R. E. Sompson, D. A. Russel, M. J. Cook, A. B. Horn, S. C. Thorpe, *Sensors and Actuators B,* 29, **1995**, 353.

[34] B. Schollhorn, J. P. Ggermain, A. Pauly, C. Maleysson, J.P. Blanc, *Thin Solid Films*, 326, **199**, 245.

[35] J. Kaufhold, K. Haufe, *Ber. Bunsenges. Phys. Chem.*, 69, **1965**, 168.

[36] D.D. Eley, *Nature* (London) 162, **1948**, 819.

[37] R.G. Derwent, in *Air Pollution and Health*, (edited by S.T. Holgate), J. M. Samet, H.S. Koren, R.L Maynard, Chapter 4, pp.51-62 (Academic, New York, NY, **1999**).

[38] F. Fernàndez-Làzaro, T. Torres, B. Hauschel, M. Hanack, *Chem. Rev.,* 98, **1998**, 563-575.

[39] H. Tian, K.-C. Chen, *Dyes and Pigments,* 27, **1995**, 191-196.

[40] M.E. Azim-Araghi, D. Campbell, A. Krier, R.A. Collins, *Semicond. Sci. Technol.,* 11, **1996**, 39-43.

[41] H. Lars, G. Heiland, *Thin Solid Films*, 149, **1987**, 129.

[42] M. S. Mindorff, D. E. Brodie, *Can. J. Phys.*, 59, **1981**, 249.

[43] F. W. Karasek, J. C. Decius, *J. Am. Chem. Soc.*, 74, **1952**, 4716.

Chapter 2

2.1 X-ray Reflectometry

2.1.1 Introduction

The X-ray reflectometry technique (XRR) is a powerful method for investigating monolithic and multilayered film structures. XRR studies are highly sensitive to electron density gradients irrespective of the crystalline nature of the system investigated [1]. It is also one of the few methods that, with great accuracy, allow one to extract information not only on the free surface and the interface(s), but also to determine the mass density, the thickness and the roughness of thin layers along the direction normal to the specimen surface [2].

The birth of the experimental technique of X-ray specular reflectivity can be traced back to 1923 and is due to the contribution of Compton who was the first to report this phenomena on solid samples with flat surfaces [3]. Some decades later, this technique was approached by Yoneada who explored the manifold applications of Compton's first experimental evidence. In fact, if the studied surfaces are not ideally smooth but somewhat rough, the X-rays can be diffusely scattered in any direction: intensity modulation in the X-ray diffuse scattering were found [4].

In the early 1970's the same group published the first experimental evidences obtained by X-rays impinging samples below the critical total reflection angle [5]: the first X-ray fluorescence measurements under total reflection conditions on particle deposited on smooth substrates, were performed.

Despite this long experimental history, it is just nowadays that X-ray reflectometry based on total reflection has become a powerful tool for analysis of surfaces and interfaces (at the Ångstrom resolution) [6], and still continues to grow up further. The reason is mainly due to the significant technological developments that have been done in the last decades, especially the advent of synchrotron radiation and the progress achieved in detector technology.

The advancement of the theoretical modelling and the techniques for analyzing experimental data are also important. Of course this has been accelerated by the rapid evolution of computers.

2.1.2 Theory

Total Reflection of light is a well known phenomenon that occur when light is travelling from an optically dense medium (high index of refraction) to a less dense (low index of refraction) medium [7]. The total reflection is accompanied by an evanescent wave propagating along the interface between the two media and being exponentially damped into the less dense medium [8]. For light, air has a smaller index of refraction than most materials, and so optics textbooks [9] only mention total reflection on *internal* surfaces of materials (of glass, for example).

But for X-rays, the refractive index of most materials is smaller than that of air, albeit only slightly, so total *external* reflection occurs. This fact enables one to use the reflectometry as a tool for physical and material science studies because an X-ray beam impinging a sample (either in air or in a vacuum) can be totally reflected by it, carrying morphological information on the reflection surface.

A simplified description of the basic principles of the physical phenomena of total external reflection is given in order to understand qualitatively the theoretical background beyond this experimental method. In the next section a mathematically more correct description is provided to explain the data processing methods.

2.1.3 Refractive Index and Snell Law

The refraction and reflection phenomena are common for all travelling waves and are described by Snell's law. Measuring the incidence and reflection angles from the surface (instead of from the normal to it), figure1., this law can be written as:

$n_1 \cos\alpha_i = n_2 \cos\alpha_r$

(α_i and n_1 being the incidence angle of the primary beam and the refractive index of the first medium and α_r and n_2 the reflection angle and the refractive index of the second medium).

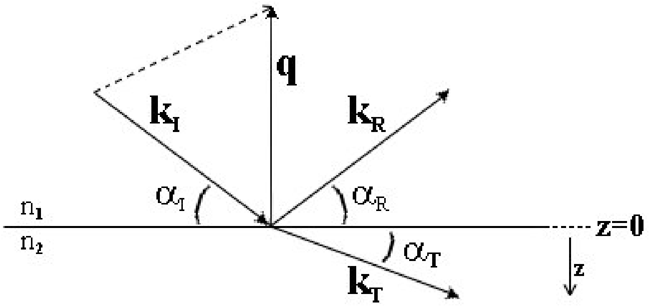

Figure 1. *Geometry of specular reflectivity. The initial and final wave vector k_i and k_f define the scattering plane.*

If $n_1 > n_2$, than $\alpha_i > \alpha_r$, $q = k_r - k_i$ consequently, there must be a value of α_i, called critical angle α_c, so that $\alpha_r = 0$. In this case $\cos \alpha_c = n_2 / n_1$. If the first medium is air, than the expression becomes: $\cos \alpha_c = n_2$.

In these conditions the beam will not be refracted any more but totally reflected.

In case of X-ray this is still true at a first approximation, and the only change required is a different definition of the refractive index [10]. The (complex) index of refraction in the X-ray region can be written as:

$$n = 1 - \delta - i\beta$$

where the real term δ is associated with the dispersion, and the imaginary term β with the absorption:

$$\delta = (\lambda^2/2\pi)\, \rho r_0 Z^2$$
$$\beta = (\lambda/4\pi)\, \mu$$

λ being the incident wavelength, ρ the material density, r_0 the classical electron radius, Z the atomic number and μ the linear absorption coefficient [11].

In this energy region, both terms are small compared to unity (about 10^{-4} to 10^{-8}), and usually β is much smaller than δ.

For all elements in the energy region away from the absorption edges, δ is a positive quantity, so the real part of the refractive index is smaller than unity. Therefore total reflection of X-rays can be observed in the region of incident angles below the critical angle of total reflection [12]:

$$\alpha_c \approx \sqrt{2\delta} = \lambda\sqrt{r_e \rho_{el}/\pi}$$

For some elements, δ has negative values for energies around the absorption edges and no total reflection process is present for these energies.

Starting from these considerations, we can rewrite Snell law for an incident X-ray beam, substituting the correct expression of the refractive index n into the equation $\cos\alpha_c = n_2$, thus obtaining:

$$\cos\alpha_c = 1 - (\lambda^2/2\pi)\, \rho r_0 Z^2 - i(\lambda/4\pi)\, \mu$$

The imaginary component, being responsible of the absorption phenomenon, will be neglected in case of total external reflectometry measurement. Indeed, the angle of incidence is very shallow and almost parallel to the surface, enhancing the signal from the surface and minimizing the penetration depth into the bulk, i.e. the absorption effect can be neglected [13].

Assuming that the incident angle is extremely small [14], the expression can be expanded till the third order in Mc Laurin series and, for a given material, at Z and ρ fixed, it becomes $\alpha_c/\lambda =$ constant.

Under the same hypothesis of small angle ($\sin\alpha \approx \alpha$), since the scattering parameter (momentum transfer) $q \cong 4\pi\sin\alpha/\lambda$, the X-ray total reflection occurs when the critical wave vector value $q_c = \alpha_c/\lambda$, is reached.

Therefore, at a very good approximation, in a total reflection experiment far from the absorption edge, the relevant parameter is not the critical angle alone, since it changes with the X-ray energy, but rather the critical angle to wavelength ratio, i.e. the critical value of the scattering parameter q_c [15], where:

$$q = 4\pi\sin\alpha/\lambda = E \sin\alpha / hc = K\, E \sin\alpha$$

(When the energy E is expressed in KeV, K = 1.0136 and q results in Ångstroms^{-1}).

As a consequence, performing a reflectivity measurement means to collect the Reflected Intensity as a function of the scattering parameter q.

In general, as it can be seen also by the approximated model described above, X-ray reflectometry can be used for determination of:

- Surface and interface roughness
- Layer thickness of thin films and multilayer samples
- Near-surface density gradients and layer density

However, in order to deduce quantitatively these information, an accurate fitting procedure based on the more rigorous theoretical model must be performed, as discussed in the next section.

2.1.4 Direct theory: Fresnel and Parratt Formalism

The basic theory of the reflection and refraction of an electromagnetic wave at an interface is given by the Fresnel formulae (round 1830). Nonetheless, it took more than 100 years, until Kiessig and later Parratt, applied these to X-rays and thus created a tool to study the structure at interfaces on a scale ranging from 10 Å to several 1000 Å. In several reviews [16-18], the theoretical concepts of the total reflection of X-rays from a single surface and multilayer have been presented.

In the previous section a simplified description of total reflection of X-rays, in analogy with visible light, was used to deduce that these phenomena occur when the incident angle equals the exit angle. In this case, the momentum transfer ($q = 4\pi \sin\alpha/\lambda$) is along the surface normal, which is chosen as the z coordinate.

The basic description of the X-ray reflectivity, model to study surfaces and interfaces, known as Parratt's formalism, was published in 1954 [19] employing Fresnel reflection and transmission coefficients as derived from electromagnetic wave propagation theory.

2.1.5 Reflectivity from an ideal surface: Fresnel Reflectivity

Let us consider the reflection and refraction of a monochromatic plane wave, polarized linearly and characterized by a wave vector k_I. This radiation impinges the interface between two non conductive, isotropic mediums, whose refractive indexes are n_1 and n_2 respectively, as shown in figure1.

As demonstrated by electromagnetism [18], a plane polarized wave (//, 'p') (or a normal polarized one ⊥, 's') produces a reflected (or refracted) wave still with the same polarization, p or s [20]. Indicating with A, R and T the amplitudes of the corresponding autostates of these waves, we can deduce the reflection (R_F, *reflectivity*) and transmission (T_F, *trasmittivity*) coefficient for the corresponding components of the amplitudes.

These coefficients are called *Fresnel coefficients*:

$$\begin{cases} R_{F,//} = \dfrac{R_{//}}{A_{//}} = \dfrac{\tan(\alpha_I - \alpha_T)}{\tan(\alpha_I + \alpha_T)} \\ R_{F,\perp} = \dfrac{R_{\perp}}{A_{\perp}} = -\dfrac{\mathrm{sen}(\alpha_I - \alpha_T)}{\mathrm{sen}(\alpha_I + \alpha_T)} \end{cases} \qquad \begin{cases} T_{F,//} = \dfrac{T_{//}}{A_{//}} = \dfrac{2\mathrm{sen}\alpha_I \cos\alpha_I}{\mathrm{sen}(\alpha_I + \alpha_T)\cos(\alpha_I - \alpha_T)} \\ T_{F,\perp} = \dfrac{T_{\perp}}{A_{\perp}} = \dfrac{2\mathrm{sen}\alpha_I \cos\alpha_I}{\mathrm{sen}(\alpha_I + \alpha_T)} \end{cases}$$

It is worthwhile to remember that these coefficients are calculated in the hypothesis of a monochromatic radiation.

In case of X-rays, the refraction index is slightly different depending on the radiation wavelength:

$$n(\lambda) = 1 - (\lambda^2/2\pi)\,\rho r_0 Z^2 - i\,\mu\lambda/4\pi$$

and affects the propagation of the radiation itself. Moreover, as the refractive index is very close to unity, the differences between the p or s polarizations of the incident beam can be neglected.

Indeed, let us consider only the z direction component of the incident ($\mathbf{k}_{I,z}$) and of the transmitted beam ($\mathbf{k}_{T,z}$) as shown in figure 2; from the Snell law, we deduce:

$$k_{I,z} = k \sin \alpha_i ,$$

$$k_{T,z} = k\sqrt{n^2 - \cos^2 \alpha_I} \approx k\sqrt{\alpha_I^2 - \alpha_c^2} \; ;$$

and the R_F and T_F coefficients become:

$$\begin{cases} R_F = \dfrac{k_{I,z} - k_{T,z}}{k_{I,z} + k_{T,z}} \overset{\alpha_I \ll 1}{=} \dfrac{\alpha_I - \alpha'_I}{\alpha_I + \alpha'_I} \\ \\ T_F = \dfrac{2k_{I,z}}{k_{I,z} + k_{T,z}} \overset{\alpha_I \ll 1}{=} \dfrac{2\alpha_I}{\alpha_I + \alpha'_I} \end{cases},$$

where

$$\alpha'_I = \sqrt{\alpha_I^2 - \alpha_c^2} = \alpha_I \sqrt{1 - \alpha_c^2 / \alpha_I^2}\ .$$

The following possibilities must be taken into account:

I. $\boldsymbol{\alpha_I \gg \alpha_c}$

It is possible to approximate α'_c with the first term of its Taylor expansion: $\alpha'_c \approx \alpha_I \left(1 + (\alpha_c / 2\alpha_I)^2\right)$ and, after a second approximation, $4\alpha_I^2 + \alpha_c^2 \approx 4\alpha_I$, we finally can rewrite the equation as:

$$R_F \cong \left(\frac{\alpha_c}{2\alpha_I} \right)^4,$$ hence it follows R ~ $1/q^4$.

This approximated R_F value deviates from the real one of less than 3% when $\alpha_I > 3\alpha_c$.

For reflectivity measurements performed above the critical angle α_c ($\alpha_i \gg \alpha_c$), this equation describes the intensity modulation which decays dramatically as the incidence angle increases.

II. $\boldsymbol{\alpha_I < \alpha_c}$

If the incidence angle is less than the critical one, than the transmitted wave number $\mathbf{k}_{T,z}$ becomes an imaginary value: $k_{T,z} = ik\sqrt{\alpha_I^2 - \alpha_c^2}$. Considering the wave as an evanescent wave propagating parallel to the surface, and substituting this new expression for $\mathbf{k}_{T,z}$, the electric field can be written as:

$$E \cong \exp(ik_{T,z}z) \cong \exp(-zk\sqrt{\alpha_I^2 - \alpha_c^2}) = \exp(-z/\Lambda);$$

Λ is the penetration depth of the evanescent wave when the wave amplitude has reached the value of $1/e$.

To calculate Λ, β can not be neglected otherwise $\Lambda \to \infty$ when $\alpha_I = \alpha_c$.
Indeed

$$\Lambda^{-1} = \frac{k}{\sqrt{2}}\left(\sqrt{\left(\alpha_I^2 - \alpha_c^2\right)^2 + 4\beta^2} + \alpha_c^2 - \alpha_I^2\right)^{1/2} \overset{\beta \to 0}{=} k\sqrt{\alpha_c^2 - \alpha_I^2},$$

choosing the negative solution only $(\alpha_c^2 - \alpha_I^2)$ of the expression

$$\sqrt{\left(\alpha_I^2 - \alpha_c^2\right)^2}.$$

As long as $\alpha_I < \alpha_c$, the penetration depth still remains very small, that means less than 30 Å. This feature is characteristic of the surface diffraction, where only the surface layers are studied.

As α_I increases, Λ gets lager too, until it becomes quasi-constant when $\alpha_I >> \alpha_c$.

III. $\alpha_I \rightarrow 0$

If $\alpha_I \rightarrow 0$, the penetration depth depends only on the electron density of the medium and it is independent on the radiation λ:

$$\Lambda = \frac{\lambda}{2\pi\alpha_c} = \frac{1}{\sqrt{4\pi r_e \rho_{el}}}.$$

2.1.6 Reflectivity from a multilayer: the Parratt Formalism

If the sample has more than one interface (i.e. a film on a substrate), the scattering from all interfaces has to be taken into account, figure 2.
Parratt developed a recursion formalism which relates the reflected and transmitted amplitude, R_j and $T_{t,}$ respectively, via:

$$X_j = \frac{R_j}{T_j} = \exp(-2ik_{z,j}z_j) \cdot \frac{R_{j,j+1} + X_{j+1} \cdot \exp(2ik_{z,j+1}z_j)}{1 + R_{j,j+1}X_{j+1} \cdot \exp(2ik_{z,j+1}z_j)}$$

where $R_{j,j+1}$:

$$R_{j,j+1} = \frac{k_{z,j} - k_{z,j+1}}{k_{z,j} + k_{z,j+1}}$$

is the Fresnel coefficient of interface j, and

$$k_{z,j} = k\sqrt{n_j^2 - \cos^2 \alpha_I}$$

indicates the wave vector component of the j layer along the z direction.

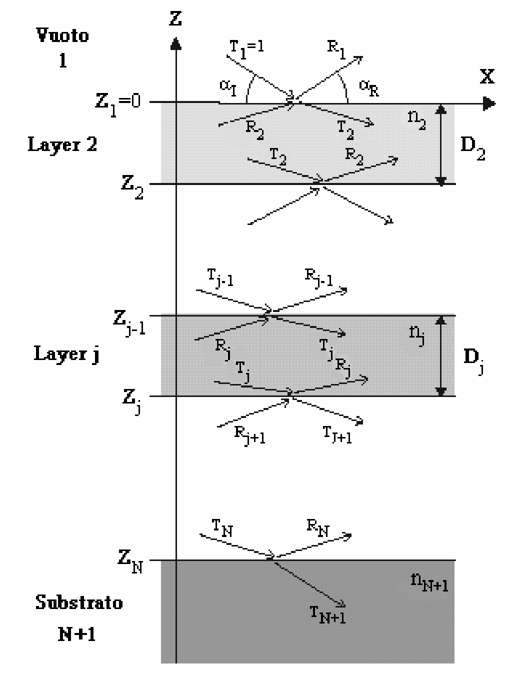

Figure 2. *A schematic diagram showing the definitions used in the Parratt formalism for a multilayered film.*

The recursion is solved using some boundary conditions:

- Incident wave normalized to unity $T_1 = 1$
- Assuming the first layer to be a semi-infinite vacuum or air, and the last layer N+1 assumed to be semi-infinite (bulk), so there will not be a recursive wave in this layer : $R_{N+1} = 0$

and the measured reflected intensity becomes:

$$R = |X_1|^2 = |R_1|^2$$

Due to the interference of waves, which are reflected from different interfaces within a system, intensity oscillations in the reflectivity can be observed. These oscillations are called Kiessig-fringes [21] and can be related to the thickness d of the film:

$$d_j = 2\pi / \Delta q_{z,j}$$

The Parratt formalism boats several notable advantages. Among them, the most remarkable is the freedom from approximations which makes it applicable from all the scattering regions that span from less than the critical angle to much higher incidence [22]. In addition it can ideally deal with an infinite number of layers.

2.1.7 Modelling of roughness in X-ray Specular Reflectivity

Ideal interfaces have been assumed in deriving the Parratt formalism, but the non ideality of the interface should be taken into account in real reflectivity calculations since most interfaces are not ideal on the length scale probed by X-rays.
To introduce the effect of rough surfaces and interfaces into the reflectivity model, a roughness factor Q_j must be introduced modelling the average electron density along the specimen normal by an error function [23, 24]. Following models are used:

- $Q_j = 1$ (i.e., an ideally smooth interface)
- $Q_j = \exp(-2k^2_{z,j}\,\sigma^2_j)$ (Debye-Waller factor [25])
- $Q_j = \exp(-2k_{z,j}k_{z,j+1}\sigma^2_j)$ (Nevot-Croce Factor [26])

The last factor was chosen and was introduced into the Parratt model in order to elaborate ad adequate fitting function. It is derived from the reciprocity principle and is based on the assumption for Gaussian distribution of the vertical roughness.

Still considering figure2, we define a function $h_j(x,y)$ to relate each point (x,y) of the interface j with a specific thickness. The term σ_j represents the root-main-square of the vertical interface roughness:

$$\sigma_j = < \left(\tilde{z}_j(x,y) \right)^2 >^{1/2}$$

with $\tilde{z}_j(x,y)$ is defined in the (x, y) point around the average interface height $h_{j,0} = < h_j(x,y) >$, and is equal to:

$$\tilde{z}_j = h_j(x,y) - h_{j,0}$$

The fluctuations around the value $h_{j,0}$ can be described by a Gaussian probability distribution: the 95% of all fluctuations are inside the interval $h_{j,0} \pm \sigma_j$. As a consequence, the refractive index n(z) changes from the value n_j to the value n_{j+1} when passing from the j layer to the j+1. In this case, the Q_j roughness term can be introduced into the Parratt formalism simply as a multiplicative factor, thus resulting:

$$\tilde{R}_{j,\,j+1} = \frac{k_{z,j} - k_{z,j+1}}{k_{z,j} + k_{z,j+1}} \exp(-2k_{z,j} k_{z,j+1} \sigma_j^2)$$

This expression is valid only if $\sigma_j << d_j$ e $\sigma_j << d_{j+1}$, i.e., the roughness is much smaller than the layer thickness.

The effect of the roughness term is to attenuate strongly the reflected intensity and to induce a damping in the Kiessig-fringes.

Moreover the missing intensity is scattered into other (non specular) directions. This diffuse scattering is sensitive to the in-plane correlations of the interface since it has a non-zero component of the momentum transfer in the plane: $q_{x,y} \neq 0$

Finally, in figure3, an example of reflectivity patterns is shown; the differences between a Fresnel reflectivity pattern (on the left) and the reflectivity collected from a thin film on a substrate (right) are evident. In the first case the reflected intensity decays more than exponentially as calculated previously, and the critical parameter is easily deduced by the position of the reflection edge.

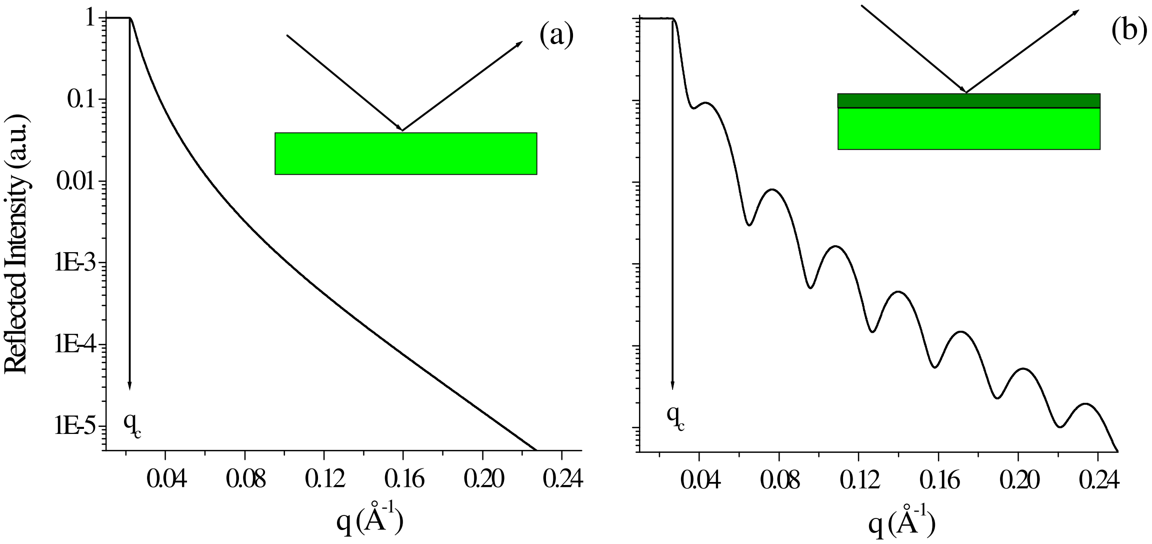

Figure 3. (a) Fresnel reflectivity of a blank surface, the critical scattering parameter is deduced. (b) Reflectivity of a flat surface with a 200 Å surface layer and an interface roughness of 5 Å.

In the second case the characteristic Kiessing fringes are visible and the Parratt model calculated for two layers can be applied in order to deduce all morphological information.

2.2 Energy dispersive X-ray Reflectometry

Since a reflectivity measurement consists in collecting the reflected intensity as a function of the scattering parameter [27],

$$q = 4\pi \sin\alpha/\lambda = KE \sin\alpha$$

which depends on the radiation energy and of the scattering angle, there are two methods available to perform the q scan and to draw the reflected intensity profile as a function of it [28]:

- The first is to use a monochromatic beam (fixed Energy), for instance a fluorescence line produced by a laboratory X-ray tube, and to make an angular scan: angular dispersive mode (AD).
- The second consists in utilizing a continuum spectrum radiation, for example the bremmestrahlung of the same X-ray tube (often called *white beam* in analogy with visible light), and to maintain the scattering angle fixed: energy dispersive mode (ED).

Even if the distinction between the two possibilities was already known at the end of the 1960 [20,30], the first one is still the most conventional method. In fact, although the second possibility has been known for long time, only in this period have solid state detectors with an acceptable resolution appeared, enabling the construction of a new kind of reflectometers/diffractometers. Advantages [31-33] and disadvantages [34] of one method on the other have been fully discussed but in this section a brief summary is given in order to understand why such a technique has been chosen to accomplish all X-ray reflectometry measurements.

When an X-ray reflectivity measurement is performed, the advantages of the ED mode are remarkable and the disadvantages become irrelevant.

In fact, the experimental geometry remains unchanged during data collection, which is a fundamental advantage for *in situ* studies [35-37]. Indeed, in the grazing incidence geometry, required in reflectivity measurements, any misalignments may induce relevant relative errors during the angular scan necessary to collect the reflectivity pattern in the Angular Dispersive mode. The use of in situ ED X-ray reflectivity, prevents this problem (the sample is not removed from its location and no instrumental movement is required) and allows film morphology modifications to be followed with extreme accuracy [38,39].

But the most important feature may be related to the resolution in the k space. A single spectrum collected at fixed angle, using the whole white beam of a conventional W anode X-ray tube, covers typically a range of some 10^{-2} $Å^{-1}$. A few hundred points, whose number is decreased by a factor 5 (groups of 5 adjacent points are summed to encounter the SSD resolution), are collected in this range.

To get the same resolution using the k_α of a Cu anode tube as primary beam, in the same k range, angular steps of 0.001° are required. Moreover, even if such angular movements may be performed by extremely accurate goniometers, the time expanse to collect all points constituting the reflectivity pattern, would not allow to perform real time measurements.

The increase of signal intensity and the parallel collection of the spectra, together with the fixed geometry, make the Energy Dispersive mode the best reflectometry technique to perform *in situ* and *time resolved* measurements.

On the other hand, the decrease in q resolution due to the uncertainties on both the angle and the energy:

$$\Delta q/q \approx \Delta E/E + \text{cotg}\,\alpha\,\Delta\alpha,$$

which is the main drawback of the ED mode in diffraction measurements, does not significantly affect the reflectometry patterns, because they are characterized by broad peaks or long period oscillations.

References

[1] M. Tolan, *X-Ray Scattering from Soft-Matter Thin Films,* Springer Tracts in Modern Physics, vol. 148, **1999**, Springer Heidelberg.

[2] R. Felici, *The Rigaku Journal*, 12 (1), **1995**, 11-17.

[3] A.H. Compton, *Philos. Mag.*, 45, **1923**, 1121.

[4] Y. Yoneada, *Phys. Rev.*, 113, **1963**, 2010.

[5] Y. Yoneada, T. Horiuchi, *Rev. in Sci. Instrum*., 42, **1971**, 1069.

[6] L. G. Parratt, *Phys. Rev.,* 95, **1954**, 359.

[7] E. Amaldi, R. Bizzarri, G. Pizzella, *Fisica Generale*, Vol. 2, (Zanichelli Editore), **1991**.

[8] R. M. Richardson, S. J. Roser, *Liquid Crystals,* 2 (6), **1987**, 797-814.

[9] M. Born, E. Wolf, *Principles of Optics*, (Oxford: Pergamon), **1970**.

[10] M. J. grundy, R. M. Richardson, S. J. Roser, J. Penfold, R. C. Ward, *Thin Solid Films,* 159, **1988**, 43-52.

[11] J. Penfold, R. K. Thomas, *J. Phys.: Condens. Matter,* 2, **1990**, 1369.

[12] L. Ljaer, J. Als-Nielsen, L. A. Helm, P. Tippman, H. Mohwald, *J. Phys. Chem.,* 93, **1989**, 3200.

[13] J. B. Hayter, H. A. Mook, *J. appl. Cryst.,* 22, **1989**, 35.

[14] J. Lekner, *Theory of Reflection,* Nijhoff Publ.: Dordrechet, The Netherlans, **1987**.

[15] W. E. Wallace, W. L. Wu, *Appl. Phys. Lett.,*67 (8), **1995**, 1203.

[16] B. Lengeler, M. Huppauff, J. Fresenius, *Anal. Chem.*, 36, **1993**, 155-161.

[17] D. K. G. De Boer, A. J. G. Leenaers, W. van den Hoogenhof, *X-ray Spectrometry*, 24 (3), **1995**, 91.

[18] X. L. Zhou and S. H. Chen, *Physics Reports*, 257, **1995,** 223.

[19] L. G. Parratt, *Phys. Rev.,* 95, **1954**, 359.

[20] P. Beckmann, A. Spizzichino, *The scattering of Electromagnetic Waves From Rough Surfaces,* (Pergamon, N.Y.), **1963**.

[21] H. Kiessig, *Ann. Phys.* 10, **1931**, 769-788.

[22] H. Zabel, *Appl. Phys. A*, 58, **1995**, 159.

[23] L. Névot, *Acta Electronica*, 24 (3), **1981/1982**, 255-265.

[24] S. K. Sinha, Z. B. Sirota, S. Garoff, H. B. Stanley, *Phys. Rev. B,* 38, **1988**, 2297-2311.

[25] J. Penfold, R. K. Thomas, *J. Phys.: Condens. Matter,* 2, **1990**, 1369.

[26] L. Névot, P. Croce, *R. Phys. Appl.,* 15, **1980**, 761-779.

[27] S. J. Roser, R. Felici, A. Eaglesham, *Langmuir*, 10, **1994**, 3853.

[28] J.C. Malaurant, H. Duval, J.P. Chauvineau, O. Hainaut, A. Raynal, P. Dhez, *Optics Comm.*, 173, **2000**, 255-263.

[29] B. C. Giessen, G. E. Gordon, *Science*, 159, **1968**, 973.

[30] J. M. Prober, J. Schultz, *Appl. Crystallogr.*, 8, **1975**, 405.

[31] T. Egami, *J. Mater. Sci.,*13, **1978**, 2587.

[32] K. Nishikawa, T. Iijima, *Bull. Chem. Soc. Japan,* 57, **1984**, 1750.

[33] B. Paci, A. Generosi, V. Rossi Albertini, E. Agostinelli, G. Varvaro, D. Fiorani, *Chem. Mater.* 16, **2004**, 292-298.

[34] R. Caminti, V. Rossi Albertini, *Int. Rev. Phys. Chem.,* 18 (2), **1999**, 26.

[35] E. Chason, M. Chason, *J. Vac. Sci. Technol. A*, 12(4), **1994**, 1565.

[36] K. Orita, T. Morimura, T. Horiuchi, K. Matsushige, *Synt. Met.*, 91, **1997**, 155-158.

[37] A. Plech, U. Klemradt, H. Metzger, J. Peisl, *J. Phys: Condens. Matter*, 10, **1998**, 971-982.

[38] J. Mio Bertolo, A. Bearzotti, A. Generosi, L. Palummo, V. Rossi Albertini, *Sensors and Actuators B,*111-112, **2005**, 145-149.

[39] B. Paci, A. Generosi, V. Rossi Albertini, P. Perfetti, R. de Bettignies, M. Firon, J. Leroy, C. Sentein, *Applied Physics Letters,* 87 (1), **2005**.

Chapter 3

3.1 Experimental Apparatus

3.1.1 Introduction

A critical operation in the construction of a sensor is the physical deposition of the phthalocyanine film onto the electronic substrate. If a series of sensing films (with reproducible electronic characteristics and vapour response) are to be produced the growth conditions, influencing morphology, uniformity and thickness must be controlled [1].

3.1.2 Physical Evaporation Systems

The deposition of the sensing films is generally carried out in a vacuum or low-pressure plasma environment. “A vacuum” is defined as an environment where the air pressure is much lower than the ambient atmospheric pressure, while a plasma is a gaseous environment where there are enough free ions and electrons to assure an appreciable electrical conductivity. Generally, these definitions are referred to processes in which atoms or molecules are deposited “one at a time”, such as in physical vapour deposition (PVD) or low-pressure chemical vapour deposition (LPCVD) processes. They can also be applied to other deposition processes such as low-pressure plasma spraying (LPPS).

The deposition processing in vacuum, increases the "mean free path" for collisions of atoms and high-energy ions and helps reduce gaseous contamination to an acceptable level. When establishing a plasma in a vacuum, the gas pressure plays an important role in the enthalpy, the density of charged and uncharged particles and the energy distribution of particles in the plasma. A plasma in a "good vacuum" provides a source of ions and electrons that can be accelerated to high energies in an electric field. In PVD processing, these high-energy ions can be used to sputter a surface, as a source of deposition material and/or bombard a growing film to modify its properties. Ion bombardment effects can also be found in LPCVD. The plasma may also be used to "activate" reactive gases and vapours in reactive deposition processes and to fragment the chemical vapour precursors in plasma-enhanced chemical vapour deposition (PECVD).

PVD: Physical vapour deposition processes are methods where material vaporized from a solid or liquid source is transported as a vapour through a vacuum or low-pressure gaseous or plasma environment. When the vapour get in contact with a substrate, it condenses. The vaporized material may be an element, alloy or compound. Some PVD processes can be used to deposit films of compound materials (reactive deposition) by the reaction of depositing material with the gas in the deposition environment (e.g., TiN) or with a co-depositing material, such as TiPc or even a combination of the two.

Typically, PVD processes are used to deposit films with thicknesses in the range of a few nanometres to thousands of nanometres; however, they can be used to form multilayer coatings, thick deposits and free-standing structures.

Vacuum evaporation: Vacuum evaporation (including sublimation) is a PVD process where material from a thermal vaporization source reaches the substrate "without collision" with gas molecules in the space between the source and substrate. The trajectory of the vaporized material is "line-of-sight." Typically, vacuum evaporation takes place in a gas pressure range of 10^{-5} to 10^{-9} Torr, depending on the level of contamination that can be tolerated in the deposited film. For an appreciable deposition rate to be attained, the material vaporized must reach a temperature where its vapour pressure is 10 mTorr or higher. Typical vaporization sources are resistively heated stranded wires, boats or crucibles (for vaporization temperatures below 1,500° C) or high-energy electron beams that are focused over the surface of the source material (any temperature).

Advantages of vacuum evaporation:

- High-purity films can be deposited from high-purity source material.
- Source of material to be vaporized may be a solid in any form and purity.
- The line-of-sight trajectory and "limited-area sources" allow the use of masks to define areas of deposition on the substrate and shutters between the source and substrate to prevent deposition when not desired.
- Deposition rate monitoring and control are relatively easy.
- It is the least expensive of the PVD processes.

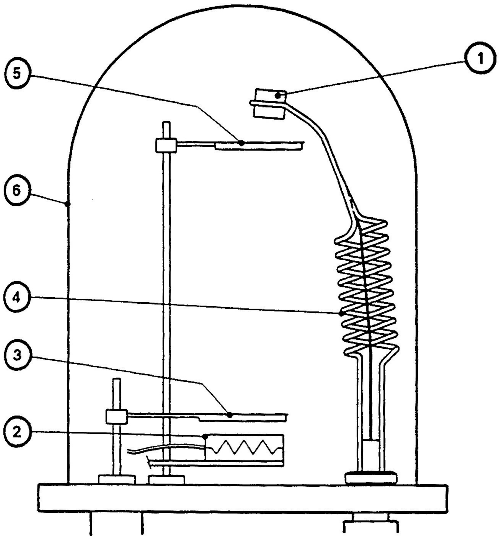

Figure 1. Schematic sketch of the sublimation apparatus. The most important parts are the: 1. Crystal head, 2. Source, 3. Source shutter, 4. Water cooled crystal holder, 5. Source shutter, 6. Bell jar.

Vacuum sublimation is usually used for depositing most un-substituted phthalocyanine compounds and is performed heating a small quantity of purified material at temperatures ranging from 300° to 500°C.

All films examined in this paper, were obtained by PVD vacuum sublimation according to the standard procedure [2]. Briefly, an Edwards Auto 306 vacuum coater, figure 1, with diffusion pumping system was used to prepare the phthalocyanine films on different substrates and the growth was observed by an Edwards FTM5 film thickness monitor, measuring the change in the resonance frequency of a quartz crystal balance [3].

The morphology of the phthalocyanine films is variable and strongly affected by the sublimation conditions: it ranges from amorphous [4] to highly crystalline [5]. Furthermore, the particular conditions by which a deposition is conducted may have a pronounced effect on the response to vapours since film morphologies are dependent on these conditions. In order to control these parameters the Energy Dispersive X-ray reflectometry (EDXR) was used.

3.1.3 Energy Dispersive X-ray Reflectometer

All reflectometry measurements were performed by a non-commercial [6] Energy Dispersive machine at the EDXR-group laboratories, Dipartimento di Chimica, Università di Roma La Sapienza and at the X-ray laboratory, I.S.M., C.N.R., Area della ricerca di Tor Vergata, Roma.

From a geometrical point of view, the energy dispersive (ED) reflectometer (figure 2) is similar to a conventional angular dispersive (AD) one: the main differences concern the detection and the absence of monochromator [7].

Another difference is about the arms motion since, although both in AD and ED the arms have to be rotated around the sample, the rotation plays a different role in the two cases. Indeed, while in AD it is carried out during data collection (the rotation angle being independent variable), in ED the rotation is executed prior to the measurement. Therefore, in the latter case, it can be regarded as an instrumental parameter like the arms lengths or the setup values of the spectroscopy amplifier.

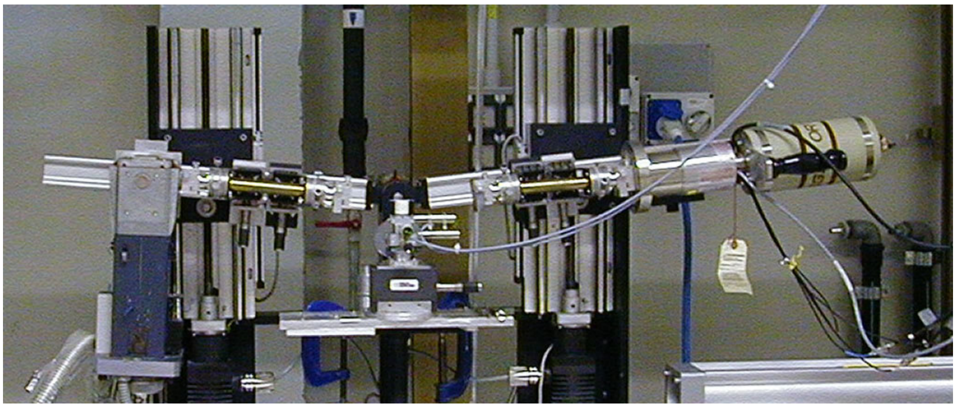

Figure 2. Sketch of the energy dispersive X-ray Reflectometer. The fundamental components are as follows: (1) X-ray source (W anode tube), (2) collimation slits, (3) sample holder, and (4) Ge single crystal energy-sensitive detector.

The instrument is mechanically very simple [8], with two arms contained in the vertical plane, pivoting around a single central axis. The arms are moved by two linear actuators driven by step motors and the tangent of the inclination angle is read by two linear encoders. Both the minimum step movement and the resolution of the encoders are 1μm, leading to a minimum angle increment and reproducibility of $(4\text{x}10^{-4})°$ [9].

An ordinary X-ray source [10] can be used as the radiation source, and in figure 3, the typical spectrum produced by a hot cathode W tube (Philips, model PW 2214/20) is shown: the tungsten L fluorescence lines and the continuous Bremmstrahlung hunch (white beam) can be recognized.

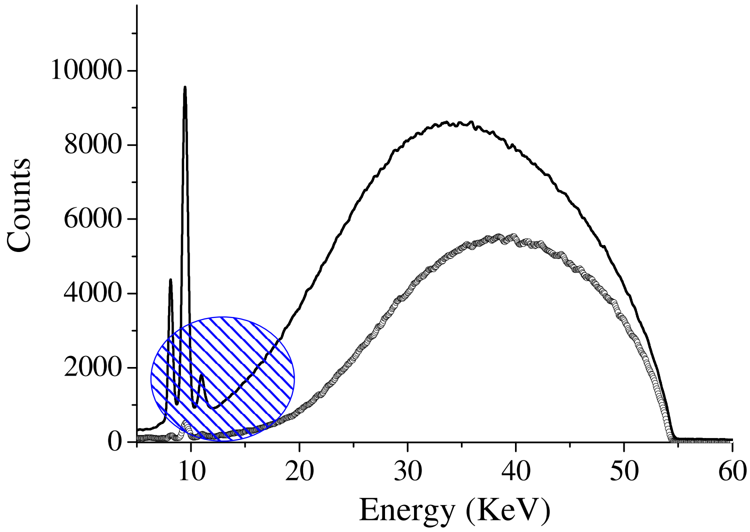

Figure 3. Two spectra produced by a conventional W anode X-ray source are shown. The black pattern is collected without any filter, while the dotted one is collected with an Al 2mm filter. The blue circle enhances the energy range which is filtered by the presence of the Al lamina.

The first are produced by the de-excitation of tungsten atoms when ionized by the fast electrons beam impinging the target. On the contrary, the white beam is not a quantized phenomenon: it is due to a deceleration of the same electrons in the electrostatic field present in the tungsten crystalline lattice. This deceleration produces the emission of radiation, according to classical electro dynamical laws [11].

Since this phenomenon depends on non quantized variables, the energy of the emitted radiation ranges from zero (the electron motion is not disturbed) to the whole kinetic energy of the electrons (the electrons are completely stopped by a single interaction).

In the angular Dispersive mode, the white beam must be removed from the primary beam or, at least, reduced as much as possible by filtering or by monochromatization.

In contrast, in the Energy Dispersive mode, all the energy components must reach the sample and then be collected by the detector. In ED the fluorescence do not disturb the measurement and, hence, do not represent a problem [12]. This X-ray optical path is defined by four variable collimation slits (2 mm W) mounted on the arms, which reduce the angular divergence of the beam.

The X-ray detection is accomplished by an EG&G Solid State Detector (SSD) whose sensitive part is a semiconducting high purity germanium single crystal. This crystal is doped by another suitable element (lithium) in order to create a p-n junction inside it and make it behave like a diode that, in working conditions, is directly polarized by applying a high voltage at its sides.

When a photon of a certain energy penetrates the crystal and is absorbed, many different mechanisms of excitation are activated in the Ge lattice. Nevertheless, the final result is a redistribution of the energy from the higher-energy excitations to the lowest-energy excitations, i.e. the electron-hole pair formation. The external voltage pushes the components of each pair in opposite directions, producing their separation. Therefore, the charge drift along the crystal, until they reach the ohmic contacts, where a current pulse can be detected.

The integral over time of this pulse gives the total charge, that is the number of electron- hole pairs. Since this number is directly proportional to the energy of the absorbed photon, the intensity vs energy graph can be plot. The SSD is connected via ADACAM hardware to a personal computer running a Maestro software to visualize and record the data through a multi-channel analyzer. This device can be schematically represented as a frequency histogram with the horizontal axis, divided into discrete intervals, corresponding to the energy. The average value of energy in each interval is a linear function of the index of that interval. In this way a digital reconstruction of the energy spectrum of the scattered radiation is accomplished.

The energy resolution is ca. 1.5% with a maximum counting rate of 10 kcounts/s.

References

[1] A. D’Amico, *Sensors for Domestic Applications*, Proceedings of the 1st European School of Sensors (by Italy European School on Sensors **1994** Lecce).

[2] R. Caminiti, A. Capobianchi, P. Marovino, A. M. Paoletti, G. Pennesi, G. Rossi, *Thin Solid Films*, 382, **2001**, 74.

[3] R. D. Gould, *Thin Solid Films*, 125, **1985**, 63.

[4] F. W. Karasek, J. C. Decius, *J. Am. Chem. Soc.,*74, **1952**, 4716.

[5] M. Assida, N. Uyeda, E. Suito, *J. Cryst. Growth,* 8, **1971**, 45.

[6] R. Caminiti, C. Sadun, V. Rossi Albertini, F. Cilloco, Patent No. 01261484, Italy, **1993**.

[7] R. Caminti, V. Rossi Albertini, *Int. Rev. Phys. Chem.*, 18 (2), **1999**, 263-299.

[8] R. Caminiti, C. Sadun, V. Rossi Albertini, F. Cilloco, R. Felici, *Proceedings of the 25th National Congress of POhysical Chemistry*, Cagliari, Italy 17-21 June, **1991**.

[9] R. Felici, *The Rigaku Journal,* 12 (1), **1995**, 11-17.

[10] K. Nishikawa, T. Iijima, *Bull. chem. Soc. Japan,* 57, **1984**, 1750.

[11] R.W. James, *The optical principles of the Diffraction of X-rays,* Woolbridge, Connecticut: Ox-Bow Press, p. 464,**1982**.

[12] B. Paci, A. Generosi, V. Rossi Albertini, E. Agostinelli, G. Varvaro. *J. Of Magnetism and Magnetic Materials* 272-276 (2004), E873-E874.

Chapter 4

4.1 Bis (phthalocyaninato)titanium (IV): [Ti(Pc)$_2$]

4.1.1 Introduction

Metal phthalocyanines have been intensively investigated as molecular electrical conductors or semiconductors [1-4]. Among the various species examinated, sandwich-like bis(phthalocyaninato)metal complexes of formula M(Pc)$_2$ (M = Sn [5,6], a lanthanide or an actinide [7,8]) include the well known intrinsic semiconductor Lu(Pc)$_2$ [9], and generally acquire semiconducting properties when doped with electron acceptors or donors.
Until the last decade, no examples of bis(phthalocyaninato)metal complexes in which the sandwiched atom was a first row transition series metal where known [10]. Later on the Bis (phthalocyaninato)titanium (IV): [Ti(Pc)$_2$], was synthesized [11] and its peculiar properties were studied.

4.1.2 Structure

Ti(Pc)$_2$ structure is shown in figure 1.
It consists of a sandwich-type molecule stapled by two inter-ligand C-C σ bonds between the two macrocyclic rings [10].

This is the most peculiar feature of this structure and it is unique to the present since there are no examples of such inter ligand connection within the molecule for similar sandwiched systems of formula $M(Pc)_2$ [12,13] or porphirin complexes $M(L)_2$, where L is the porphirin dianion [14].

Certainly, the stapled form of the two phthalocyaninato groups in [TiL] must be the combined result of the small ionic radius of Ti^{IV} and its strong Lewis acidity.

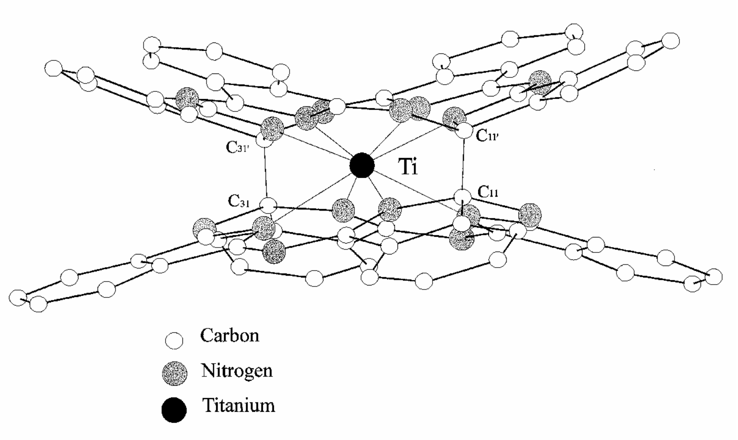

Figure 1. The structure of a $TiPc_2$ unit is shown. The central Ti atom coordinates two phthalocyanine units connected to each other via *C-C* single bonds.

The inter ligand bond distances are just a little longer than expected for normal C-C σ bonds [15]. Each of the C(11), C(11'), C(31) and C(31') atoms forms four σ bonds, thus partially breaking the π-electron delocalization otherwise fully extended on each of the two macrocyclic rings.

This particular X-ray crystal structure confirms the unusual yellow-orange colour of the $Ti(Pc)_2$, different from colours observed for 'normal' phthalocyanine systems (purple, green or blue in the crystalline state).

4.1.3 Properties as NO_2 transducer

The $[Ti(Pc)_2]$ metal complex shows a very good sensitivity toward NO_2 detection [16] and its modifications after exposure to this gas have been investigated [17]. Moreover its reversibility has been proven and finally this material has been patented [18] as a transducer for NO_2 detection [19].

Furthermore, despite this material is an insulator, ($\sigma < 10^{-12}\ \Omega^{-1}\ cm^{-1}$), it is worth remembering that the detection of a gas corresponds to a conductivity change between two different states, and it is the value of this change (D) that should be big enough to be detected.

From data reported in literature, it can be deduced that in the case of monomeric phthalocyanines the D value is large enough for the detection, but their use as sensors is limited by the response time and the poor durability of the materials.

On the other hand, when intrinsic semi conducting phthalocyanines were used as gas detector, the conductivity variation is less important in magnitude but impurities play a role not very significant [20].

In the case of titanium bis-phthalocyaninato sandwich, which is purely insulating when undoped, the effect on NO_2 on the electrical conductivity is higher in magnitude if compared with that obtained by $LuPc_2$ and the effect of oxygen (air) is negligible (an essential requirement in order to use the material as air pollutant sensing device).

Like other diphthalocyanines, the system also exhibits changes in optical absorption and this property makes it advantageous for likely incorporation of this material into optical devices as well. Indeed, this compound is characterized by three well defined absorption bands in the visible region (λ = 506, 675 and 720 nm) which undergo spectral changes in the presence of nitrogen dioxide.

Furthermore, as a result of exposure to NO_2, the charge carriers generated by the gas interaction are well identified as two chemical species (each one characterized by different conductivity and colour) which are in equilibrium during the process, as follows:

$$Ti(Pc)_2 + NO_2 \leftrightarrow (Ti(Pc)_2^{+}\ NO_2^{-})$$

$$(Ti(Pc)_2^{+}\ NO_2^{-}) + NO_2 \leftrightarrow [(Ti(Pc)_2)^{++}\ 2NO_2^{--}]$$

The kinetics associated with these equilibriums are completely different, since the first one is much faster than the second.

As visible from the redox equations, in this system the presence of NO_2 gas produces two oxidised species, monocation and bication, responsible for the conductivity increase. Despite both species are present at the maximum of the conductivity value, the hypothesis that the monocationic species is the only one responsible for the conduction process, was validated [17].

In conclusion, the main features of Bis (phthalocyaninato)titanium (IV) as NO_2 sensing material, can be summarized as follows:

- High selectivity of $Ti(Pc)_2$ in regards to NO_2.
- No interference coming from SO_2, CO, ambient air, and NH_3.
- Perfectly reversible when UV treated: no fade of the physical or chemical properties.
- $[NO_2]$ = 1ppm detection limit.

Because of these properties and of the possibility of co-working with the research group that patented this material as a sensor, the $Ti(Pc)_2$ represents a very good starting point in order to approach the NO_2-film interaction from a morphological point of view.

4.2 Ex-situ EDXR measurements

4.2.1 NO_2 – $TiPc_2$ interaction: preliminary test

At first, a set of $TiPc_2$ thin films of different nominal thicknesses was deposited on Si <111> substrates. The substrate was chosen, among others (Mica, Ge, Au, etc.), for various reasons:

- It can be considered as atomically flat when processing the reflectivity data, i.e. its surface roughness is neglected ($Q_{Si} = 1$).
- The density contrast between the Si substrate and the phthalocyanine films is good, which implies a high amplitude of the Kiessing Fringes in the reflectivity patterns.
- Low cost.
- Easy to cut to obtain adequate (in shape and size) substrates.

A series of different reflectivity measurements was performed in order to find the best experimental conditions and the most convenient instrumental setup.

The energy range was chosen between 10 and 55keV, thus covering the widest possible q-range and the reflection angle between 0.080° and 0.150° degrees. With these conditions MPc films between 15nm and 200nm can be accurately measured and the morphological parameters can be deduced by the Parratt fitting equation.

4.2.2 NO_2 – $TiPc_2$ interaction: a systematic study

A set of films of different nominal thicknesses (20-150 nm) were grown and studied by EDXR in order to characterize their morphological properties as deposited. Of course the "nominal" thickness measured on line by a quartz balance during the vacuum deposition, gives only an approximate value of the actual thickness, while its precise value is determined by EDXR. Nevertheless, the samples under study will be identified by their approximate nominal thickness, i.e. an integer number, for the sake of clarity and simplicity rather than by their actual thickness value.

As previously discussed, these films are patented as NO_2 detectors, since their electronic behaviour undergoes drastic changes when the $TiPc_2$ gets in contact with the oxidizing gas. In order to investigate if this electrical response may be related to a morphological and structural one, the films underwent an NO_2 500 sccm gas flow (NO_2 100ppm in air) treatment for several hours and, then, were replaced back into the X-ray reflectometer and re-measured.

This is the typical example of ex-situ measurements: the experimental conditions are reproduced (X-ray beam energy, slits aperture, scattering angle, etc.) but, after the removed sample is placed back, the uncertainties on its position, on the scattering volume, on the reflecting portion of the sample, could be considerable, and this may induce relevant errors. However, this repositioning error does not influence the thickness value obtained by the fit. Indeed fact, various test measurements were performed repositioning samples which had been removed from the experimental chamber after an initial measurement. The fitting procedure always reconfirmed the thickness value obtained previously within an uncertainty of ± 1 Å.

This is because the oscillation frequency is almost insensitive to the setup once the angle is defined. Instead, the fringes resolution and the slope of the reflectivity curve are strongly affected by the correct reproduction of the experimental conditions and the surface roughness is directly dependent on such two parameters. Therefore in order to make a correct interpretation of the reflectivity data, the roughness values are not quantitatively considered when ex-situ measurements are performed.

For this reason, we may be confident that the curve shift witness a real change in the morphology due to the gas exposure (figure 2). This happens regardless the initial thickness thus indicating a general trend for the morphological evolution.

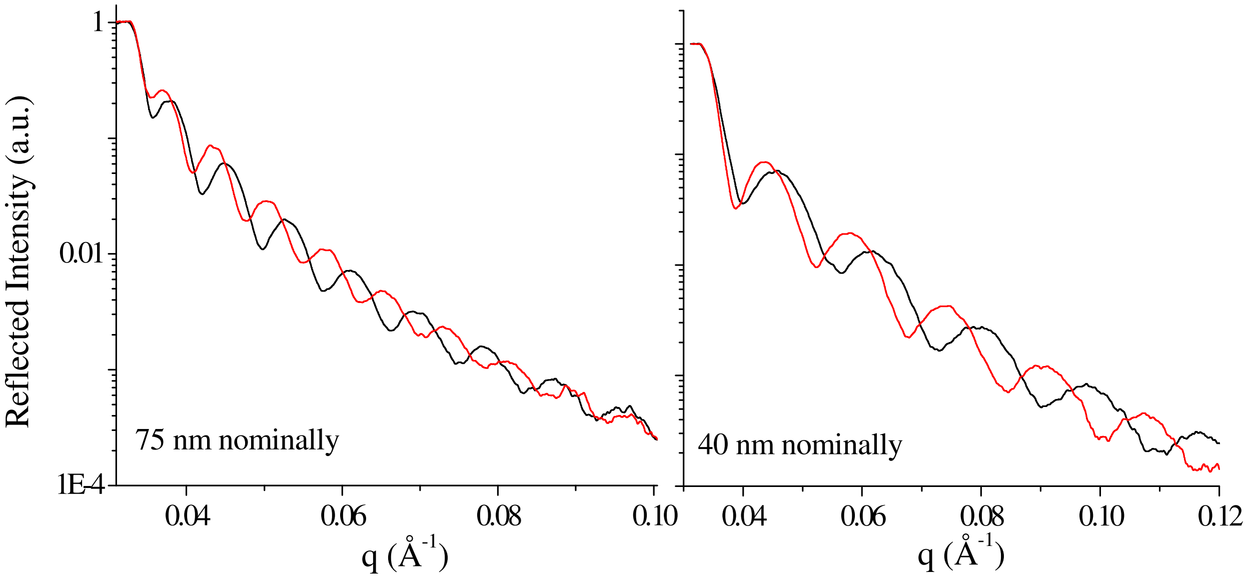

Figure 2. The reflectivity patterns of a 75 and 40 nm nominally thick $TiPc_2$ films before (black line) and after (red line) the exposure to a 50sccm NO_2 gas flow are shown. The oscillating fringes are visibly more frequent after the gas exposure: the films have grown thicker.

A first result was plotting the final thickness d_2, namely after exposure to gas, against the initial one d_1, both obtained by X-ray reflectivity data processing.

The overall increase of the thickness of each film turned out to be proportional to its initial value, as can be seen in figure 3, where all the points plotted lie on a straight line crossing the axis origin, the linear regression $y = a + bx$, fitting the points being:

$$y = (1.080 \pm 0.007)\, x + (0.090 \pm 0.450)$$

This indicates a "breathing like" behaviour of the film in presence of the gas, much like the thermal expansion of a metal heated to a temperature higher than the initial. However these first considerations are limited by the fact that, in ex-situ measurements, the surface roughness can not be accounted quantitatively and the time evolution of this swelling can be described only phenomenologically.

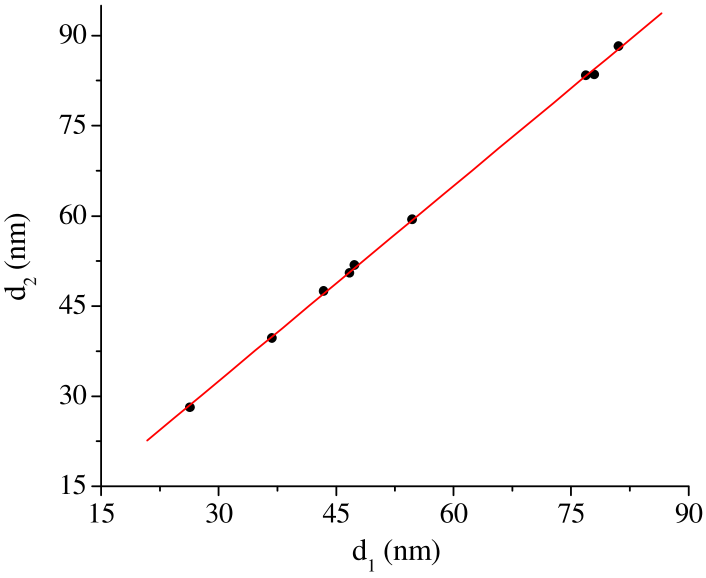

Figure 3. The final thickness versus the initial thickness for all the films studied is shown. The red line is the linear function fitting the points.

In order to study the real time evolution of the gas-film interaction and thus describing morphological change quantitatively, further EDXR measurements in the in in-situ time resolved mode are required.

4.3 In-situ EDXR measurements

4.3.1 Experimental setup and considerations

In order to perform the in situ X-ray reflectivity measurements on thin gas sensing films operating at room temperature and at ambient pressure, an experimental chamber was designed and realized as shown in figure 4.
The chamber is made of a single block of aluminium, the block sides crossed by the beam are thinner so that in the selected energy range (10-55keV) the radiation is not remarkably damped by absorption effects.

An in-situ time resolved experiment consists of collecting a certain number of reflectivity spectra over a number of hours (to be determined), the acquisition time being the same for each spectrum. During this collection, the instruments geometry has to remain unchanged. As a consequence the overall mechanical stability is of crucial importance.

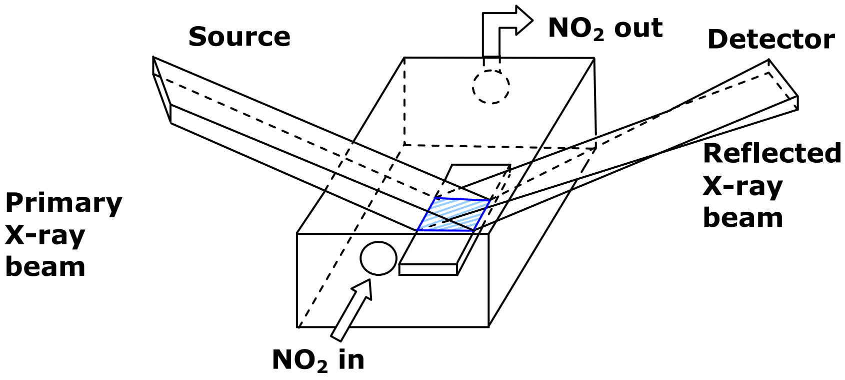

Figure 4. Schematic sketch of the experimental chamber.

For this reason, various preliminary stability tests were performed to check the immobility of the experimental chamber on its holder and of the sample in the experimental chamber itself.

In figure 5 (a) an example of these stability tests is shown. A 32 nm nominally thick $TiPc_2$ film was placed in the chamber and a sequence of reflectivity patterns was collected for 4 days at the rate of a pattern each half an hour. No artefact resulting in an apparent morphological change was noticed as visible also by naked eye looking at the figure: no phase shift or change in the slope of the reflectivity patterns takes place in the observation time.

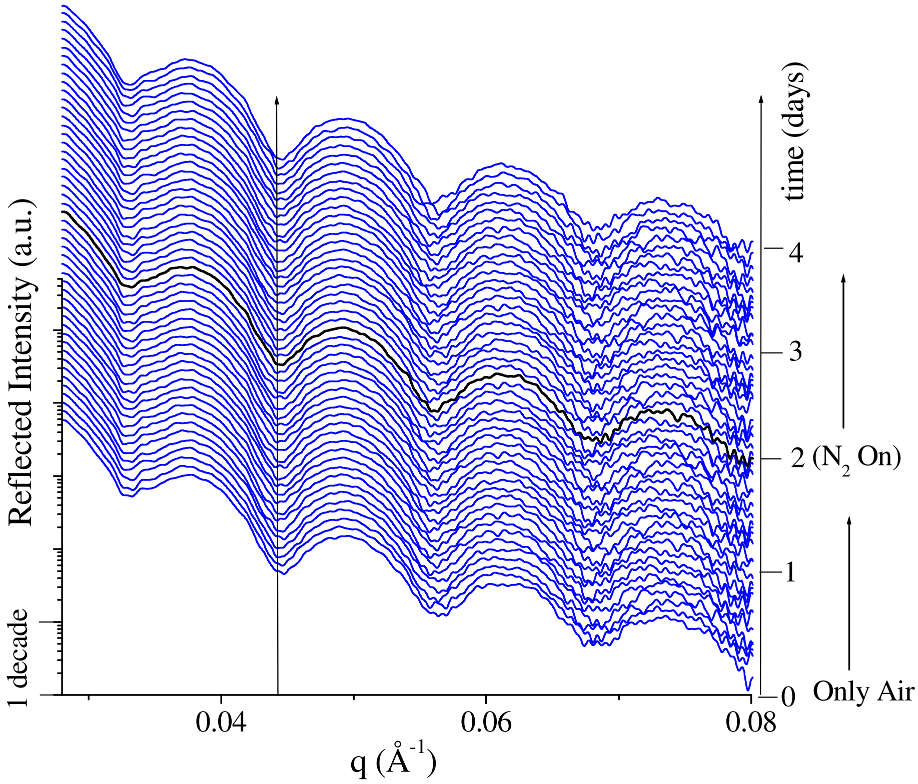

Figure 5. *Sequence of reflectivity patterns collected every 30 minutes in air (first two days) and in N_2 gas atmosphere (for another two days), respectively. The arrow connecting the minima of the first oscillation underlines that no phase shift has taken place.*

Moreover, an N_2 180nmol/esc. gas stream was fluxed into the chamber and analogous test was made for another 2 days, proving the stability of the setup in presence of a gas.

The spectra were collected in the same experimental conditions and are plotted in figure 5 (b) as a sequence together with the patterns previously collected Furthermore no morphological interaction occurs between the $TiPc_2$ film and the N_2 molecules, as expected, since the reflectivity patterns are perfectly reproducing the spectra collected in air. So N_2 was chosen to be the drift stream in the further coming experiments, being an inert gas towards $TiPc_2$ films from a morphological point of view.

Moreover, the determination of the most suitable experimental conditions to perform in situ measurements was made during the preliminary tests: beam energy = 55keV; scattering angles ranging from 0.070° to 0.150° depending on the films thicknesses; collimation slides shape: square; slides apertures ranging from 20μm*20μm to 100μm*100μm.

Besides these mechanical choices, the duration of each reflectivity pattern collection is to be made considering two competing factors:

- Decreasing the acquisition time, the resolution of the d and σ temporal curves improves, since the sampling frequency increases.

- The signal to noise ratio gets worse and, as a consequence, increase the uncertainty on the d and σ values as obtained by the curves fit.

These two different factors have to be well balanced every time an in situ time resolved X-ray reflectometry measurement has to be performed.

4.3.2 NO_2 – $TiPc_2$ interaction: a systematic study

In order to monitor the overall characteristics of the film-gas interaction process, a first cycle of time resolved EDXR investigations were performed submitting a series of samples (of different nominal thickness ranging from 27 to 120 nm) to a flux ϕ of 20nmoles/sec of NO_2 (concentration = 50ppm) in an N_2 stream (180nmoles/sec).

As an example of the results obtained, in figure 6, the EDXR spectra collected in-situ in the case of a film having a nominal thickness of 80nm are reported.

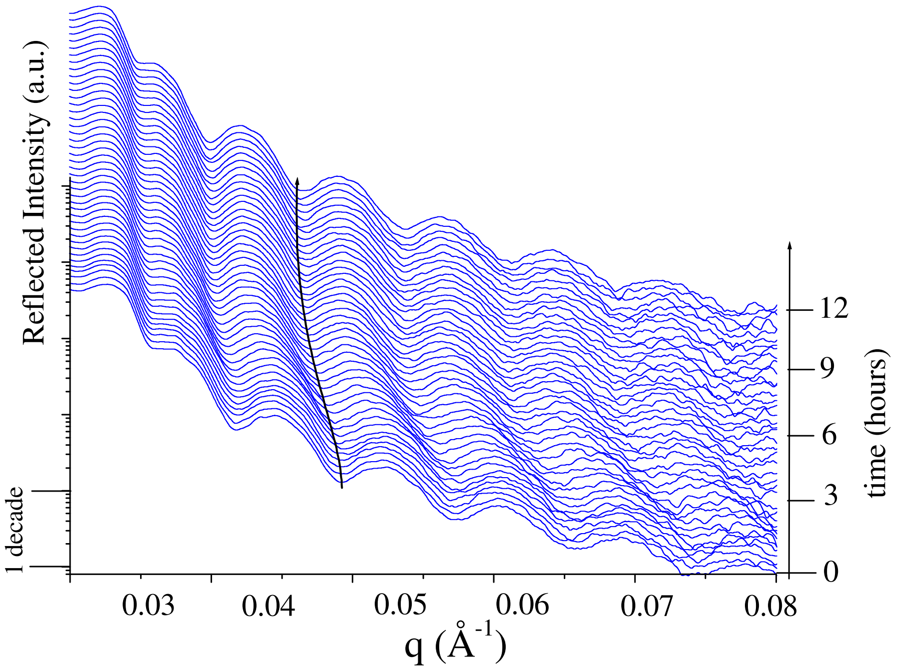

Figure 6. *Sequences of time-resolved EDXR spectra for a 80nm $TiPc_2$ film exposed to an NO_2 gas flux of 20nmol/sec. The arrow connecting the minima of the second oscillation evidences the phase shift.*

The change in the period of oscillations and in their damping are related to the variation of film thickness d and of its roughness σ, respectively. The progressive compression of the curves (evident by observing the line connecting the minima of the second oscillation), indicates an increase in the films thickness.

However, the change of σ is difficult to detect by naked eye, and can only be revealed by a proper fit of the reflection patterns.

After these preliminary observations, a more accurate calculation of the change occurring in the two morphological parameters upon gas exposure was made analyzing the sequences of spectra relative to the various films, according to Parratt's theory for X-ray reflectivity.

The shape of the thickness vs time curves [d(t)] are similar for all the samples in study, and as an example, the d and t curves obtained by processing the spectra in figure 6, are plotted in figure 7a.

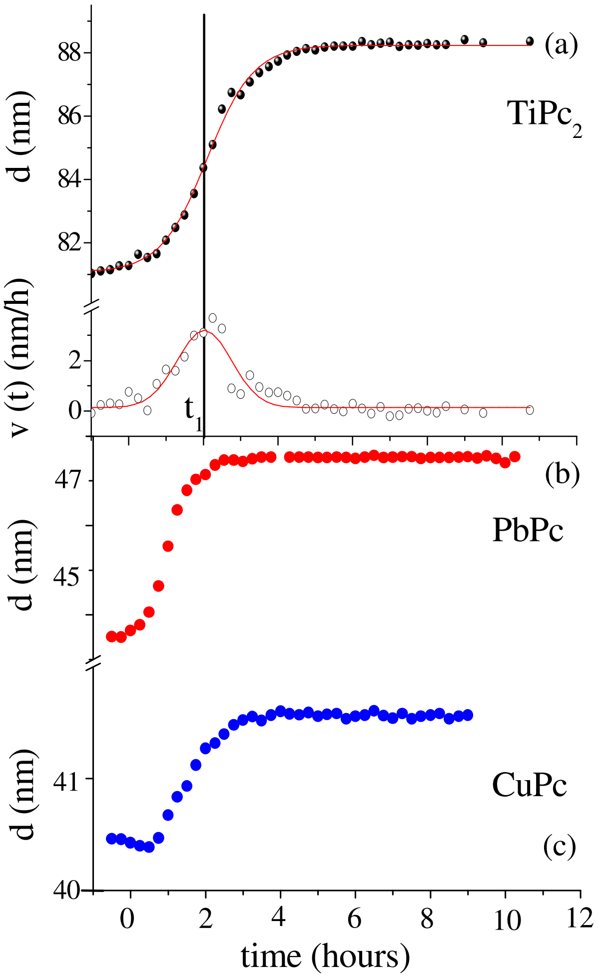

Figure 7. a)The thickness time evolution of an 80 nm nominally thick $TiPc_2$ film is shown with its derivative. The process is well fitted by a Boltzmann growth.
In b) and c) the same time evolution is shown in case of a PbPc and a CuPc film respectively. The kinetic evolution of the thickness are similar in all cases.

As expected, the former curve has a profile similar to that of the line in figure 6, which is well fitted by a simple Boltzmann growth. The "breathing like" process accounting for the d(t) trend, previously hypothesized by the ex-situ measurements, can be easily interpreted considering the d(t) derivative, namely the film growth speed v(t).

As the gas starts flowing in the cell, the film bulk response is not immediate: at the beginning the d(t) profiles remains almost flat, so that v(t) is small (induction time of about 1hour). Then v(t) starts increasing rapidly, until it reaches a maximum value. In the following stage, the process slows down and, finally, v(t) approaches zero, indicating that the film thickening has concluded.

This film expansion, as expected, is similar to that observed in other gas sensing Metal-Phthalocyanine (MPc) films when exposed to the same pollutant, and can be related once more to the bulk diffusion process.

As shown in figure 7b and 7c, when MPcs with M= Cu and Pb are considered, the thickness expansion follows the same kinetic behaviour, despite the different metal involved and the different film packing characteristics [21-23].

However, the roughness evolution of the same $TiPc_2$ film (figure 8a), shows a completely different behaviour with respect to the other MPc considered (figure 8b and 8c).

Indeed, the surface response usually consists of a monotonic increase of roughness during the first part of the exposure to the gas, followed by a plateau, when the saturation is reached, as can be seen in figure 8b and c, where the two $\sigma(t)$ curves relative to the PbPc and the CuPc film are reported for comparison. While the latter follow a Boltzmann-like trend, the $Ti(Pc)_2$ $\sigma(t)$ curve exhibits a peak, i.e. after a normal initial rise, it reaches a maximum value and, then, begins to decrease until a final constant value is reached. This is comparable with the initial value or only slightly higher.

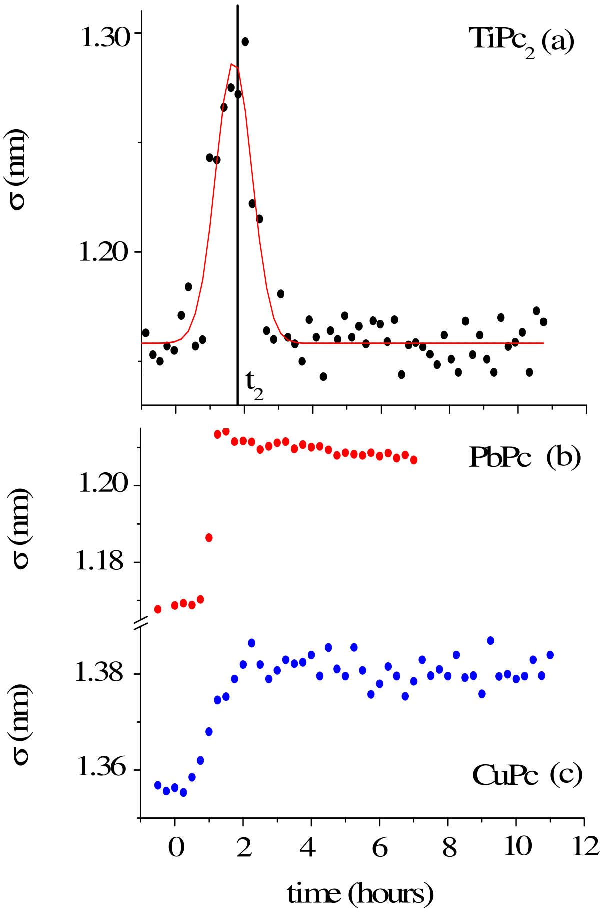

Figure 8. a) Time dependence of the Ti(Pc)$_2$ film roughness thickness σ obtained by analysing the EDXR spectra recorded in real time. Roughness curves obtained for a PbPc and a CuPc film are shown in b) and c) respectively. They both show a step growth until a plateau is reached, the final value being considerably higher than the initial value.

Observing figure 8a, it is evident that the time t_2 at which the surface roughness reaches its maximum value coincides with the time t_1 of maximum growth speed: t_1 = 1.75 (± 0.25) hours and t_2 = 2.00 (± 0.25) hours.

The same roughness evolution upon gas exposure, described above, is reproduced systematically by all the Ti(Pc)$_2$ samples studied.

Furthermore, the coincidence of t_1 and t_2 mentioned above was demonstrated to be a general characteristic of the Ti(Pc)$_2$ films upon NO$_2$ gas exposure, i.e. the time t_2 at which the surface roughness is maximum always coincides with the time t_1 of the growth maximum speed, within the error bar.

Two different explanations, both consistent with this anomalous appearance of a peak in the $\sigma(t)$ curves of Ti(Pc)$_2$, may be proposed:

1. the first is the attribution of such behaviour to a thermodynamic effect.

2. the second is the attribution to a kinetic effect.

1. In the case of a thermodynamic effect, the $\sigma(t)$ peak would represent the transformation from an initial arrangement of the layer formed by the NO$_2$ – Ti(Pc)$_2$ molecules interacting at the film surface to a final arrangement, passing through an intermediate phase.

In this case, the transformation might be described as a transition from the original structure of the film surface, consisting of a progressive increase of the roughness due to the appearance of a new surface structure represented by a NO$_2$ -Ti(Pc)$_2$ layer, up to a threshold value. After this value, the layer relaxes to a second phase, which exhibits a roughness comparable with that of the original film surface.

2. Alternatively, a kinetic explanation can be provided assuming that the interaction layer does not possess a well defined geometric structure but represents only the molecules statistical occupancy of the receptive sites at the film surface. In this case, the increase of $\sigma(t)$ (left side of the peak) would correspond to the random deposition of an increasing number of gas molecules that, by interacting with the film surface, form a disordered inter-phase layer to which the increase of roughness can be attributed.

Since the penetration inside the film (diffusion) takes a certain time, the "crowding" of the molecules at the surface augments progressively. Indeed, in agreement with previous observations of an induction time required for the film to display its sensor properties [17], a certain delay between the beginning of the exposure and the response of the film (see figure 7a) is observed. Therefore, in this kinetic model, the "crowding" of the molecules on the surface must reach a critical concentration before the diffusion can occur, which implies a progressive increase of roughness. When the diffusion mechanism becomes effective, the molecules penetrate inside the film, whose thickness rapidly increases.

As a consequence, the surface layer goes back to its equilibrium conditions and the roughness returns, approximate to its initial value.

In the former case (thermodynamic effect), the $\sigma(t)$ peak height should not be influenced by the deposition rate of the molecules, i.e. the gas flux, as long as the quasi-equilibrium conditions are preserved. On the contrary, in the latter case (kinetic effect), the "crowding" should be a function of the deposition rate, since the more intense ϕ is, the more rapid the increase of σ (t) should be and, as a consequence, the higher the σ (t) peak.

4.3.3 $TiPc_2$ films vs. different NO_2 concentrations

A systematic analysis of the $TiPc_2$ thin films response towards different NO_2 concentrations was performed in order to evaluate morphological response of the sensing material when a certain NO_2 concentration range is taken into account.

In order to establish which of two hypotheses related to the anomalous behaviour of these films roughness applies, in situ time resolved EDXR measurement(s), taken while submitting the gas sensing films to NO_2 gas fluxes of increasing intensities, were carried out.

An example of the results is reported in figure 9, where the EDXR spectra collected during the exposure of a 91 nm $TiPc_2$ film to a gas flux of

30nmol/sec are shown (graph analogous to that of figure 6). In this case, the higher concentration of NO_2 gas molecules produces a decrease in the response time of the film, as expected.

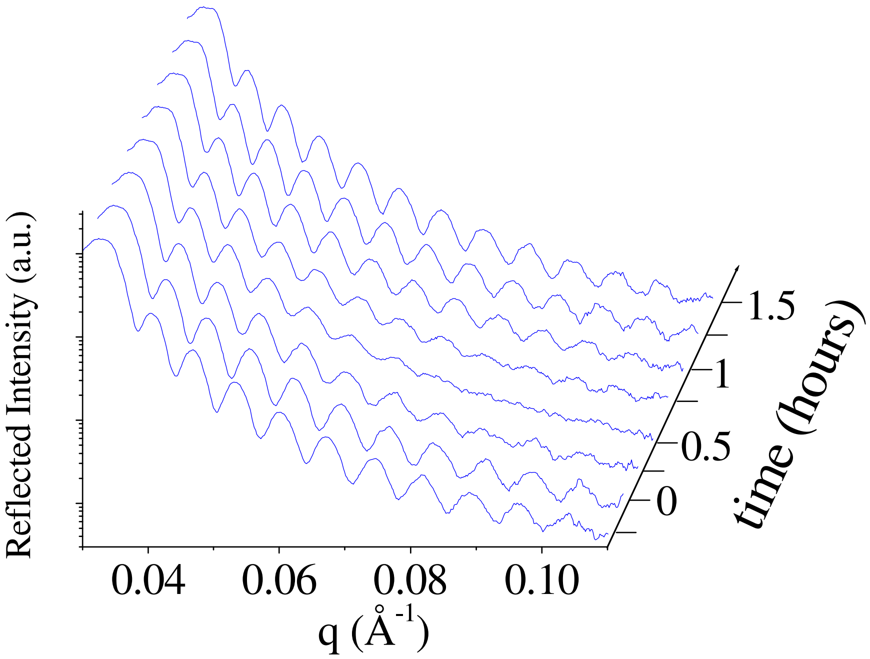

Figure 9. Sequences of time resolved EDXR spectra for a 91 nm thick $TiPc_2$ film exposed to an NO_2 gas flux of 30nmol/sec.

It is evident that the 4th spectrum showed in figure 9, recorded after 30 minutes from the gas aperture, is characterized by a much larger damping of the oscillations (i.e. much larger surface roughness of the film) with respect to both the first and the last ones shown in the figure.

Indeed, when the flux is as high as 30nmol/sec, the change in the film roughness upon gas exposure is so dramatic that the $\sigma(t)$ trend can be predicted just looking at the raw EDXR patterns, despite the fact that normally this parameter can only be calculated by data processing.

Therefore in the above example, the σ vs t curve obtained by analysing this sequence of spectra (line with triangles in figure 10a) will exhibit a maximum in correspondence with the spectrum recorded after 30 min.

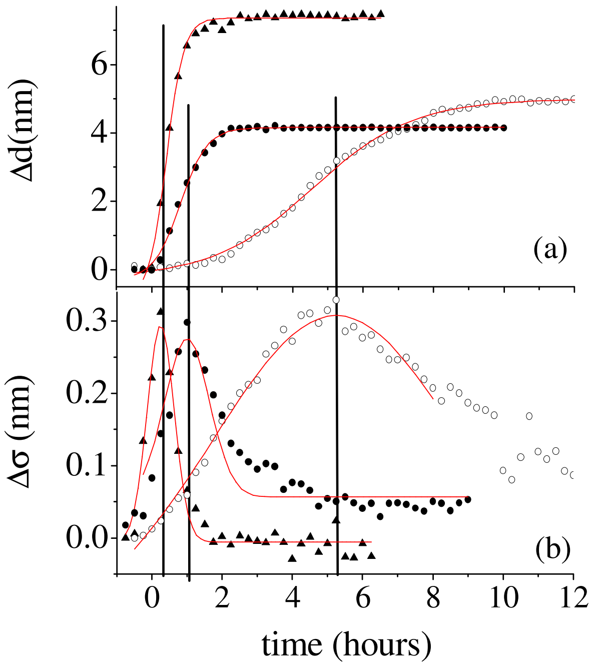

Figure 10. a) Comparison of the relative variation of the Ti(Pc)$_2$ film thickness over time: 91nm film exposed to a gas flux ϕ = 30nmol/sec (triangle), 57nm film exposed to a gas flux ϕ = 20nmol/sec (circle) and 71nm film exposed to a gas flux ϕ = 10nmol/sec (open circle).
b) The relative variation of the Ti(Pc)$_2$ layer roughness over time for the same films as in figure a.

In figure 10a, a selection of curves (films 91, 57 and 71 nm thick), describing the relative increase in thicknesses, [$\Delta d(t)=d(t)-d_1$], are shown. The data points obtained for a gas flux ϕ =30, 20 and 10 nmol/sec, respectively, are plotted.

The characteristic times of the two processes are shorter for higher concentrations, both for the thicknesses and the roughness variations, being associated to the different gas diffusion times.

In figure 10b, the relative roughness variation [i.e. the $\Delta\sigma$ (t)= $\sigma(t)-\sigma_I$ curves, where σ_I is the initial value the $\sigma(t)$ curve] of the same films are reported. As expected, when the gas flux intensity ϕ increases, the position of the maximum of the $\Delta\sigma(t)$ curves shifts to lower time values.

Of great importance is the fact that the maximum value reached by the $\Delta\sigma$ vs t curves is about the same. On the other hand, the $\Delta\sigma(t)$ peak height is independent of the gas molecules deposition rate, which indicates that the phenomena responsible for the anomalous behaviour of the films surface roughness is, indeed, a thermodynamic effect.

The results can therefore be interpreted as a surface morphological rearrangement of the $Ti(Pc)_2$ films.

At this point a last doubt may arise. The previous measurements were carried out at various concentrations of NO_2. However, such concentrations might be too elevated from the sensor's response point of view. Indeed the sample holder is a closed experimental chamber saturated by the gas mixture at the given concentration, but this situation may not be reliable with the true working conditions of the sensor in which the polluting gas should be a trace to detect in air. To confirm that the results not dominated by such saturation effects, due to the excessive abundance of stimulating agent, further measurements were performed by exposing the films to a 20 nmoles/s NO_2 flux and to a pure N_2 flux alternatively.

Moreover, in the case of a kinetic crowding effect of the NO_2 gas flux, the observed roughness behavior would take place only during the exposure of the film to the gas flux containing NO_2 molecules and relax under pure N_2 flux.

Figure 11 shows that this is not the case: in figure 11a the film, submitted to NO_2 gas, exhibits, as expected, the same thickness and roughness evolution observed previously.

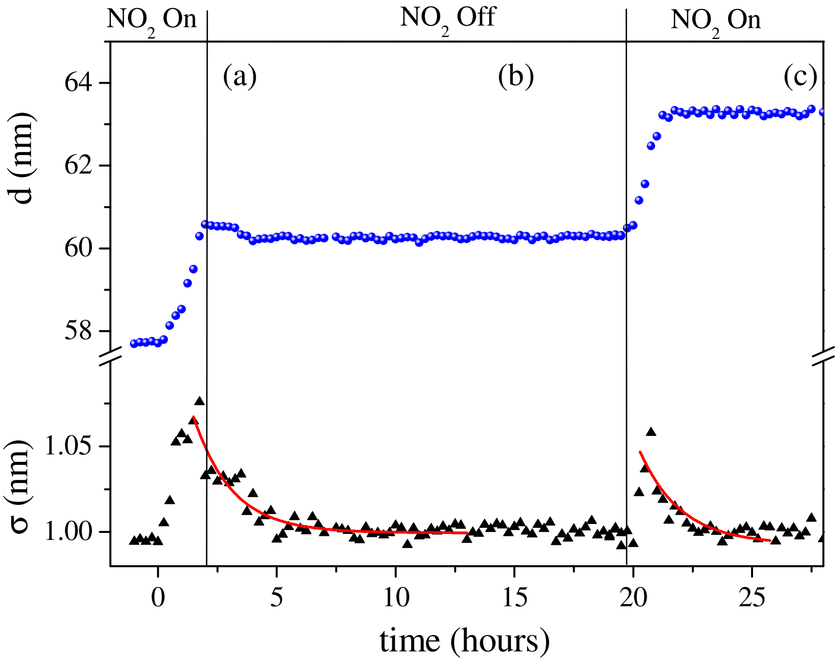

Figure 11. Time dependence of the $Ti(Pc)_2$ film thickness d and the roughness σ, during the exposition of the film alternatively to NO_2/ N_2 (a, c) and N_2 only (b) gas fluxes.

Then, before the gas absorption process is completed, the NO_2 gas flux is interrupted, and the film is exposed to the flux of N_2 gas only (figure 11b): the film thickness decrease [24] is almost negligible, while its roughness does not return to the original value instantaneously but reaches its equilibrium value only after the washing action of the N_2 is completed. The whole reset process takes about 3 hours (similarly to what observed in the previous case).

However, since the gas absorption process was not completed, when the NO_2 is fluxed again on the film (figure 11c), the film thickness and roughness evolution restart until their conclusion.

It must be stressed that the roughness, after having reached its maximum, decreases following the same trend both when the gas flux contains NO_2 molecules and when it is formed by N_2 molecules only. This shows that, after the critical roughness is reached, the exposure to further NO_2 molecules is irrelevant to the evolution of the process.

In summary, the results of this first systematic EDXR study [25] showed that:

- during exposure to NO_2 gas molecules, the $Ti(Pc)_2$ film thickness increases, following a Boltzmann growth, as also observed in other Metal-Pc. This indicates that the film undergoes a "breathing like" expansion as the gas diffuses inside the bulk.

- the response of the surface roughness showed an unexpected anomalous behavior. A second sequence of EDXR measurements, submitting the samples to different gas fluxes, allowed the attribution of this effect to a re-arrangement of the layer formed by the NO_2 – $Ti(Pc)_2$ molecules interacting at the film surface, passing through an intermediate phase characterized by an increased roughness.

This study provides experimental evidence for the use of EDXR technique as a valuable tool to monitor the gas sensing behaviour of thin $TiPc_2$ films from a morphological point of view. It claries by the in-situ time resolved method, the kinetic evolution of the film's morphology. Moreover, it allows to observe a surface phase rearrangement in these gas sensing films, induced by the interaction with NO_2 molecules.

4.3.4 $TiPc_2$ thin films: sensors reversibility and second cycle performances

In order to test this material as a gas sensor (from a morphological point of view), the restore conditions must still be evaluated. In fact, the EDXR has proved the $TiPc_2$ films sensitivity towards NO_2 and the detection limits at different concentrations of the pollutant: the morphology response reproduces the results already known by conductivity measurements, and is able to add information about the gas-film interaction.

The only information still to verify is whether the morphology recovers, when the sensing device is restored, or if the columnar stacking of the $TiPc_2$ is irreversibly modified by the diffusion process, and so is the morphology.
It is well known that the introduction of an inert gas or the evacuation of gas under vacuum (10^{-2} Torr) at room temperature, are used to restore the staring material. Treatment under vacuum at 100-130°C gives the same result in a few minutes (15min.) [26]. The whole redox $TiPc_2$-NO_2 interaction is reversible and the oxidation process can be driven back also by light (Hg emitting lamp).

A series of $TiPc_2$ films were exposed to an NO_2 gas flux of 20nmol/sec, in the same experimental conditions as described previously. These films were then (ex-situ), by the following reset procedures:

- 130° at 10^{-2} Torr for 30 minutes (figure 12a)
- 200° at $^{-2}$ Torr for 30 minutes (figure 12b).
- Hg lamp at RT for 15 minutes (figure 12c).

The films were placed back into the experimental chamber and EDXR spectra were collected. In figure 12 a,b and c, the reflectivity patterns of a 50nm, 60 nm and 65 nm nominally thick $TiPc_2$ films are shown. The black line represents the pattern of the film as deposited, the blue is relative to the film morphology after the NO_2 interaction and the reflectivity spectra collected ex situ after the different restore processes is plotted in red.

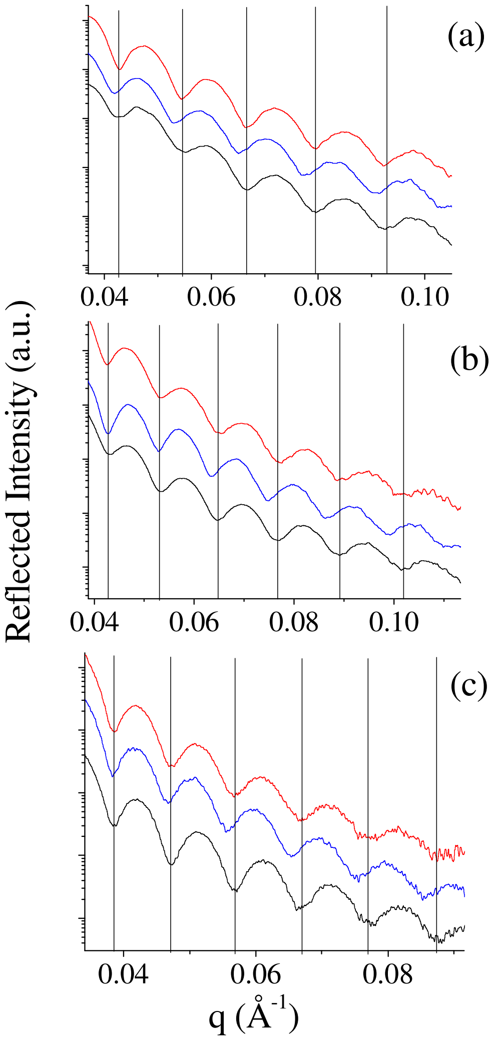

Figure 12. The reflectivity patterns of a $TiPc_2$ film before (black line) and after (blue line) the exposure to an NO_2 50ppm gas flux are compared to the spectra (red line) obtained after a 130°C (a), a 200°C (b) and an Hg light (c) treatment respectively. The grid lines connecting the minima of the first and the last spectra, show that the morphological reset has taken place.

Whenever the thermal treatments (130°C or 200°C) or the Hg lamp exposure are used as reset methods, the related oscillations of the EDXR patterns are in phase with those of the as deposited spectrum, collected before the gas exposure. Indeed, as expected, the reflectivity spectra after the exposure to the NO_2 are visibly de-phased if compared to the first and the restored pattern.

Therefore, the films returned to their original thickness as a consequence of heating at the different temperatures, and of the Hg lamp light exposure, as confirmed by the fitting procedure. The same behaviour was observed for all samples studied, showing that the chemical reversibility of the sensor is related to the recovery of the initial film thickness, i.e. the morphology restoration.

However, a remark must be done. When heated at temperatures as high as 200°C, which are very close to the evaporation limit of the material, the initial thickness is recovered, but the film roughness increases strongly. Indeed, this temperature likely induces the onset surface melt, thus changing the surface roughness when the film is cooled down.

It is now necessary to investigate if this morphological recovery is connected to a functional recovery of the sensing material or if the sensing performances are worsened by such treatments. In order to prove the morphological efficiency of the thin $TiPc_2$ films, the performances during a second cycle of NO_2 treatment, were monitored. The results, as expected, confirms the morphological efficiency of the sensing films.

4.4 Combined conductivity and EDXR measurements

Finally, in order to correlate the morphological behaviour to the electrical response of the $TiPc_2$ films when exposed to an NO_2 gas flux, in situ time resolved EDXR measurement were combined to the standard conductivity measurements.

To perform the measurements jointly, the $TiPc_2$ films were grown upon interdigitate Au electrodes, previously deposited on Si <111>, and shown in figure 13.

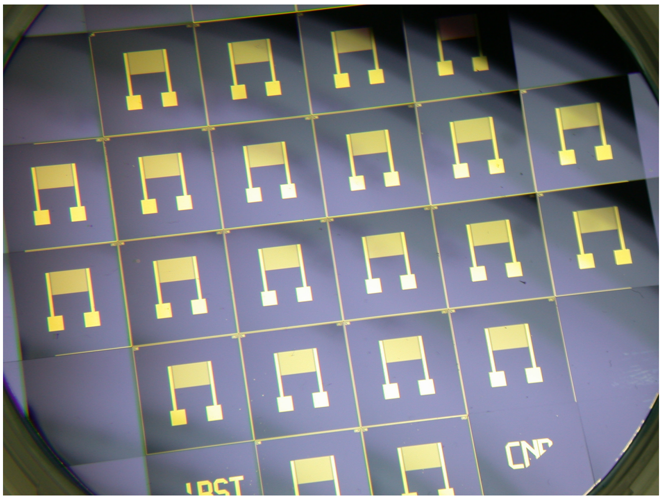

Figure 13. *Series of interdigitated Au electrodes deposited upon a Si wafer.*

As discussed above, concerning Ti-phthalocyanines in general, this is an insulating material expected to become semiconducting when interacting with NO_2. At first a 2 contact measurement was performed, applying a voltage to the thin film and monitoring the current intensity changes occurring as a function of the duration of the gas exposure. The experimental conditions (voltage = 0.8 V, NO_2 concentration = 50ppm) were chosen as suggested by literature in order to have a first comparison with previously published data.

After this preliminary measurements, the combined EDXR and conductivity measurements were performed.

In figure 14 the thickness evolution (a) of a 60nm nominally thick $TiPc_2$ film, is plotted as a function of time together with its current intensity change (c). The film was exposed to the NO_2 gas (50ppm, 20 nmol/sec in 180nmol/sec N_2) to activate the chemical redox process. The diffusion process of the gas into the bulk of the film is fitted by the usual sigmoidal curve having a characteristic time of t_c = 0.80 hours as is evident by its derivative (figure 14 b).

Indeed, the conductivity peak, corresponding to the formation of the monocation species ($(Ti(Pc)_2^+ NO_2^-)$), coincides with the maximum velocity of the diffusion process. As the redox reaction goes on, the equilibrium is shifted towards the second process and the dicationic species $[(Ti(Pc)_2)^{++} 2NO_2^{--}]$, not as conductive as the monocationic, coexist with the latter inducing a decrease in the intensity until the saturation is reached.

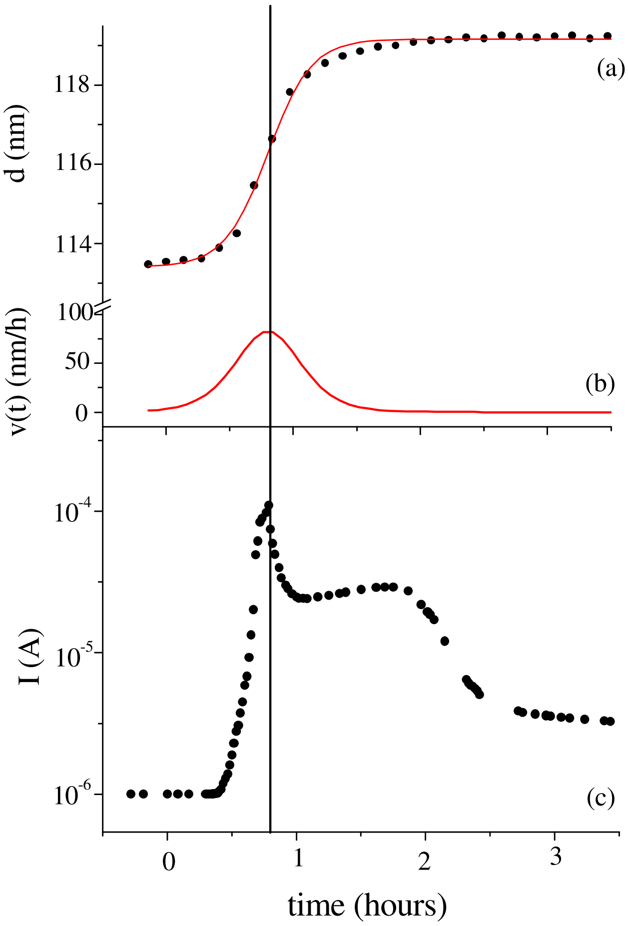

Figure 14. (a) Evolution of the parameter d of an 110nm nominally thick $TiPc_2$ film as a function of time when exposed to an NO_2 50ppm gas flux. (b) The derivative of d vs t is plotted. (c) Evolution of the current intensity as a function of time as in figure (a).
Both processes are characterized by the same characteristic time.

The second maxima of the conductivity pattern corresponds to the dynamic electrical equilibrium taking place between the two cationic phthalocyanine species. This corresponds to the saturation of the diffusion process of the gas molecules into the bulk. Finally, when the conduction sites are saturated too (slightly later than the morphological saturation) the conductivity decreases and reaches a plateau some units above its starting value.

In order to deepen the electrical investigation, the NO_2 stream was interrupted and only N_2 was fluxed upon the sample when the morphology had saturated. The removal of NO_2 from the experimental chamber, shifts the overall redox equilibrium back to the previous equilibrium value: indeed the monocathionic specie ($Ti(Pc)_2^+$ NO_2^-) get more numerous thus increasing the conductivity, see figure 15. In this way, a second conductivity maximum is reached followed by a very slow decrease of the conductivity since the charge carriers start to disappear.

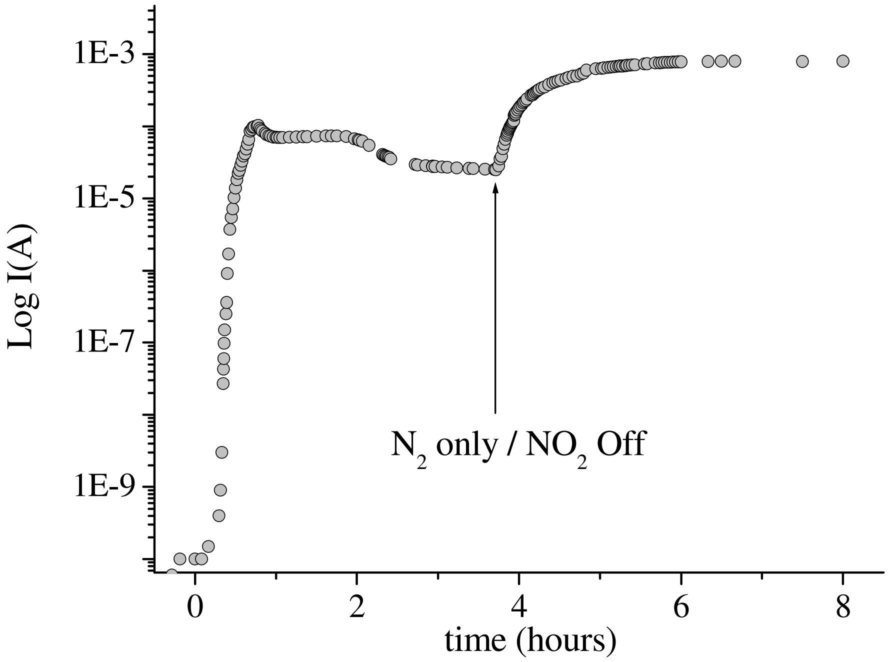

Figure 15. The conductivity variation of a 50 nm thick $TiPc_2$ film as a function of the duration of the exposure to an NO_2 (20 nmol/s) and an N_2 (180 nmol/s) gas flux respectively, is plotted.

References

[1] J. R. Ferraro, J. M. Williams, *Introduction to Synthetic Electrical Conductors,* Academic Press, Florida, **1987**, p. 219.

[2] M. Y. Ogawa, J. Martinsen, S. M. Palmer, J. L. Stanton, J. Tanaka, R. L. Green, B. M. Hoffman, J. A. Ibers, *J. Am. Chem. Soc.,* 109, **1987**, 1115.

[3] T. Inabe, J. G. Gaudiello, M. K. Moguel, J. W. Lyding, R. L. Burton, W. J. McCarthy, C. R. Kannewurf, T. J. Marks, *J. Am. Chem. Soc.,* 108, **1986**, 7595.

[4] M. Hanack, U. Keppeler, H.-J. Schulze, *Synth. Met.,* 20, **1987**, 347.

[5] W. J. Kroenke, M. E. Kenney, *Inorg. Chem.*, 3, **1964**, 251.

[6] W. E. Bennett, D. E. Broberg, N. C. Beazinger, *Inorg. Chem.*, 12, **1973**, 930.

[7] C. Clarisse, M. T. Riou, *Inorg. Chim. Acta*, 130, **1987**, 139.

[8] R. Guilard, A. Dormond, M. Belkalem, J. E. Anderson, Y. H. Liu, K. M. Kadish, *Inorg. Chem.*, 26, **1987**, 1410.

[9] M. Maitrot, G. Guillaud, B. Boudjema, J.-J. André, H. Strzelecka, J. Simon, R. Even, *Chem. Phys. Lett.*, 133, **1987**, 59.

[10] C. Ercolani, A. M. Paoletti, G. Pennesi, G. Rossi, A. Chiesi-Villa, C. Rizzoli, *J. Chem. Soc. Dalton Trans.*, **1990**, 1971-1977.

[11] V. L. Goedken, G. Dessy, C. Ercolani, V. Fares, L. Gastaldi, *Inorg. Chem.*, 24, **1985**, 991.

[12] K. Kasuga, M. Tsutsui, R. C. Petterson, K. Tatsumi, N. Van Opdenbosh, G. Pepe, E. F. Meyer jr, *J. Am. Chem. Soc.*, 102, **1980**, 4836.

[13] A. De Cian, M. Moussavi, J. Fisher, R. Weiss, *Inorg. Chem.*, 24, **1985**, 3162.

[14] J. W. Buchler, B. Scharbert, *J. Am. Chem. Soc.*, 110, **1988**, 4272.

[15] F. H. Allen, O. Kennard, D. G: Watson, L. Brammer, A. G. Orpen, R. Taylor, *J. Chem. Soc., Perkin Trans.,* 2, **1987**, S1.

[16] A. Capobianchi, A. M. Paoletti, G. Pennesi, G. Rossi, S. Panero,

Synth. Metals, 75, **1995**, 37-42.

[17] A. Capobianchi, A. M. Paoletti, G. Pennesi, G. Rossi, *Sens. Actuators B,* 48, **1998**, 333-338.

[18] A. Capobianchi, A. M. Paoletti, G. Pennesi, G. Rossi, *Italian Patent* No. RM 2000 A 0000 28.

[19] F. Baldini, A. Capobianchi, A. Falai, G. Pennesi, *Sens. Actuators B,* 51, **1998**, 176-180.

[20] M. Tromoter, R. Even, J. Simon, A. Dubon, J. Y. Laval, J. P. Germain, C. Maleysson, A. Pauly, H. Robert, *Sens. Actuators B,* 8, **1992**, 129.

[21] T. V. Basova, E.K. Kol'tsov, I.K. Igumenov, *Sensors and Act. B*, 105, **2005**, 259-265.

[22] J.C. Hsieh, C.J. Liu, Y.H. Ju, *Thin Solid Films*, 322, **1998**, 98-103.

[23] Y.-L. Lang, W.-C. Tsai, J.-R. Maa, *Appl. Surf. Sci.,* 173, **2001**, 352-361.

[24] Y.H. Ju, C. Hsieh, C.J. Liu, *Thin Solid Films*, 342, **1999**, 238.

[25] A. Generosi, B. Paci, V. Rossi, Albertini, P. Perfetti, G. Rossi, A. Capobianchi, A.M. Paoletti, G. Pennesi, R. Caminiti, *Appl. Phys. Lett.*, 87 (1), **2005**.

[26] S.-R. Kim, S.-A. Choi, J.-D. Kim, K.H. Choi, S.K. Park, Y.H. Chang, *Synth. Met.,* 71, **1995**, 2293-2294.

Chapter 5

5.1 Ruthenium Phthalocyanine: $(RuPc)_2$

5.1.1 Introduction

Exploration of the synthesis, chemical properties, and reactivity of ruthenium phthalocyanine derivatives appears not to have been so far adequately extended [1-3], especially if compared with that of some first transition series metal phthalocyanines [4]. Recently some more details have been reported [5,6] because of its interesting structural and chemical peculiarities, and this material was selected to carry out morphological investigations in the view of possible use in gas sensing devices. In fact, while undoped phthalocyanine are insulating materials ($\sigma < 10^{-12}\ \Omega^{-1}\ cm^{-1}$), the ruthenium phthalocyanine is an intrinsic semiconductor [7].

5.1.2 Synthesis

The $(RuPc)_2$ complex was obtained by removal of DMSO from the adduct $[PcRu\ (DMSO)_2 \bullet 2DMSO]$ [7,8] by heating at 330°C and 10^{-2} mmHg [9]. As obtained, $(RuPc)_2$ shows only traces of C, H and N. However, all the samples examined, even if freshly prepared, show a certain content of oxygen (1.0-1.5%), probably due to contaminants released during the drastic elimination of DMSO.

This procedure results in the formation of an amorphous solid material, whose detailed description follows in the next section. However, in order to prove that such material is always formed (with the same properties), regardless the nature of the adduct used, samples of $(RuPc)_2$ can be prepared from the bis(quinoline) and bis(pyridine) [10].

Indeed, $[PcRu(quinoline)_2]$ and $[PcRu(pyridine)]_2$ were recently reported to be also appropriate precursors of the ruthenium phthalocyanine. The powders obtained from these N-base adducts consist all of the same material and the aggregates are indistinguishable from those prepared from the DMSO adduct, as proved by X-ray data, IR and UV-visible spectra, magnetic behaviour and electrical conductivity properties.

5.1.3 Structure and properties

X-ray diffraction analysis has shown that ruthenium phthlocyanine, obtained as an amorphous material from the adduct $[PcRu(DMSO)_2] \bullet 2DMSO$, is dimeric: $(RuPc)_2$, as shown in figure 1.

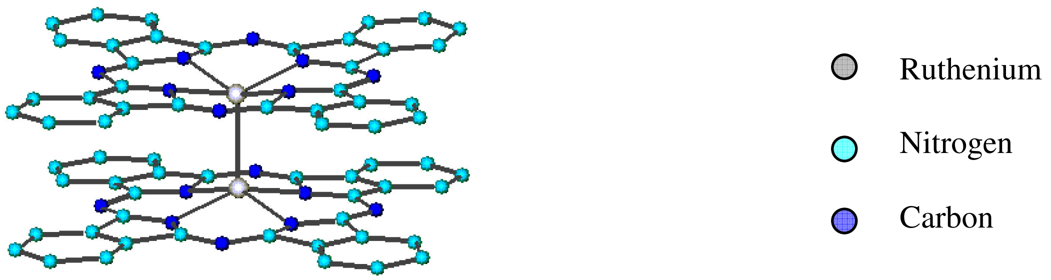

Figure 1. Sketch of the dimeric $(RuPc)_2$ adduct. The Ru atoms are bound to each other with a double σ,π bond and coordinating two phthalocyanine rings.

Recently, the solid state structure was shown to consist of dimeric units, $(RuPc)_2$, held together by a direct Ru-Ru bond (2.40 Å) and linearly chained to give an aggregate of formula $[(RuPc)_2]_n$ (average n =6), with the examers disorderly arranged in the solid amorphous material [11], see figure 1. The couple of Ru atoms (d^{12}) within the dimer was assigned the electronic structure $\sigma^2\pi^4\delta^2\delta^{*2}\pi^{*2}$ (in the Molecular Orbital approach) perfectly coherent with the presence of a clean Ru (II) = Ru (II) double bond.

Moreover, the semiconducting properties ($\sigma_{RT} = 1 \times 10^{-5}\ \Omega^{-1}\ cm^{-1}$) of the material could be attributed to the $\pi-\pi$ interaction between adjacent macrocycles within the stacked assemblies formed by the dimeric units. By now, participation of the Ru centres has been excluded on the basis of the "internal" location within the dimer of the strongly interacting Ru couples and of the long interdimer Ru-Ru contacts (4.32 Å).

Furthermore, in case of proving good properties as nitrogen dioxide detector, this material would be processed as thin film, so the more important information are related to the study of this aggregation state rather than of the precursor powder.

Fortunately, X-ray studies have recently been reported [5,6,12] characterizing the ruthenium phthalocyanine film structure; in particular the Energy Dispersive mode was successfully applied on this amorphous material. These diffraction data indicated that, in the passage from the bulk to the film, the dimeric structure of the compound was maintained, the only change being the different length of columnar packing of dimeric molecules, more wide ranging in the film than in the bulk material.

Indeed, 10 dimers were in columned along the stacking direction (parallel to the Ru = Ru bonds), whereas six units were found in the bulk material.

The higher order observed was also supported by conductivity measurements [5], the arrangement in a one-dimensional stacking being responsible for the improvement of the electrical properties: $\sigma_{RT} = 1 \times 10^{-4}\ \Omega^{-1}\ cm^{-1}$, one order of magnitude better than in the powder $(RuPc)_2$.

Furthermore, this material has shown such a strong reactivity towards small molecules, like nitrogen dioxide, to raise the doubt that the metal may be somewhat interacting. Indeed, it has been found that UV- visible spectra registered during the interaction of the $(RuPc)_2$ film with NO_2, clearly indicated the formation of new species with characteristic spectral features.

However the $(RuPc)_2$ film-NO_2 gas interaction is still very unclear: the reaction mechanism is not known, the role of the metal and of the macrocycle in the oxidation process is not completely clarified.

In order to achieve these physical-chemical information and to deepen the study of the sensing characteristics of the $(RuPc)_2$ films, the same morphological approach, previously discussed for the $Ti(Pc)_2$, was adopted.

5.2 Ex-situ EDXR measurements

5.2.1 NO_2 – $(RuPc)_2$ interaction: preliminary test

At first, a set of $(RuPc)_2$ thin films of different nominal thicknesses was deposited, as mentioned above, on Si <111> substrates.

The films were deposited choosing a "nominal" thickness range between 200 Å and 1500 Å, the first being the lowest thickness required in order to obtain a reflectivity pattern with a sufficient number of fringes to fit, i.e. to deduce the morphological parameters d and σ accurately, the latter being close to the resolution threshold, i.e. the limit to detect the single fringes separated and not merged together, as previously described in the section devoted to $TiPc_2$.

A first set of reflectivity measurements was performed and in figure 2 the reflectivity profiles (dots) of five samples (chosen as an example) are shown in semilog. graphs, together with their Parratt fits (line). The so obtained values of thickness and roughness are reported in table 1.

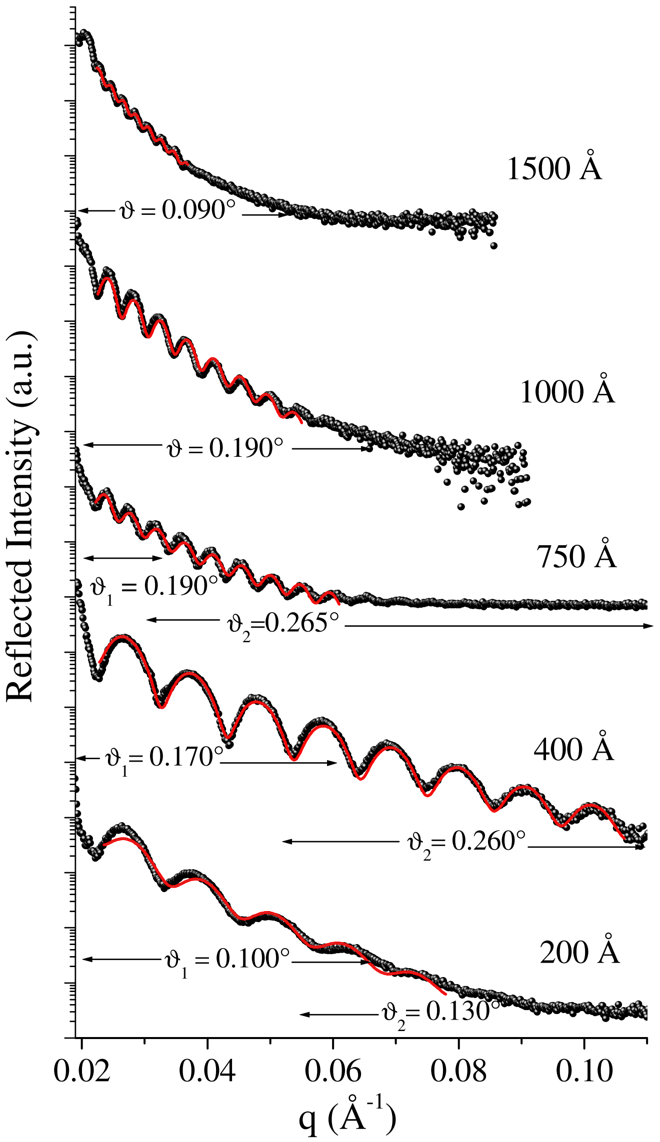

Figure 2. Total Reflection measurements of ruthenium phthalocyanine thin films (dots) and calculated data (lines) as a function of the scattering parameter. The reflection angles chosen to perform the measurements are reported.

A first observation is that the measured surface roughness statistically increase with the increase of the film thickness. In fact, since the Si surface is assumed to be almost flat, the surface roughness is determined by the phthalocyanine film and, as expected, increasing the deposition time, i.e. increasing the thickness, the 'memory' of the sharp substrate is progressively lost.

Nominal thickness (Å)	Measured thickness (Å)	Roughness (Å)
200	254.5	8.2
400	328.3	6.4
750	658.0	9.4
1000	732.3	14.3
1500	1949.3	24

Table 1. Thickness and roughness of the $(RuPc)_2$ films calculated by the Parratt Fit from the experimental data, versus the nominal values deduced during the deposition process.

As a second experimental step, the two samples showing the reflectivity profiles with the most accurate fit (400 Å and 1000 Å nominally thick), were exposed to a NO_2 500 sccm gas flow (NO_2 100ppm in air) for a couple of hours, and then measured again.

Furthermore, this means the ex-situ measurements are a good test to establish if the morphology of the thin $(RuPc)_2$ films undergoes any change when exposed to the NO_2 gas flux (i.e. the $(RuPc)_2$ may be somewhat sensitive to this gas) or not.

The comparisons between the reflectivity spectra before and after the gas treatment were carried out normalizing the reflected intensity (above the q_c) with the Fresnel reflectivity of the Si substrate, in order to isolate the oscillating signal coming from the thin film only. This procedure is equivalent to the subtraction of the form factor from the X-ray diffraction pattern of an amorphous sample in order to isolate its oscillating part (static structure factor). In figure 3, these signals are shown for the 400 Å and the 1000 Å nominally thick films respectively.

From figure 3 some interesting information can be deduced.

First of all, the morphology undergoes a change in thickness and roughness when the film is exposed to the NO_2 gas, and, as demonstrated in case of $Ti(Pc)_2$, we can deduce that an interaction has taken place.

Indeed, the oscillations gets out of phase (d is increased) and are damped in the second measurement (σ is increased).

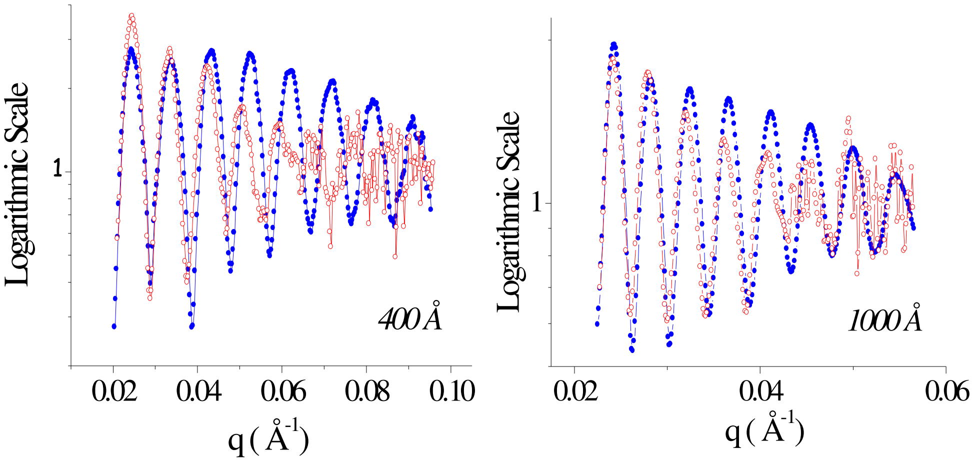

Figure 3. $(RuPc)_2$ film signal before (blue dot-line) and after (red dot-line) interaction with NO_2. Changes in frequency and amplitude are visible due to the solid/vapour interaction.

Furthermore, the interaction does not appear to be restricted to the surface of the film only and, therefore, is not in agreement with a model of absorption or chemisorption of a gas molecule layer.

$(RuPc)_2$ films	400 Å nominally	1000 Å nominally
d before exposure	328.3 Å	732.3 Å
d after exposure	355.0 Å	745.0 Å
σ before exposure	6.4 Å	14.3 Å
σ after exposure	15.5 Å	18.8 Å

Table 2. Thickness d and roughness σ of two $(RuPc)_2$ films before and after exposure to an NO_2 gas flux (50 ppm NO_2 in N_2).

Indeed, if so, the increase in the thickness of the two samples should be comparable (or even exactly the same) whereas it appears to be quite different, table 2. However, trying to deduce some more quantitative information from these data, does not seem reasonable. In fact, the ex-situ procedure, consisting in comparing the spectra before and after the exposure to the gas, can give some hints on the mechanism of the process, but in this preliminary analysis, it can't be conclusive. Moreover this were the first measurements upon $(RuPc)_2$ thin films and the experimental conditions still require to be adjusted and optimized.

In particular, the roughness values may be affected mostly by this experimental setup, so it is reasonable to notice the roughness increases in both films after the gas exposure, but not to try to correlate the numerical values.

Some authors had hypothesised [13] that the gas sensitivity of other MPc sensors increase with film thickness. To explain the gas-film interaction, various adsorption models for the surface interaction, as well as a Fickian model describing the diffusion inside the film, had been proposed [14,15]. In contrast, our preliminary experimental results show, that the interaction is not uniform. Furthermore, both films have been exposed to the NO_2 gas flux in the same experimental conditions and for the same time, but we have no experimental evidence that these conditions were the most suitable in order to achieve the best response from the $(RuPc)_2$ films and we could not even be sure that the flux was sufficient to act on both films in the same way.

In conclusion, this preliminary EDXR test proved a morphological change occurring on the $(RuPc)_2$ films as a consequence to the exposure to the NO_2 gas [16], i.e. the films are sensitive to the pollutant, this being the essential condition to perform deeper investigation.

5.2.2 NO_2 – $(RuPc)_2$ interaction: a systematic study

Since the preliminary tests proved that NO_2–$(RuPc)_2$ interaction takes place, ex situ EDXR measurements were systematically performed on several $(RuPc)_2$ films of various nominal thicknesses, in order to achieve statistically accurate information.

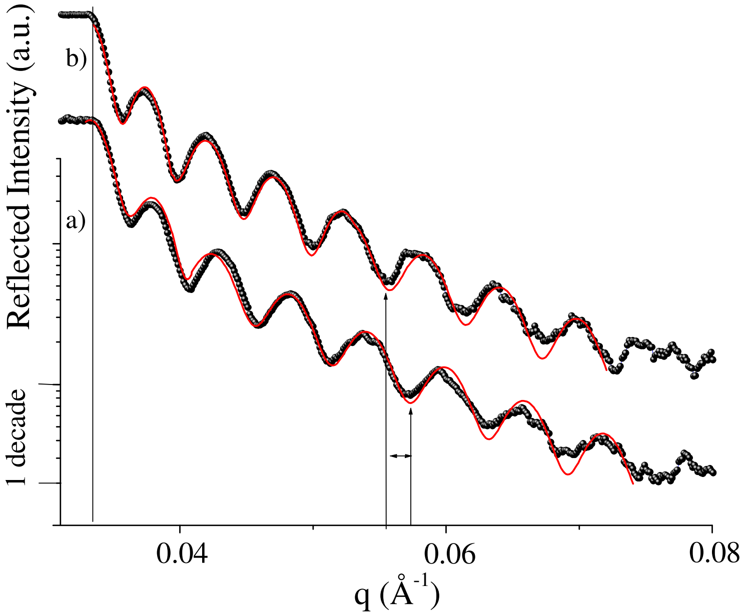

Figure 4. Reflectivity spectra, collected before a) and after b) the NO_2-$(RuPc)_2$film interaction, are plotted as a function of the scattering parameter. The fact that oscillations shift towards lower q-values indicates that the $(RuPc)_2$ film is swallowing.

The ex-situ reflectivity spectra of a 103 nm thick film, collected before and after exposure to NO_2 (50ppm, 20 nmol/s in N_2), are reported in Figure 4 as an example, together with the Parratt fitting functions.

The shift towards lower q-values of the (b) spectrum oscillations indicate that the film becomes thicker as a consequence of exposure to the gas, as expected.

Finally, as a result of the whole systematic study, the final thicknesses of the films (d_2) can be plotted versus their initial values (d_1) to get an overview of the swelling process, shown in figure 5.

The most straightforward explanation to account for this thickness increase is that the film undergoes a "breathing like" mechanism as an effect of a gas diffusion process [17]; in this case the final d value (d_2) should be proportional to the initial film thickness.

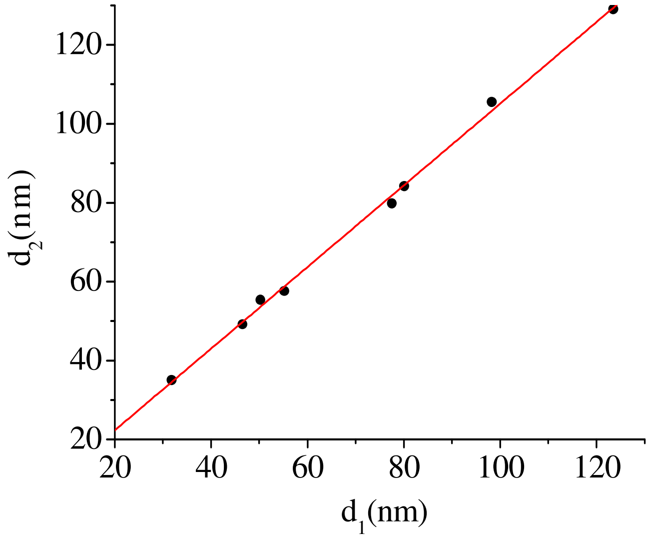

Figure 5. The overall increase in thickness is shown schematically for a selected number of $(RuPc)_2$ samples. Their initial thickness d_1 is plotted versus the final d_2 (dots) and the systematic behaviour fits a linear function (straight line).

However, the experimental points plotted figure 5 give indication that this hypothesis is not completely fulfilled in the present case. Indeed, the data follow a linear trend whose linear fit is:

$$d_2 = d_1\,(1.038 \pm 0.021) + (1.68 \pm 1.44)$$

namely, a straight line with an almost unitary slope coefficient, and that does not cross the origin of the axes.

This suggests that the film growth is due to two contributions, the first being a constant increase of about 1.7 nm, independent of the initial film thickness d_1, while the second is proportional to d_1.

This observation implies that the growth process actually involves two distinct mechanisms, each producing one of these two effects. Therefore the previous hypothesis on the growth has to be partially modified. It consists of a contribution proportional to the initial thickness and a constant one that does not involve the bulk, but the surface only. This model would explain why the latter contribution does not change in relation to film thickness. The proportional contribution, instead, would be the result of a bulk observed in other MPcs thin films.

To validate the former hypothesis, in situ EDXR measurements could be helpful since this technique is able to monitor the morphological changes during the gas-film interaction, as shown in the previous chapter.

The next step therefore consisted of following the morphological evolution of the $(RuPc)_2$ films upon exposure to the NO_2 gas.

5.3 In-situ EDXR measurements

5.3.1 Stability and reproducibility test

In order to perform the in situ X-ray reflectivity measurements on $(RuPc)_2$ thin films, the same experimental chamber described in the section devoted to $Ti(Pc)_2$ and the same experimental conditions were used, i.e. room temperature, NO_2 50 ppm, 20 nmol/s and N_2 as driving stream.

To ensure the N_2 gas flux does not interact with the $(RuPc)_2$ films, and to test the stability of the experimental setup, a sequence of preliminary in situ time resolved measurements was performed. This allowed also to find the most appropriate geometry to execute this kind of acquisitions, i.e. the appropriate scattering angle, the slides apertures, the photon flux.

The experiment consists of collecting a certain number of reflectivity spectra over a number of hours (to be determined), each spectra being acquired for a fixed time. The choice of the duration of each collection is to be made considering two competing factors:

- ➢ Decreasing the acquisition time, the temporal resolution of the d and σ vs t curves improves, since the sampling frequency increases.

- The signal to noise ratio gets worse and, as a consequence, increase the uncertainty on the single d and σ values as obtained by the curves fit.

These factors have to be well balanced every time an in situ time resolved X-ray reflectometry study has to be performed.

In figure 6 an example of a sequence of (time resolved) reflectivity patterns collected in-situ is shown. In this figure, a 125nm nominally thick $(RuPc)_2$ film was measured while fluxing an 180nmol/s N_2 gas flux into the sample holder. Each pattern was acquired for 15 minutes, automatically stored. Than a new collection started in the same modality, the geometry of the apparatus remaining fixed during the whole experiment.

The sequence of patterns is plotted in figure 6.

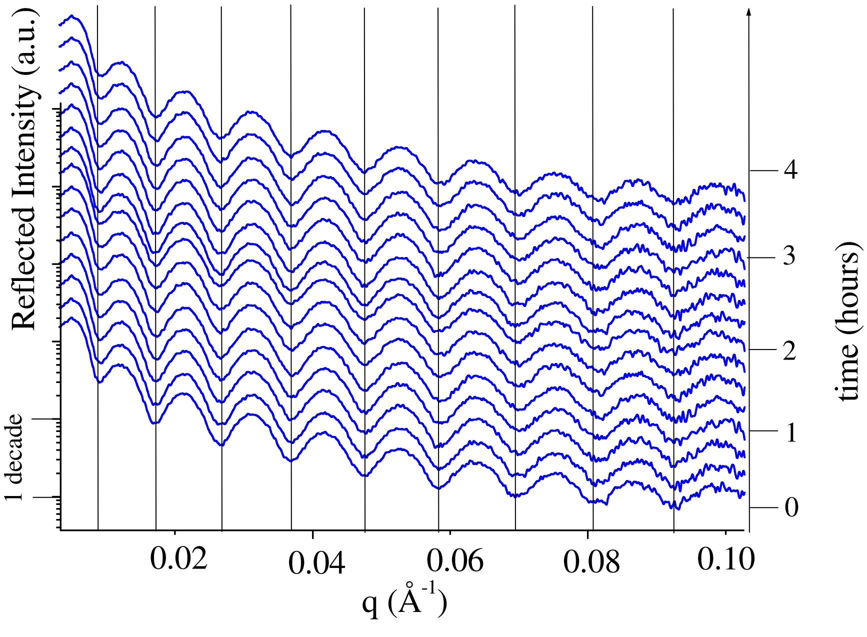

Figure 6. Sequence of reflectivity patters collected during the exposure of a $(RuPc)_2$ film to an N_2 (180 nmol/s) gas flux. As enhanced by the vertical grid lines, the periodicity of the oscillations remains unchanged during the exposure, i.e. the films thickness is stable.

The curves are shifted to improve the visibility. In this way the temporal evolution (if any) can be directly observed. In the present case change either in the amplitude nor in the damping of the oscillations is visible.

This is confirmed by the patterns fit, which provides differences among the various d (and σ) values within the uncertainty of the experimental determination. For this reason, we can be confident that, if any change will be detected in the patterns during the exposure of the films to the gas, it will have to be attributed to the effect of their interaction, rather than to experimental artefacts.

Furthermore the reflectivity patterns show that the sample position remains stable despite the gas stream and, most importantly, no morphological changes take place when N_2 only is fluxed onto the film.

As expected, the $(RuPc)_2$ is not influenced by the nitrogen flux, so this will be chosen as the driving stream when working with the NO_2 oxidizing gas.

5.3.2 NO_2 – $(RuPc)_2$ interaction: preliminary tests

The present section concerns a preliminary test of the real time evolution of two $(RuPc)_2$ 300 Å and 500 Å nominally thick films (as measured during deposition), when submitted to an NO_2 gas molecules flux.

The measurements were performed in the same experimental conditions as described in the previous section. Moreover, the samples were left in the NO_2 atmosphere for 12 hours and, then, the gas flux was interrupted maintaining the N_2 stream only.

The two sequences of the reflected intensity spectra, relative to the two samples, are plotted in figure 7 a) and b), after being normalized to the energy-dependent primary beam.

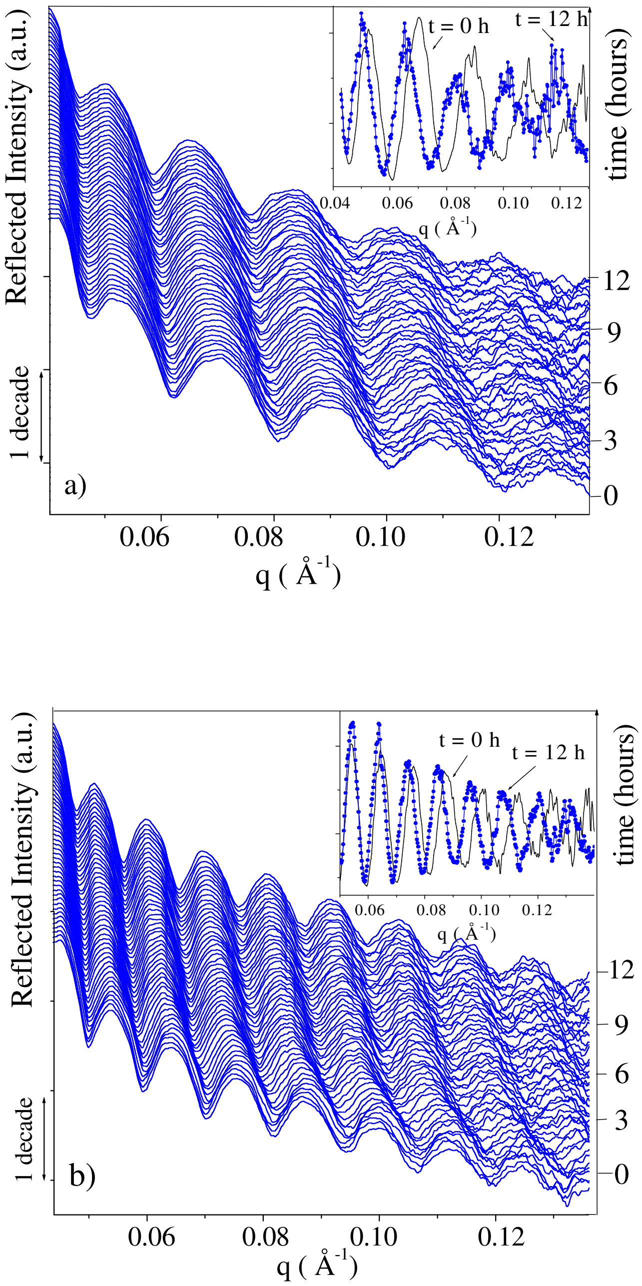

Figure 7. Plot of the real time evolution of the x-ray reflectivity spectra: a) for the 300Å and b) for the 500Å thick films. In the insets: the oscillating contribution to the reflectivity (at the beginning and after 12 hours of exposure to the NO_2 gas) is isolated.

A progressive de-phasing of the spectral oscillations is clearly observable: in particular a continuous shift of minima and maxima towards lower q values as a function of time is evident (figure 7 b).

Since the thickness is connected to the fringes period Δq by the approximate relation $d = 2\pi/ \Delta q$, this shift witnesses the increase of d as a consequence of the gas exposure.

In the inset, the first and the last spectra are compared after being normalized to the Fresnel reflectivity contribution, as discussed above.

The change in the period and in the damping of the oscillations are quantified, in rigorous terms, by fitting the EDXR spectra according to Parratt's formula for X-ray reflectivity.

By fitting each reflectivity spectrum, the thickness and roughness parameters are deduced and the d and σ versus time experimental points can be plotted (see figure 8).

In order to estimate the characteristic times of the overall process, the curves were fitted by an increasing upper-limited exponential function:

$$x(t) = x_1 + (x_2 - x_1)\ [1\text{-}\exp -(t/\tau)],$$

describing the case of a progressive increase of a given parameter x, from its initial value x_1 till its asymptotical value x_2 (saturation) in a characteristic time τ. In this equation, x(t) represents the evolution over time of the film thickness and roughness as obtained from the d vs. t and σ vs. t curves.

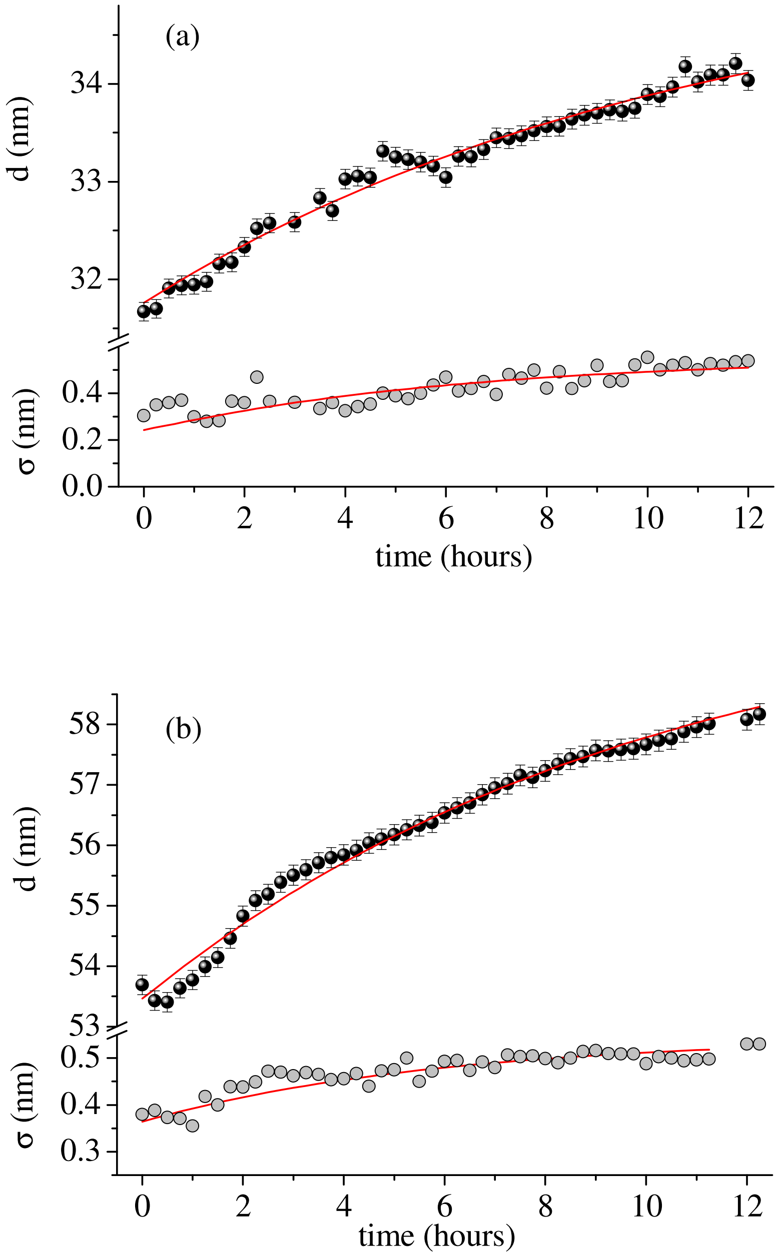

Figure 8. *Curves of the films thickness (full dots) and roughness (open dots) as a function of time, obtained by the Parratt's model, for the 300 Å (a) and 500 Å (b) films, respectively. The solid line represents the fit of the data points according to an upper-limited exponential function describing the saturation process.*

Comparing the figures 8 a and b, it is evident that the data related to the 500 Å sample are of higher quality with respect to those of the 300 Å.

This is due to the fact that the reflectivity spectra of a thicker sample are characterized by a higher number of oscillations; which allow a better fit.

The values of the fit parameters are reported in table 3. The increase in thickness is of the order of 10% in both samples (11% for the 300 Å film and 13% for the 500 Å), namely the increase is proportional to the original thickness. Instead, the roughness value experiences a growth that is independent of the original film thickness.

Nominal d(Å)	Initial d_1(Å)	Final d_2(Å)	Time τ_d (h)
300	318 (1)	352 (1)	10.7 (0.5)
500	534 (1)	603 (1)	9.9 (0.5)
Nominal d(Å)	Initial σ_1(Å)	Final σ_2(Å)	Time τ_σ (h)
300	2.4 (3)	5.6 (3)	6.2 (0.5)
500	3.6 (3)	5.5 (3)	5.9 (0.5)

Table 3. *Values of the calculated morphological parameters obtained fitting the EDXR spectra.*

The two characteristic times, τ_d and τ_σ are about the same for the 300 Å and the 500 Å film: τ_d is approximately 10 hours and τ_σ approximately 6 hours for the two samples, respectively.

These first in-situ time resolved EDXR experimental results of the $(RuPc)_2$ film-NO_2 interaction [18], confirm that this interaction occurs involving both the surface and the bulk of the film, as hypothesized previously by the ex-situ measurements:

- the surface interaction, inducing the increase in roughness, is more rapid and not influenced by the underlying bulk.
- the bulk process, involving the intercalation of the gas molecules inside the film, needs a longer time.

5.3.3 NO_2 – $(RuPc)_2$ interaction: a systematic study

In order to obtain more accurate information on the different interaction mechanisms taking place between the $(RuPc)_2$ films and NO_2 gas, a systematic analysis of the adsorbtion and desorption cycles on various films of different thickness was performed.

The gas sensing films were grown with thicknesses ranging from 20 nm to 150nm, with a surface area of ≈ 1 cm^2.

They were placed in the experimental chamber and exposed to a gas flux of N_2 containing 50 ppm of NO_2 , which corresponds in our setup to a rate of 20 nmol/s. After a complete saturation was reached, each film was submitted to a desorption treatment by flushing the systems with pure N_2 gas at 180 nmol/sec for another day and, finally, the samples were left in air (room conditions) and periodically (every month) re-measured (ex situ EDXR) to check their morphological stability.

As an example, two sequences of reflectivity spectra are shown in figure 9, in the case of two films having nominal thicknesses of 50nm (a) and of 100nm (b), respectively.

Both sequences represent spectra acquired during the first 12 hours of exposure to the N_2/NO_2 flux, since this time range was found to be longer than the characteristic saturation time for the $(RuPc)_2$ thin films in these working conditions (gas flux, room temperature and pressure).

A first of evidence is the thickening discussed above. Indeed, a progressive compression of the curves in figure 9 towards low q-values can be followed by the naked eye till a certain time.

Then, such compression stops, indicating that the sensing film is saturated with NO_2 and that the thickness no longer changes.

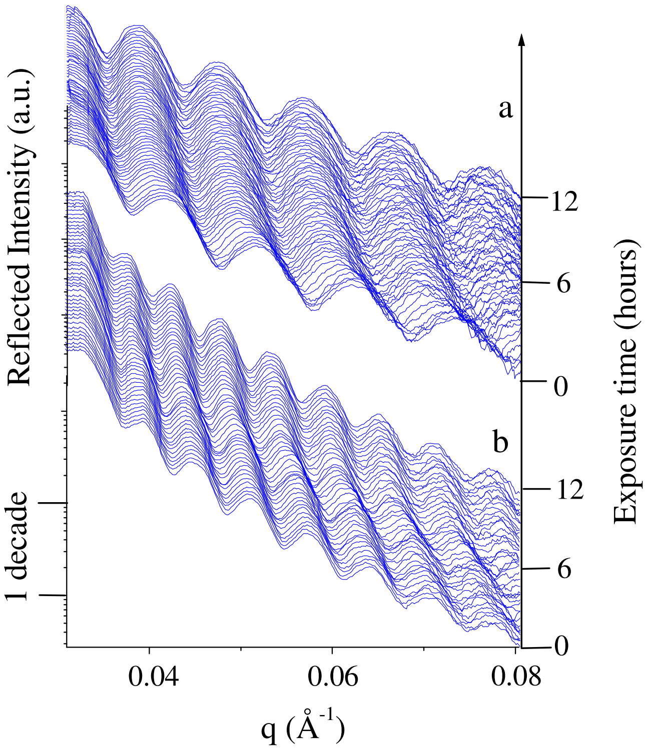

Figure 9. Reflectivity spectra, collected during the NO_2-film interaction, are plotted as a function of the scattering parameter: a) 50 nm thick film; b) 100nm thick film. The fact that the oscillations shift towards lower q-values indicates that the $(RuPc)_2$ film is swelling.

This kind of preliminary observation, i.e. the general features of the reaction kinetics, represents a constrain on the results of data processing. Indeed, the thickness vs. exposure time curve will have to describe a trend consistent with this observation, so that possible artefacts will be easily revealed.

The resulting real time evolution of the thickness parameter is reported in detail in figure 10a.

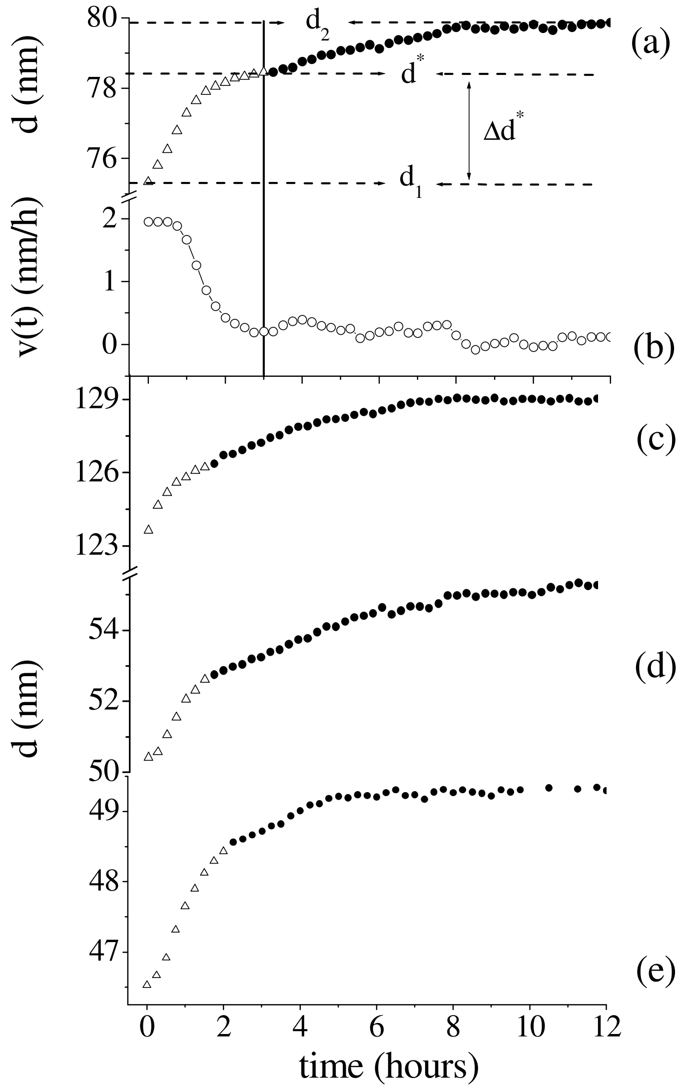

Figure 10. The kinetic evolution of film thickness during the NO_2-$(RuPc)_2$ interaction as a function of time, is shown in the case of four different samples (a, c, d, e). Different fonts are used to point out the two different reaction stages (triangle, first step; dot, second step;), i.e. the thickness crossover value d*. In figure b, the derivative of 'a' is represented, to make the crossover value more evident.

Instead, the real-time evolution of the thickness parameter is peculiar to the in situ X-ray reflectometry investigations.

The values of the initial and final data point of the curves, are exactly the information that can be deduced by the ex situ analysis, as discussed above. As expected considering the preliminary overview of the raw pattern sequences in figure 9, two trends can be observed, which are separated by a crossover value, defined as d*.

Two different symbols are used in the graph to distinguish such different behaviours, separated by a sudden change in the slope of the curve in correspondence of a certain threshold value d*. The visibility of the crossover can be enhanced by calculating the d(t) curve derivative (figure 10b). This two-fold behaviour was exhibited by all the $(RuPc)_2$ films studied, as shown in figure 10c, d and e, where a selection of the d(t) curves is plotted.

The next step was to analyse the relevant parameters of each d(t) curve separately.

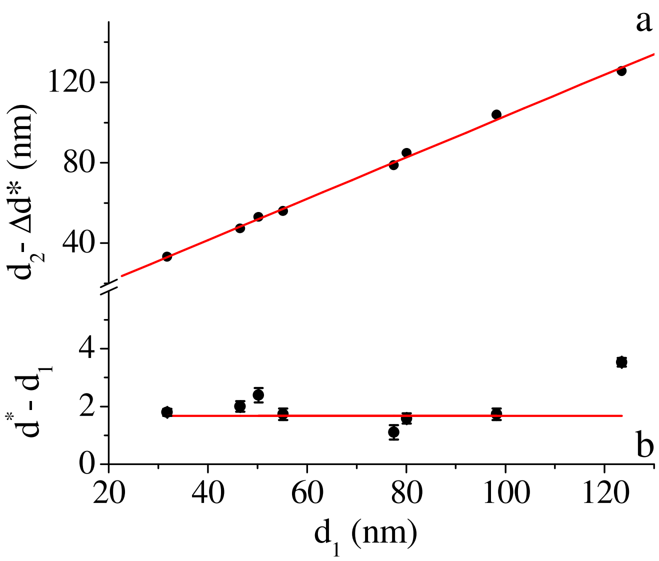

Figure 11. The evolution of the different reaction stages as a function of the initial thickness is reported for a selection of samples: a) second step thickness growth, i.e. proportional increase; b) first step contribution only, i.e. constant increase; the error bars are estimated as the uncertainty in the d* determination.

In figure 11a, we report the $\Delta d^* = (d^* - d_1)$ values corresponding to the amplitude of the first branch of the curve, as a function of d_1. In figure

11b, the (d_2 – Δd^*) values (amplitude of the second branch of the curve) are plotted as a function of d_1.

The first part of the whole thickness increase (Δd^*) is a constant, namely is independent of d_1. It can be fitted by the equation:

$$\Delta d^* = (1.68 \pm 1.5)$$

which is approximately the same value of the intercept of the linear function fitting the overall process (see figure 5).

The second part of the thickness increase (d_2 – Δd^*) can be fitted by the equation:

$$(d_2\text{-}\Delta d^*)= (1.027 \pm 0.02)\ d_1 + (0.43 \pm 0.30)$$

which is a linear function with the same slope of that related to the whole process (figure 5), but crossing the axis origin.

The conclusion is that the hypothesis made on the basis of ex-situ data can be confirmed by analysing time resolved in situ data.

Indeed, the latter allows to distinguish the two distinct processes that take place upon exposure of the $(RuPc)_2$ sensing film to the NO_2 flux to be distinguished.

A further confirmation to the two step model can be obtained by using the same measurements to calculate the other morphological parameter detected by X-ray reflection, namely the film surface roughness σ.

Two σ versus t curves are shown in figure 12.

In comparison with the corresponding d vs. t curves, it can be noticed that, at the same time when the crossover occurs for the latter, also the σ vs t curves, change their slopes.

Of particular interest is the fact that the initial linear increase of σ (t) is followed by an almost flat profile. This is fully consistent with the proposed model since it hypothesizes a growth of the surface roughness below t^* and is relative to the thickness crossover value d^*. This corresponds to the conclusion of the surface process, after which no further change of σ is expected (i.e. above t^*).

Finally, when the bulk process is also concluded, the $(RuPc)_2$ thin films do not desorb and the parameters d and σ remain constant, even if the samples are exposed to a N_2 flux, in our case (180 nm/sec). Moreover, no interaction with air is detectable, even after a number of weeks.

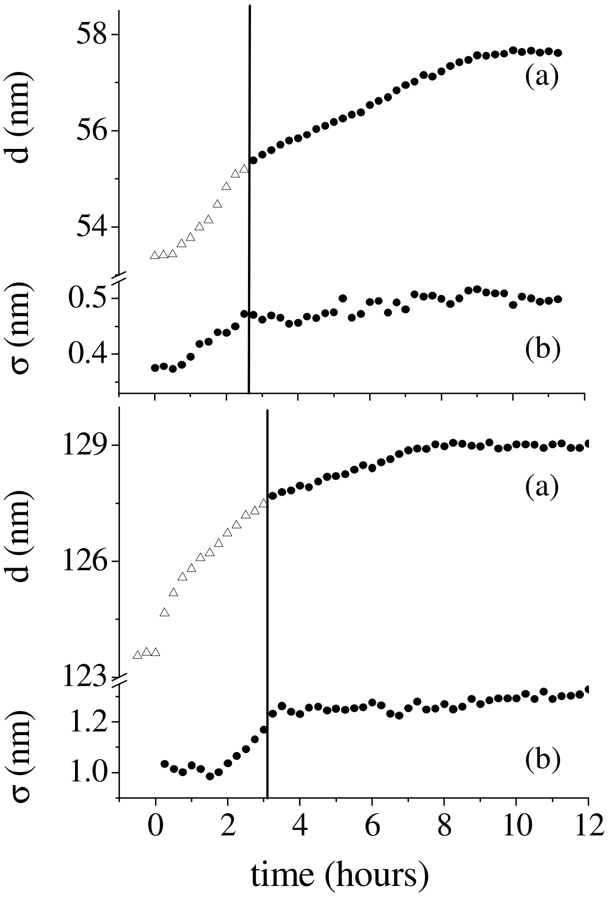

Figure 12. The kinetic time evolution of thickness (a) and roughness (b) is shown for two different samples: 1) 52nm thick film; 2) 123 nm thick film. In both cases there is a straightforward correlation between the two-step thickness evolution and the roughness

This means that the $(RuPc)_2$ thin films are stable at room temperature and ambient pressure conditions, and their reflectivity spectra taken at any time are perfectly overlapping, i.e. d_2 remains unchanged.

In conclusion of this systematic analysis, we can affirm that, by the time-resolved EDXR, a two-fold reaction mechanism between $(RuPc)_2$ and the active gas is evident.

This can hardly be attributed to the one step diffusion mechanism observed in the other MPc. Therefore a two step process can be inferred.

The first step can be related to a surface mechanism with a negligibly small (or no) induction time; the second, to a diffusion process involving the film bulk. This is consistent with the fact that the packing of the $(RuPc)_2$ thin film is very different from the other MPc, frequently encountered in previous studies.

However, determining the reason for the peculiar behaviour of $(RuPc)_2$ thin films upon exposure to NO_2 gas is not possible on the basis of the EDXR data only. It might be possibly due to the expansion of the film lattice induced by the penetration of gas molecules, or might involve more complex chemical reactions, such as a Ru-NO_2 redox process. Therefore, further investigations are required to clarify whether the Ru metal, which is responsible for the structure and the packing of the films, plays a role in the process of film growth or not.

5.3.4 $(RuPc)_2$ thin films: sensor reversibility and second cycle performances

In analogy to what discussed in the section devoted to the $Ti(Pc)_2$ film's reversibility towards NO_2 gas exposure, this paragraph is devoted to the study of the morphological/sensing behaviour of $(RuPc)_2$ films when submitted to thermal treatments. These treatments aimed to reset the device by inducing the release of the trapped NO_2 gas.

A new series of films with various thicknesses (20-120 nm nominally) was grown and the experimental procedure adopted can be summarized as follows:

- STEP-1. a first exposure of the samples to NO_2 gas: the absorption kinetics of the films on first exposure to the gas was studied

- STEP-2. an ex-situ thermal treatment: recovery of film morphology is induced by thermal treatment, two different results being obtained (depending on the temperatures applied): either the films return to their original condition (total recovery) or to a well defined intermediate state (partial recovery).

- STEP-3. a second exposure to NO_2 gas: the kinetics of a second absorption process is recorded and compared with the first.

STEP-1 As already described, the films under measurement were exposed at room temperature to a gas flux of NO_2 molecules (20nmoles/sec) until a stationary condition was reached, i.e. the reflection spectra didn’t show any further changes.

Such time resolved collection of reflectivity spectra provided a very accurate description of the evolution of morphological parameters upon the first gas treatment.

To quantify the change of d and σ, the spectra were fitted according to Parratt's model. The d and σ vs. t curves for sample-1 having an actual thickness value of 44nm, and sample-2 being actually 76nm thick samples (taken as an example) are plotted in figures 13 (a) and (b) and 14 (a) and (b), respectively. They are characterized by a first rapid increase from the initial value d_1 up to a crossover value d*, followed by a slower growth to reach the final plateau at d_2, as discussed in the previous section.

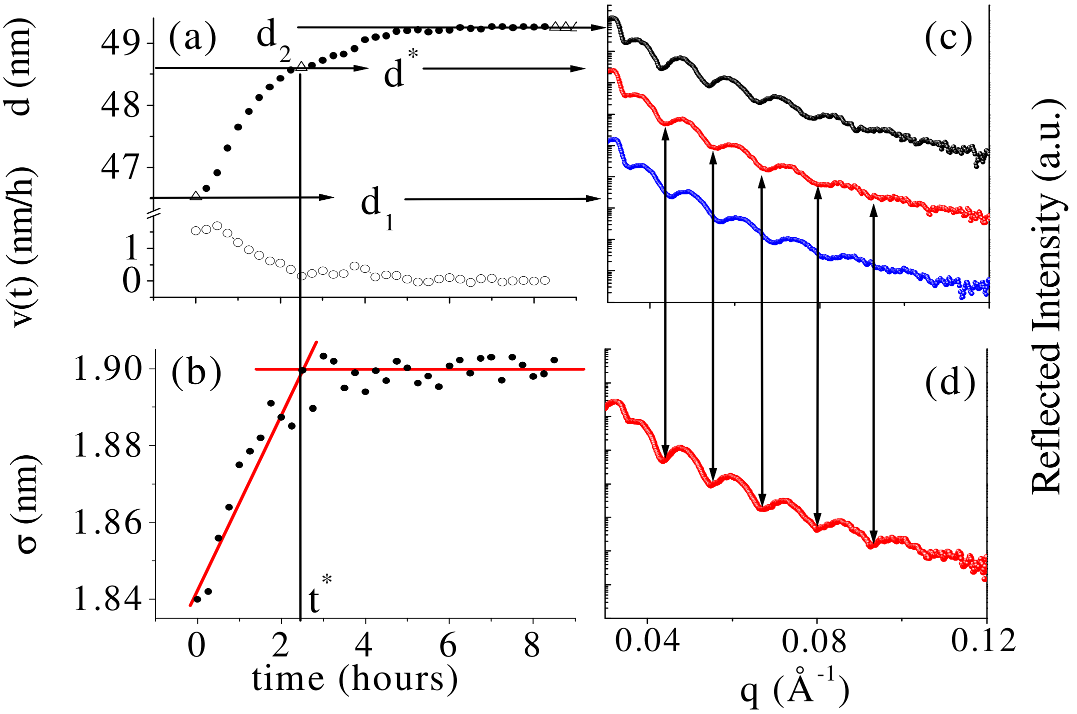

Figure 13. (a) Time dependence of the $(RuPc)_2$ layer thickness d (full dots) and its derivative v(t) (open dots), for sample-1.

(b) Time dependence of the $(RuPc)_2$ layer roughness σ (full dots).

(c) Reflectivity profiles relative to the d_2, d^* and the d_1 values recorded in- situ.

(d) The bottom spectrum is recorded ex-situ after heat treatment of the same sample at T=130°.

STEP-2 In order to test possible reversible behaviours of the phenomena described above, the samples were removed and submitted to a thermal treatment for 30 min in a vacuum at 10^{-2} torr, the heating temperature being 130°C and 200°C (Sample-1) and (sample-2), respectively.

STEP-3 The samples where placed back and measured again by EDXR. The reflection spectra corresponding to the three characteristic points of the d(t) curve obtained during the first exposure, namely d_1, d* and d_2, are reported in figure 13c for sample-1 and in figure 14c for sample-2.

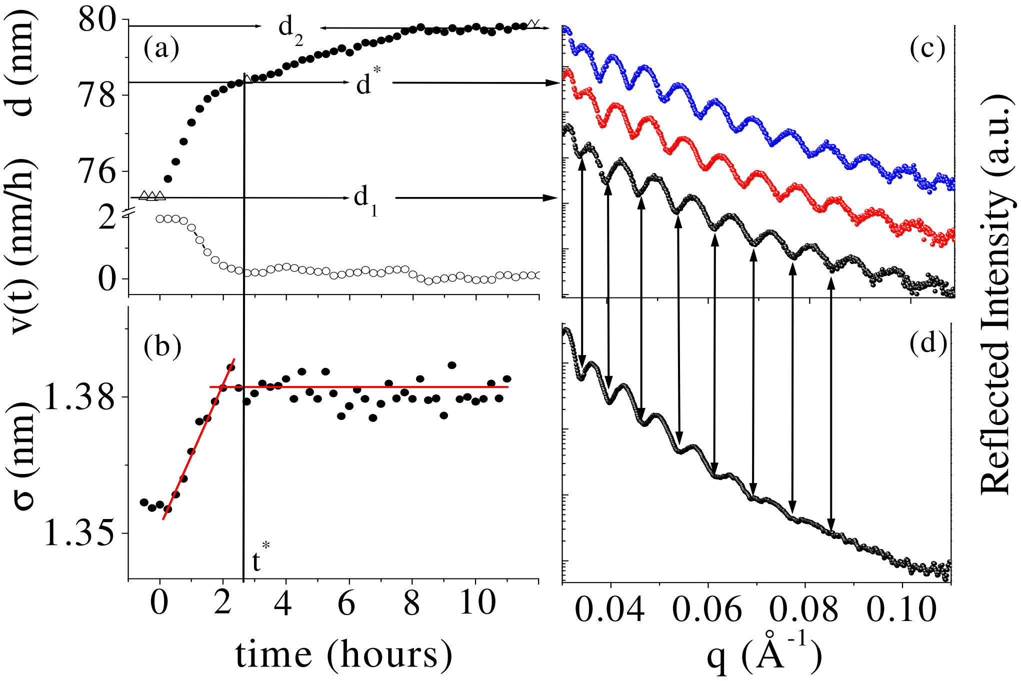

Figure 14. (a) Time dependence of the $(RuPc)_2$ layer thickness d (full dots) and its derivative v(t) (open dots), for sample-2.
(b) Time dependence of the $(RuPc)_2$ layer roughness σ (full dots).
(c) Reflectivity profiles relative to the d_2, d^* and the d_1 values recorded in- situ.
(d) The bottom spectrum is recorded ex-situ after heat treatment of the same at T=200°.

The above spectra must be compared with the spectra collected after the thermal treatment, in figure 13d (sample-1) and 14d (sample-2).

In both cases, the oscillations of the spectra recorded after the thermal treatment are characterized by longer q-periods, with respect to the spectra obtained at the end of the gas exposure.

This indicates that, the gas desorption due to heating always induced a reduction of the film thickness that is different for the two samples.

Indeed, in the first case (figure 13 d, sample-1, reset at 130 °C), the oscillations of the spectrum collected after the thermal treatment are in phase with those of the spectrum relative to the value d* while, in the second case (figure 14 d, sample-2, reset at 200°C), they are in phase with those of the spectrum relative to d_1.

On the basis of these EDXR data, several pieces of experimental evidence confirm the occurrence of two distinct and independent mechanisms in the gas-film interaction.

They are summarized as follows:

1) As mentioned previously, the increase in film thickness as a function of time, reported in figures 13a and 14a, cannot be represented by a simple exponential growth or by a Boltzmann curve, which usually fit reaction processes.

Rather, it seems that the d(t) curves are composed of two distinct branches: a rapid increase from the initial value d_1 to a crossover value d*, followed by a slower growth up to the final plateau at d_2. This double trend is more evident when the d(t) derivative, namely the film growth speed v(t), is plotted (figure 13a and figure 14a, open circles). As the gas starts flowing in the cell, the increase of d is very rapid. Then it slows down until the derivate approaches a constant value, corresponding to d^*, indicating that the first (rapid) part of the film growth is concluded. Subsequently, a second "slower" increase in d takes place from d^* to d_2.

2) Keeping the working conditions (namely the temperature and gas flux) unchanged, the first part of the increase in thickness (i.e. from d_1 to d^*) has the same duration regardless of the initial thickness of the film, the time t^* at which d(t) reaches its crossover value d^* being about 3 hours. The second part, on the other hand, has a duration that is proportional to the initial thickness.

3) Another notable point that emerges from in-situ EDXR measurements is the shape of the curve of the film surface roughness as a function of the exposure time (σ(t) curve). In the case of $(RuPc)_2$ samples, see figure 13b and figure 14b, this σ (t) curve increases (linearly) until the time t^* (defined in point 2) and, then it remains stationary. This behaviour demonstrates that the surface morphology evolves only until t^*, no further modifications being detected after this point.

Points 1 to 3 are indicative of the fact that the first part of the film growth upon gas absorption is dominated by a surface process (adsorption), which is not influenced by the amount of underlying material. The second part, however, appears to be essentially connected with the interaction between the gas molecules and the film bulk.

4) More evidence is obtained from further EDXR measurements, performed after the film was treated thermally. Indeed, depending on the temperature at which the samples had been heated, only two results were obtained: the thickness can either go back to the intermediate d* value (*intermediate recovering*), or to the original d_1 value (*total recovering*), no other values being observed. This indicates that the removal of the gas molecules trapped in the film is a two-step process ruled by two different activation energies E_1 at $T \leq 130°C$ and E_2 in the temperature region $130°C \leq T \leq 200°C$. From the above considerations, attributing the decrease in thickness to the release of the molecules trapped in the film is straightforward, the first part of the process being essentially due to the release from the film bulk and, the second, from the film surface.

5) Finally, more information on the surface vs bulk interaction mechanisms was obtained from the in-situ collection of reflectivity spectra during a new exposure of the samples to NO_2 (STEP-3): the resulting d(t) curves are compared with those obtained during the first gas exposure in figure 15 a for sample-1, and in 15 b for sample-2.

Concluding, the starting values are d* for the partially recovered samples (case of sample-1) and d_1 for the totally recovered samples (case of sample-2). It is remarkable that the d(t) curves for both samples reproduce the same behaviour as the second part of the curve observed during the first absorption: a simple Boltzmann growth, consistent with a pure bulk absorption process, the final value being d_2 for sample-1, and about d_2-d* for sample-2.

Moreover, the shape of the σ (t) curve (fig. 15a and fig. 15b) is different with respect to that of the first exposure: the rapid σ increase, which reveals a drastic change of the surface morphology during the first exposure to the gas, is no longer present.

It is worth noticing that the initial roughness value at the second exposure is higher than that of the final value of the first exposure. This effect, although always present, is much more evident in the case of the samples reset at 200°C, indicating that the thermal treatment at higher temperatures increases the surface roughness.

Therefore, during the second exposure of the films to the gas the morphological evolution of the films can be regarded as a pure bulk absorption process, similar to the second part of the process present in the first exposure. On the other hand, the fact that the surface layer was preserved in the case of sample-1 (and not in sample-2) does not affect the bulk diffusion process and the final thicknesses of the films, confirming that the two processes occurring in the first cycle are independent. This implies that, in the second absorption treatment, both the partially and the totally recovered samples provide a response (in the form of a bulk diffusion process) similar to that exhibited on the first gas exposure, regardless the surface layer was preserved or not during heating.

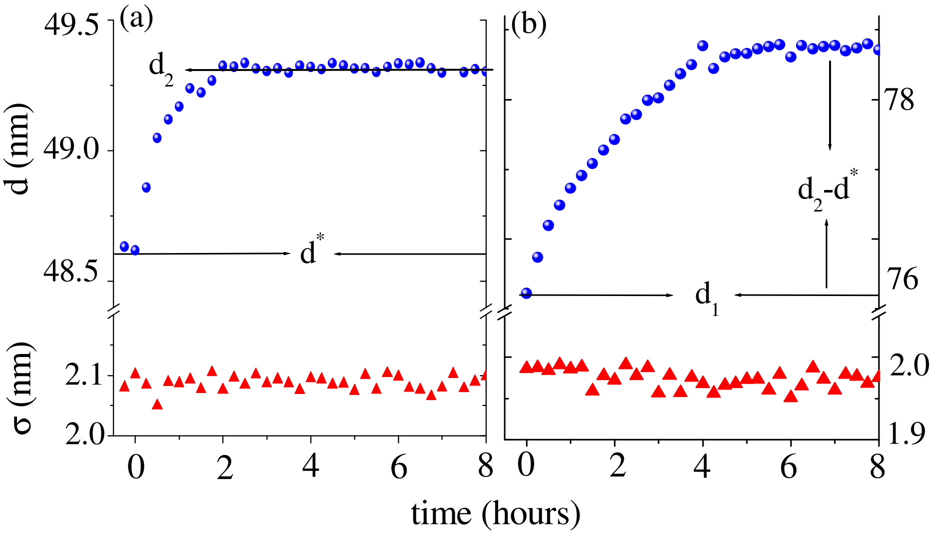

Figure 15. Time dependence of the $(RuPc)_2$ layer thickness (full dots) and roughness (triangles) at the second submission to the gas. (a) The thickness of sample-1 increases from d^* to d_2. (b) The thickness of sample-2 increases from d_1 to $(d_1 + d_2 – d^*)$. The σ curves do not show any significant increase.

In summary, the EDXR data demonstrate that the response of the film to gas exposure is characterized by a first, fast increase in thickness, reversible at 200°C, which can essentially be attributed to a surface adsorption, followed by a slower one, reversible at 130°C, which shows the morphological characteristics of a bulk diffusion process.

A possible explanation is that the former process induces the formation of a layer, whose thickness is (d^*-d_1), on the film surface, persisting also when the gas flux is interrupted and that can be removed only by heating the sample to a temperature close to 200°C.

This behaviour is different from the other MPc systems investigated and, in principle, could be associated with the interaction of the NO_2 molecules with the Ru metal atoms. Moreover, the micro-structural characterization of these films reveals a peculiar packing and long-range structure, anomalous with respect to the microcrystalline structure of the other MPc films, possibly inducing a different behavior in gas diffusion.

However, since the difference is essentially restricted to the interaction at the film surface, it seems more likely that the metal, rather than the film packing, is responsible. The observation that the two steps of gas desorption require rather different energies (desorption is fully accomplished only at higher temperatures) suggests that gas diffusion is mediated by strong interactions.

Unlike the other MPc, for instance $Ti(Pc)_2$, in addition to the expected interaction between the Pc ring and the gas, the metal is believed to play an active role in the $(RuPc)_2$ matrix, giving rise to a chemical bond with NO_2.

Beside the clarification of the mechanisms involved in the film/gas interaction, the importance of this unexpected result lies in the great technological relevance given by the possible use of these films as optical/conductometric sensors. Indeed, the EDXR measurements indicate that the interaction between the NO_2 gas and the sensing film does not compromise the recovery of the initial film morphology.

Moreover, the recovery of the film morphological parameters does not affect the second stage of the gas absorption process, both for the partially reset sample and for the totally reset one.

In other words, the bulk absorption process is reversible upon thermal reset of the samples. This is a relevant point, since the EDXR technique demonstrated to be an effective tool for retrieving information on those properties that are strongly affected by film morphology, such as the reversibility. In fact, the reported measurements are the first experimental evidence [17] of the reversibility of the bulk absorption process for $(RuPc)_2$-based sensing films.

Since the film bulk provides the dominant contribution to the optical/conductometric response of a chemical sensor, these results indicate that the $(RuPc)_2$ based sensing films could be suitable candidates to use as active elements in gas sensors devices.

5.3.5 Thermal treatments

As observed previously, when $(RuPc)_2$ films undergoes different thermal treatments, at a second exposure to the NO_2 gas flux the efficiency of their morphological response is enhanced. Indeed, the overall thickness increase due to the bulk diffusion is preserved but the induction time gets vanishingly short and the breathing like response is immediate. The need of a first activating cycle to reach the best operating conditions is a classical behaviour of many sensors. In order to evaluate if this enhanced efficiency induced by the presence of NO_2, is related to the thermal treatment or is characteristic of the second cycle itself, a systematic thermal treatment was performed on various $(RuPc)_2$ films.

The films where thermally pre-treated, i.e. they where heated prior to the exposure to the NO_2 gas flux (20nmol/s in N_2 180 nmol/s). At first, the temperatures where chosen to be:

- 130°C, 30 minutes
- 170°C, 30 minutes
- 180°C, 30 minutes
- 200°C, 30 minutes

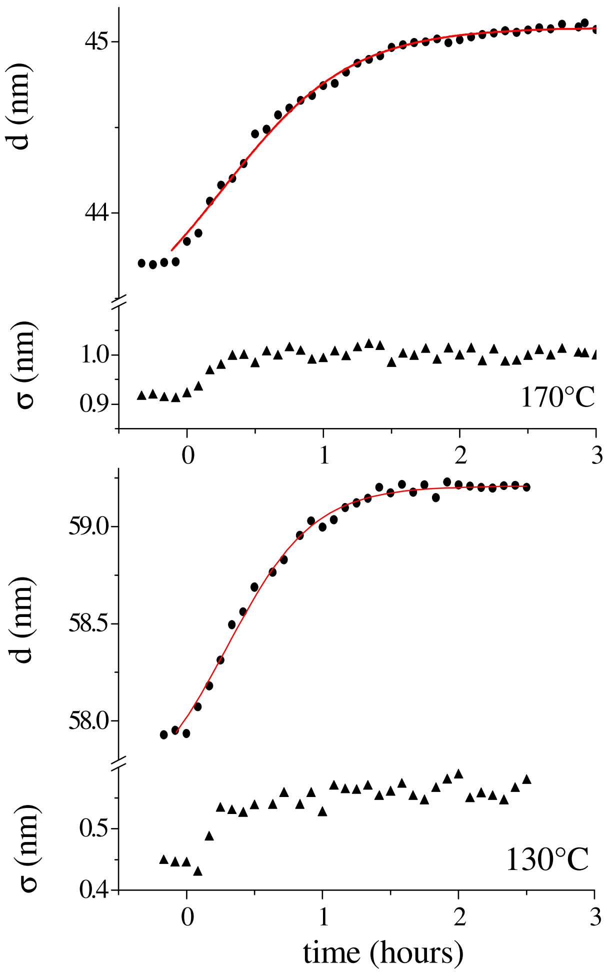

Figure 16. Time evolution of the morphological parameters d and σ of two $(RuPc)_2$ films during the exposure to an NO_2 gas flux (50 ppm). The films were previously treated at 130°C and 170°C for 30 minutes respectively.

After this thermal treatment, the films were placed into the experimental chamber and a in-situ time-resolved reflectivity measurement was performed as described above (NO_2, 50ppm, 20nmol/s). The patterns were collected every 5 to 15 minutes, and the data were processed and fitted. In fact, in figure 16, the time evolution of the morphological parameters are shown in case of films previously treated at 130°C and 170°C and then exposed to the NO_2 gas flux.

Such thermal treatment enhances the $(RuPc)_2$ films sensing efficiency. Indeed, only the bulk diffusion is visible in this case and the time responses are comparable to those taking place in other MPcs patented as devices. When the films are heated at 180°C or 200°C, no sensing response in present any longer. Neither the thickness or the roughness of the film undergo to any changes, i.e. no NO_2-$(RuPc)_2$ film interaction is present. These temperatures probably induce a surface melting process, compromising the surface structure and morphology: the mechanical conditions for the gas diffusion into the bulk are lost.

However, in the "as-deposited" films the initial conditions could be recovered to aloe their further operation as sensing devices despite they were submitted to a double thermal treatment at 130°C (for 30 minutes) and 200°C (for 30 minutes), respectively.

Therefore, further investigations were required to study the effect of high temperatures on the sensor's activity. It can be hypothesed that a stabilizing effect is induced by the 130°C thermal treatment. This temperature might stabilize the films structure, thus extending the temperature range of applicability of these materials as nitrogen dioxide sensors. To confirm this conjecture, another set of samples were kept at the following temperatures (for 30 minutes each):

PRE – TREATMENT	TREATMENT
130°C	200°C
130°C	240°C
130°C	260°C

Table 4. Schematic sketch of the thermal treatments (30 minutes each) performed on a series of $(RuPc)_2$ films.

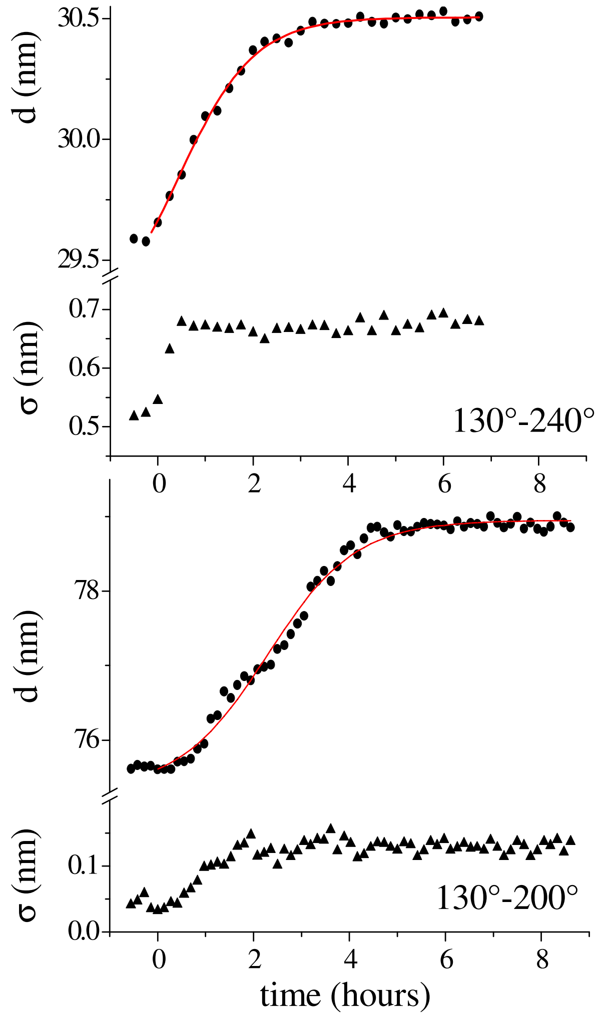

Figure 17. Time evolution of the morphological parameters d and σ of two $(RuPc)_2$ films during the exposure to an NO_2 gas flux (50 ppm). The films were previously treated at 130°C + 200°C and 130°C + 200°C for 30 minutes at each temperature.

In fact, when stabilized by the pe-treatment, the following treatment at 200°C and 240°C didn't compromise the sensing device activity, as visible in figure 17. The usual sigmoidal thickness evolution is obtained and also the surface roughness behaves as expected: the bulk diffusion occurs (no surface interaction being visible any longer) and the morphological efficiency is preserved. However, the 260°C thermal treatment not only compromised the films activity, but it was strong enough to induce the phthalocyanine sublimation. High temperatures, even very close to the sublimation one, do not affect the films structure/morphology and the thin $(RuPc)_2$ films preserves their sensing efficiency, thus showing to be suitable for high temperatures applications.

5.3.6 $(RuPc)_2$ films: in situ surface melting- sublimation

In the previous section, it has been demonstrated that the gas sensing $(RuPc)_2$ films are sensitive towards NO_2 molecules when thermally treated. However, when the films are exposed at 180° C for 30 minutes, the sensing activity is lost by the material, while at 170°C they still preserve their sensing properties.

Moreover, a thermal treatment at lower temperatures (130°C) proved to have a stabilizing effect, which allows the film to work at higher temperatures, up to 240°C. This is particularly interesting since NO_2 is a by product of industrial releases that are usually emitted in the atmosphere at high temperatures.

In order to understand the physical/chemical phenomena inducing this behaviour, a series of films where morphologically monitored while undergoing the thermal treatments mentioned above.

An especially designed oven was used as sample holder and placed in the energy dispersive X-ray reflectometer to perform in situ time resolved reflectivity measurements during the thermal treatment.

Films submitted to long thermal treatments up to 170°C, suffered no morphological change, i.e. the thickness and roughness values obtained by the fitting procedure of the spectra remained constant.

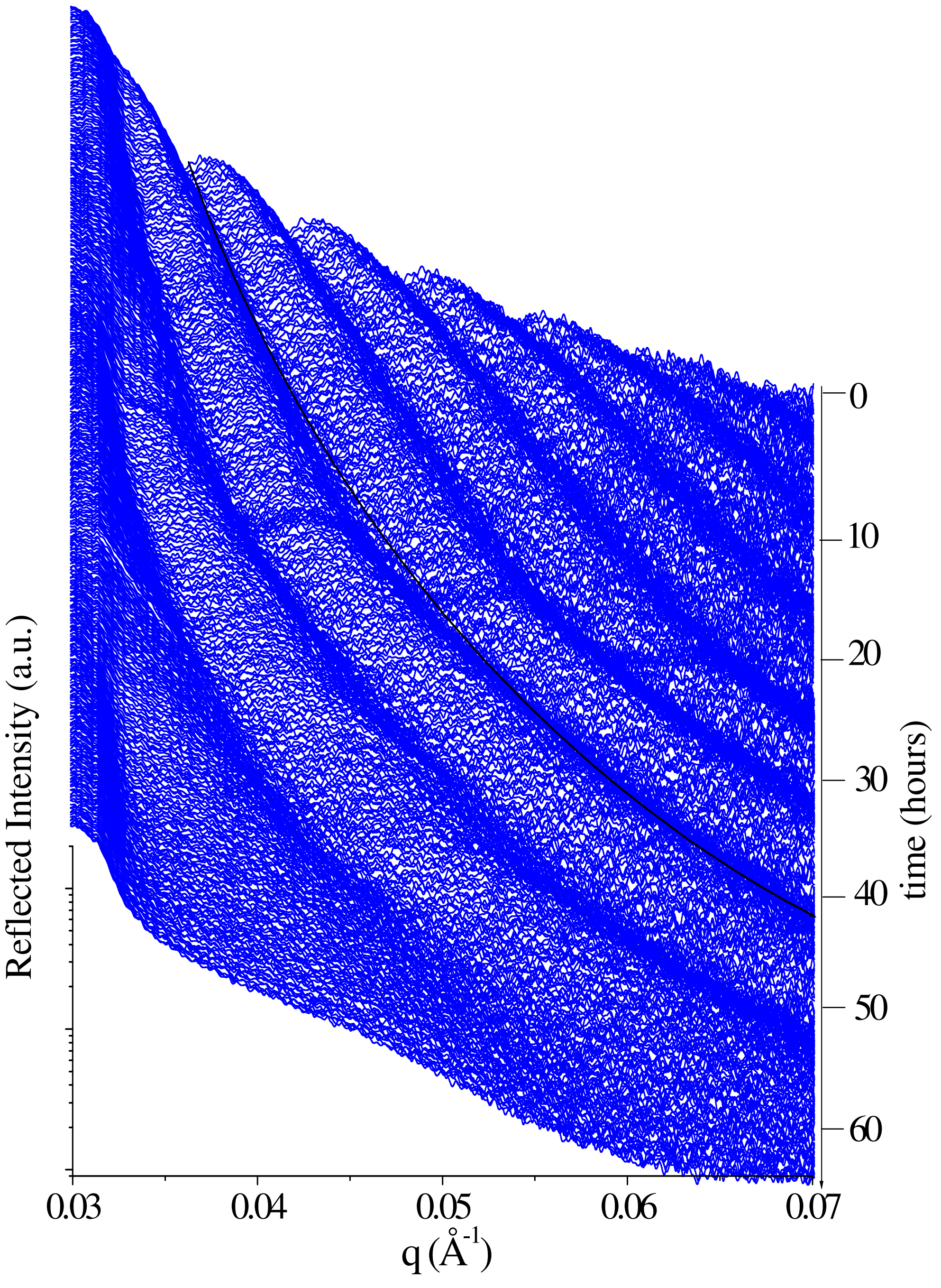

Figure 18. Sequence of reflectivity spectra collected during the thermal treatment at 180°C of a 100nm nominally thick $(RuPc)_2$ film. The red line enhances the shift of the fringes towards lower q values, i.e. the film is getting thinner as time goes by.

Instead, when a thermal treatment of 180°C was performed, the films morphology changed dramatically. In figure 18 a sequence of reflectivity patterns are shown as an example, the sample being a 100nm nominally thick $(RuPc)_2$ film submitted to an 180°C thermal treatment. The measurement lasted 3 days, during which a collection of reflection spectra (10 minutes each) was acquired until the reflectivity profile did not show any further modification.

It is evident even by naked eye that there is a constant shift of the fringes minima towards higher q values, i.e. the thickness decreases constantly. This shift is evidenced by a red line connecting the minima of the second oscillation.

In figure 19 (a) and (b) the thickness and roughness vs. time evolutions as obtained by the fit of the previous sequence, are shown respectively.

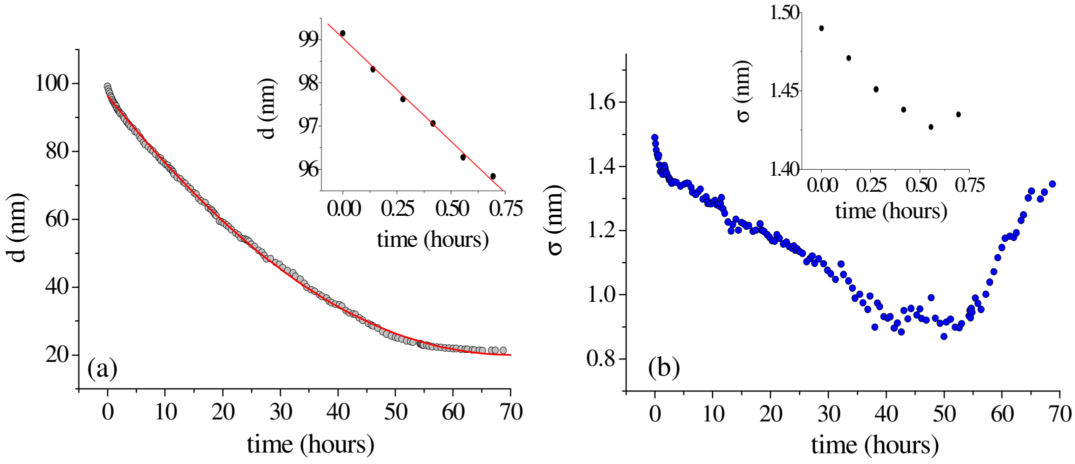

Figure 19. (a) Time evolution of the thickness of a 100nm nominally thick $(RuPc)_2$ film during a 180°C thermal treatment. The d vs. time curve has been fitted (red line) by a third order exponential decay. In the inset the d behaviour during the first 30 minutes of the treatment is enhanced and fitted by a straight line. (b) Time evolution of the surface roughness of the above mentioned sample. In the inset the s vs. time evolution during the first 30 minutes is enhanced.

A loss of material induced by the thermal treatment can be noticed, i.e. the film gets thinner and thinner. In the inset of figure 19, the behaviour of the morphological parameters is shown during the first 30 minutes of thermal treatments. Indeed after 30 minutes only, the sensing properties of the material were lost and in fact such a time is more than sufficient to induce big changes.

Moreover, the roughness behaviour is peculiar. Indeed this value decreases as long as the film is getting thinner and, finally, when the thickness approaches its asymptotic value, the roughness starts growing. This behaviour suggests the following hypothesis. Since the temperature chosen is not high enough to induce a full sublimation, the film might undergo a two-step transition, consisting of an initial melting of the surface layers followed by the evaporation of the melt. Indeed, a molten layer on top of the film would explain the decrease of roughness, which appears flatter then the original solid.

Finally, when only a few layers of $(RuPc)_2$ are left onto the Si and the thermal treatment is not strong enough to overcome the adherence of the phthalocyanine to the substrate, the remaining solid phase displays a highly defective structure. This would justify the final growth of the surface roughness value.

In conclusion this EDXR study demonstrated that the film morphology undergoes changes when submitted to a 180°C temperature for 30 minutes. These morphological changes inhibit the functionality of the film as sensing deice, proving once more the key importance of these parameters on the devices performances.

Deeper investigations are required to reinforce the hypothesis proposed on the thermodynamic behaviour of these films during the melting-evaporation process and the EDXR could be a useful tool to deepen this knowledge.

5.3.7 $(RuPc)_2$ films vs different NO_2 concentrations: detection limits of the material

A systematic time resolved EDXR study was performed in situ on Ruthenium Phthalocyanine thin films to estimate the detection limits of these materials as NO_2 transducers and the influence of the gas concentration changes on the gas-film interaction mechanisms [19]. The work validates, giving the first experimental evidence by EDXR, the use of the morphological evolution of a gas sensing film upon working as test-parameter, in alternative to the usual electro-resistive measurements. While the latter is only able to give the information of whether or not the gas is interacting with the film, the former is also able to discriminate among interaction processes of different nature (surface and bulk).

As a first step, a 30ppm NO_2 gas was fluxed upon a 50 nm nominally thick $(RuPc)_2$ film. The sequence of reflectivity spectra were collected every 15 minutes in these conditions and in order to obtain the real time changes of the morphological parameters d and σ, every pattern was fitted using the Parratt formalism.

The time variations of these quantities were obtained, the resulting uncertainties being: $\Delta d_{max} = \pm 2$ Å and $\Delta\sigma_{max} = \pm 0.5$ Å, respectively. The same experimental procedure was applied to a series of samples, while exposed to NO_2/N_2 gas mixtures at different NO_2 concentrations, from 5ppm up to 60ppm. Since an expansion of the time scale was expected at the lower concentrations and a compression at the higher once, the patterns were collected every 15 min for $[NO_2] \leq 30$ ppm, and every 5 min for $[NO_2] > 30$ ppm.

In figure 20, the time evolution of the thicknesses of $(RuPc)_2$ films is presented as a function of time, in correspondence of various NO_2 concentrations.

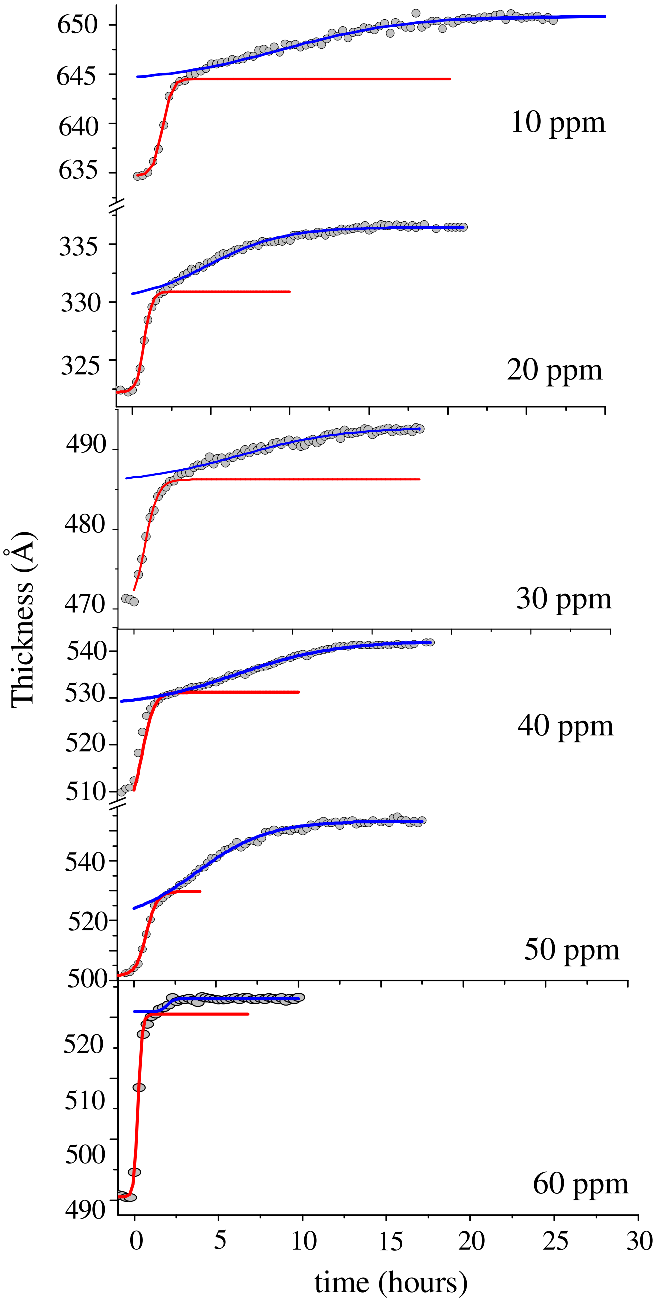

Figure 20. Time evolution of the morphological parameter d (dots), obtained by Parratt Fitting procedure of the time resolved reflectivity sequence, is shown for different NO_2 concentrations fluxed upon different thick films. The sigmoidal fit of the two distinct reaction mechanisms are shown (line) in order to obtain the characteristic times of the interactions.

In figure 21, an analogous plot for surface roughness is shown.

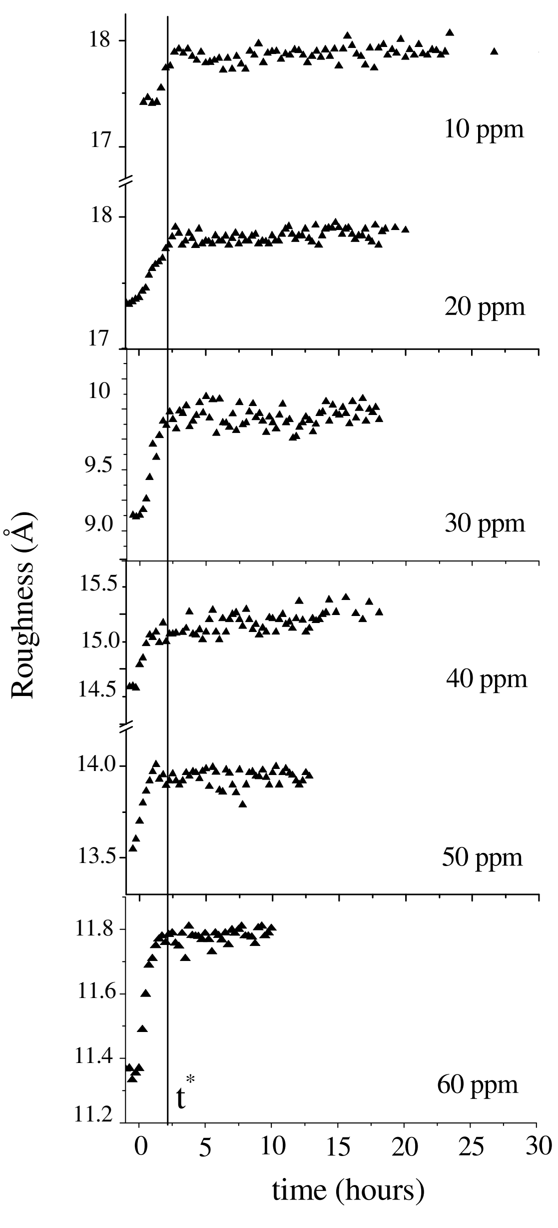

Figure 21. Time evolution of the morphological parameter σ (triangles), obtained by Parratt Fitting procedure of the time resolved reflectivity sequence, is shown. The surface roughness evolutions is independent on the different NO_2 concentrations.

The experimental detection limit was found to be equal to 10 ppm. At 5ppm, a limited number of NO_2 molecules are expected to come in contact with the thin film surface, since the gas-in and gas-out channels in the camber are located above the film: at low concentration the NO_2 molecules will be transported out of the experimental chamber by the N_2 stream, due to the lamellar (rather than turbulent) regime of the gas flux without getting in contact with the surface.

Moreover, the whole interaction process becomes slower as the concentration decreases. This allows to easily observe the characteristic two step behaviour (surface absorption and bulk diffusion) that was already detected and discussed in the previous sections.

Such two steps in the film growth, distinguishable by following the d(t) curve (dots figure 20), that is formed by two branches separated by a crossover point, were fitted by two Boltzmann functions (lines figure 20).

They were finally considered as independent processes, both starting simultaneously as the gas is fluxed in the experimental chamber, but characterized by different response times.

At lower gas concentrations, the two branches in the d(t) curves can be readily distinguished, since the surface and bulk processes differ strongly in characteristic times. However, at the highest concentration (60ppm), they appear to take place simultaneously.

The observation of the surface roughness (figure 21) is a further confirmation of such two step model. Indeed, the first step happens in the same time interval in which the surface roughness increase, indicating that it is associated with the gas-surface interaction (the roughness parameter is sensitive to surface processes only).

Once the general features of the interaction process are defined, the question of the influence of both the film (initial) thickness and the NO_2 gas concentration can be faced.

A first observation is that the characteristic time of the surface process (i.e. of the low t branch of the d(t) curve profile and of the σ(t) curve), corresponds to $t^* = (2.50 \pm 0.25)$ hours, independently of the film thickness and gas concentration (line figure 21). Therefore, by fitting the d (t) curves, it is now possible to quantify the characteristic times τ_1 and

τ_2 of the two steps of the process. The first time, τ_1, must be, for what discussed above, independent on both the film thickness and the gas concentration. As a consequence, similar values are expected to be obtained from all the curves ($3\tau_1 = t^*$).

However τ_2, the characteristic time of the bulk-related process, depends on both the film thickness and gas concentration, which are not constant in the experiments performed. For this reason, in order to study the influence on τ_2 of such two parameters independently, another series of EDXR time resolved measurements was carried out on $(RuPc)_2$ films of various thickness, at a fixed concentration of NO_2, that was chosen 50ppm. From the same Parratt fitting procedure, the time evolution of the morphological parameter d was calculated for this new set of measurements and, then ,the times τ_1 and τ_2 were deduced by a further analysis of the so obtained 'd vs time' plots.

As shown in figure 22, when the NO_2 concentration is kept unchanged, the first interaction mechanism is characterized by a τ_1 = 0.70 hours = constant (as expected), while τ_2 results to be approximately proportional to the initial thickness d_0:

$$\tau_2 = 2.40\ (0.15) + 0.03\ (0.01)\ d_0.$$

This relation enables to calculate the dependence of τ_2 on both the thicknesses and the NO_2 concentrations. Indeed, now it is possible to rescale τ_2 with respect to the film thickness, isolating its dependence on the concentration only.

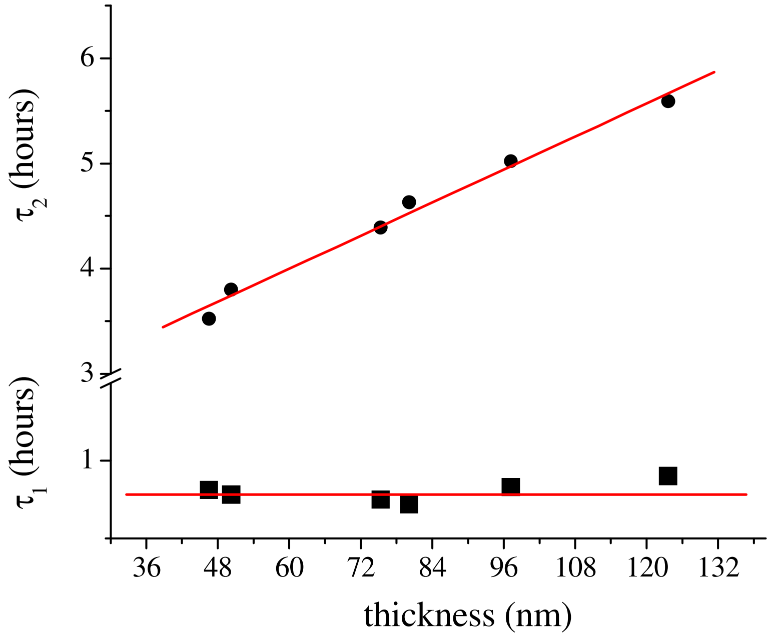

Figure 22. The characteristic evolution times, τ_1 and τ_2, of the two interaction mechanisms are shown as a function of the film thickness in the case of an NO_2 [50ppm] gas flux. The τ_1 values are independent on the thickness; The time τ_2 evolves proportionally to the thickness.

The plot of τ_2 as a function of the concentration (figure 23) can be fitted using a sigmoidal curve. τ_2 varies from 7.90 hours to 0.78 hours passing from 10 ppm to 60 ppm, which means that the bulk diffusion velocity tends to become constant below a 10ppm NO_2 concentration (lower detection limit) and it saturates above 60 ppm NO_2 (upper detection limit).

Moreover, the characteristic time τ_2 = 0.78 hours, for $[NO_2]$ = 60ppm, is very close to the τ_1 = 0.70 hours, characteristic time of the surface interaction mechanism. At concentrations higher than 60ppm, the former hides the morphological evolution due to the latter, since $\tau_2 < \tau_1$.

This represent the intrinsic detection limit of this sensing materials response to the oxidizing gas NO_2 when the distinction between the two interaction mechanism are analysed separately.

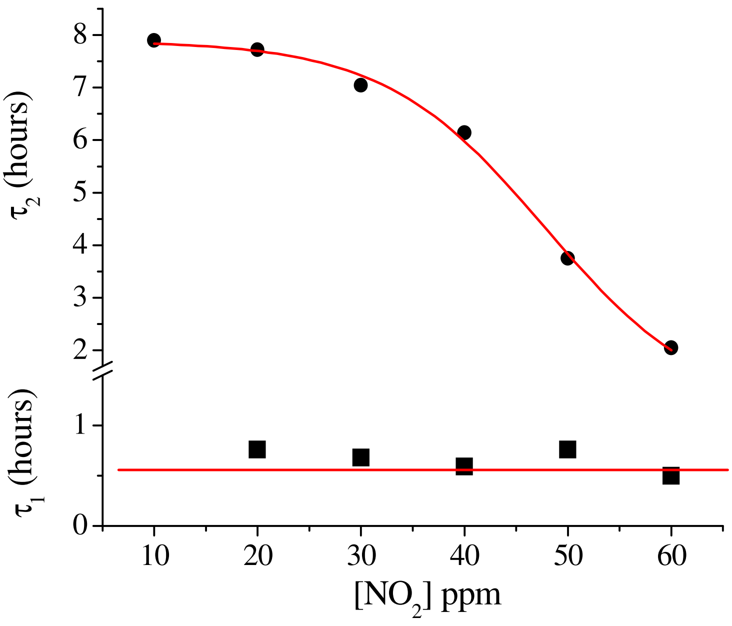

Figure 23. The characteristic evolution times, τ_1 and τ_2, of the two interaction mechanisms are shown as a function of the NO_2 concentration. The τ_1 values are independent on the [NO_2], while the τ_2 evolution is well fitted by a sigmoidal curve.

In conclusion, the in situ time resolved EDXR technique was able to determine the detection limits of NO_2 uptake into a $(RuPc)_2$ thin films from the morphological point of view and to discriminate the two step reaction behaviour as a function of the pollutant concentration.

The lowest [NO_2] concentration detectable was found 10ppm. At concentrations higher than 60ppm, the surface absorption hides the diffusion mechanism of the NO_2 intake in the film bulk since the characteristic reaction time of the former process becomes much higher than the latter. Despite this, the concentration range in which the morphological monitoring can be applied, is comparable to that of the more common electro-resistive measurements.

Moreover this systematic study confirmed once again that the gas-film interaction process is ruled by two mechanisms (a surface and a bulk one) which were confirmed to be independent.

5.4 Combined conductivity and EDXR measurements

Finally, joint in-situ/time-resolved conductivity and EDXR measurements were performed upon $(RuPc)_2$ thin films exposed to NO_2 gas fluxes. The aim of these measurements is to finally establish which of the two distinct reactive processes occurring between the thin phthalocyanine film and the NO_2 gas are associated to the electrical sensing response. On a morphological basis, we affirmed that the diffusive bulk interaction between the phthalocyanine π-electrons and the oxidizing gas, modulated the devices response versus NO_2 and now the electrical confirmation is required. Furthermore, we would like to determine if the surface reaction involving the ruthenium metal might affect the electrical properties, too.

As previously discussed in the section devoted to $TiPc_2$ films, the devices were produced sublimating under vacuum the $(RuPc)_2$ powder on interdigitated Au electrodes. In this case however, the experimental conditions and the response deriving from the sensing device are completely unknown since no data have been previously published on the subject. For this reason, the same experimental conditions held in measuring the $TiPc_2$ devices were chosen: a two contact electrical measurement was preformed applying a 0.8V voltage to one electrode and collecting the current intensity values as a function of the NO_2 exposure time.

$(RuPc)_2$ is an intrinsic semiconductor so the starting current intensity values are obviously expected to be higher than those observed for $TiPc_2$. Despite this, to classify this material as a potential electrochemical transducer, an observable conductivity change is expected.

Two preliminary test measurements were performed at different NO_2 concentrations, 50ppm and 30ppm respectively, maintaining the same flux (20nmol/s NO_2 in 180nmol/s N_2) in both cases. Each reflectivity spectrum was collected for 500 s (0.15 hours) along 12 hours.

As visible in figure 24, the morphological behaviour deduced by fitting of the reflectivity patterns sequences is as expected:

- the surface interaction (fitted by the red sigmoidal lines) is independent on the gas concentration.
- The bulk interaction (fitted by the blue sigmoidal lines) is still dependent on both the gas concentration and the film thickness as described in the previous section

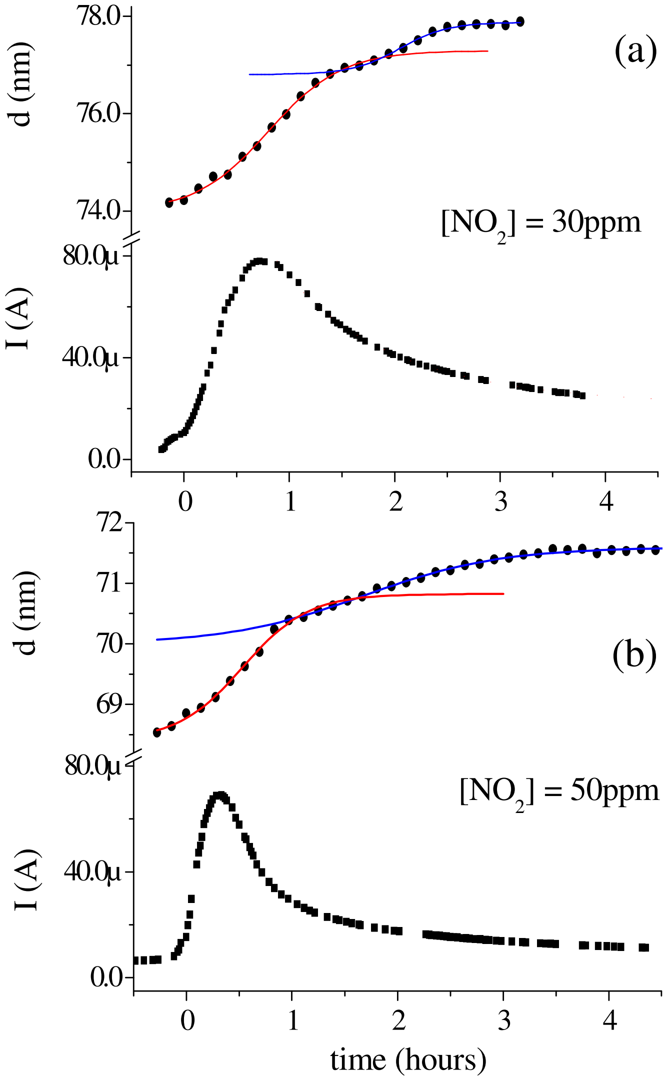

Figure 24. (a) Time evolution of the morphological parameter d of a 74 nm nominally thick $(RuPc)_2$ film is shown together with its electrical conductivity change when exposed to a 30ppm NO_2 gas flux. (b) The same parameters are shown for a 65nm nominally thick $(RuPc)_2$ film exposed to a 50ppm NO_2 gas flux.

The continuous lines are the Boltzmann fit of the first and second interaction processes occurring between the film and the gas.

In the lower part of figure 24 a and b, the electrical behaviour of the $(RuPc)_2$ films is associated to the morphological one. It is visible by naked eye that, when the NO_2 concentration is 30ppm, the electric response is slower than in case of a 50ppm concentration, i.e. the conductivity change is modulated by the pollutant concentration in its response time. However the overall conductivity change remains unchanged (slightly less than two orders of magnitude as overall increase) independently on the NO_2 concentration.

Since the surface reaction occurring between the sensing film and NO_2 is independent on the gas concentration (within certain limits) [20] while the bulk diffusion is not, this seems to be a first evidence of the correlation between electric response and bulk diffusion.

To make some more quantitative observation, the surface reaction only was taken into account and by the derivative of this process, the characteristic times τ_1 of the surface interaction were calculated, as shown in figure 25. Indeed, despite the different NO_2 concentrations, in both cases (figure 23a and b) $\tau_1 = 0.70 \pm 0.15$ hours. Furthermore, the characteristic times of the electric responses, τ_e, were deduced for the same samples and resulted different from τ_1, and, most importantly, this response is dependent on the NO_2 concentration: a) $\tau_e = 0.68$ hours, b) $\tau_e = 0.30$ hours.

This evidences excludes the hypothesis that the electrical response is connected to the surface reaction involving the Ruthenium metal. Indeed it confirms what previously deduced on the base of the morphological monitoring procedures alone, i.e. the bulk diffusion is the process responsible for the sensing properties of $(RuPc)_2$ films.

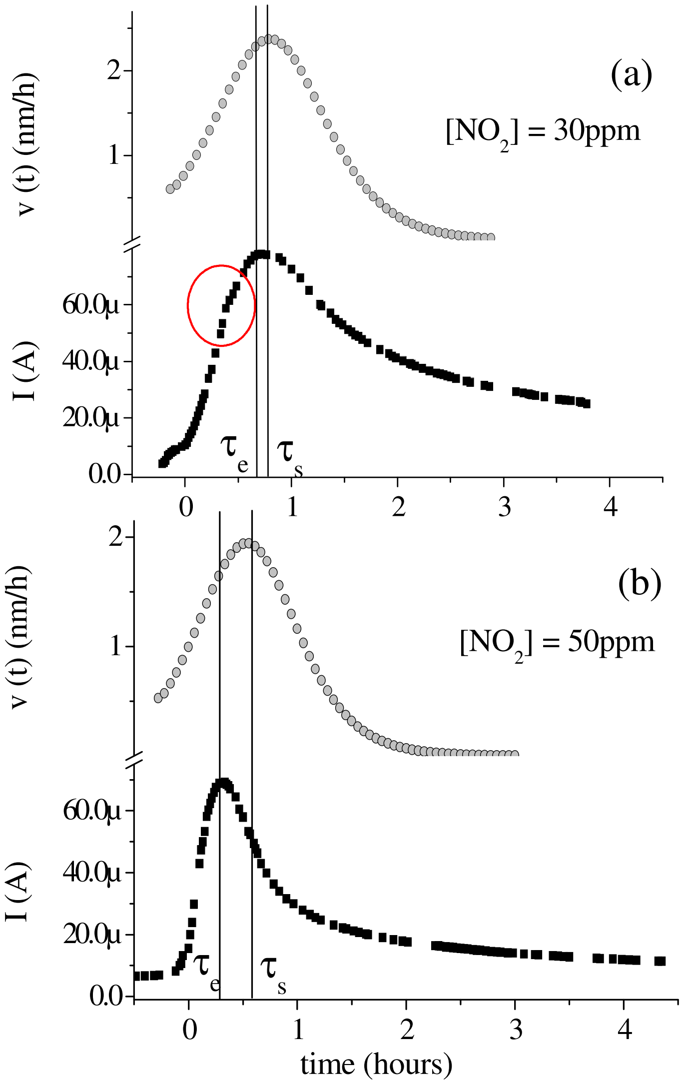

Figure 25. The derivatives of the surface reaction fit (fig. 24 a and b) of two $(RuPc)_2$ films exposed to 30ppm and 50ppm NO_2, are compared to the electrical conductivity change of the same samples. The characteristic times of the two processes τ_s and τ_e are extrapolated and do not coincide. While the τ_s remains unchanged the τ_e shifts with the NO_2 concentration.

However, at the lower NO_2 concentration, being the response mechanism slower, a more resolved conductivity peak is obtained since the statistical accuracy is enhanced. As remarked in figure 25a by a red circle, the peak seems to be the convolution of two distinct signals, the former with shorter characteristic times, the latter with a longer one. Further investigations are required varying the NO_2 concentration towards the materials detection limit (10ppm), in order to deepen this preliminary observation.

The hypothesis of a signal associated to the surface absorption, which is hidden by the dominating one associated to the bulk diffusion has to be verified, as well as, the dependence of the electrical response on the film thickness.

In conclusion, these joint electrical/EDXR measurements performed for the first time on $(RuPc)_2$ thin films upon working provided some interesting information that, although not conclusive, the potential of the combined use of the morphological monitoring and the traditional techniques.

References

[1] T. Nyokong, J. Guthrie-Strachan, *Inorg. Chim. Acta*, 208, **1993**, 239.

[2] D. Schmeisser, J. Pohmer, M. Hanack, W. Gopel, *Synth. Met.,* 61, **1993**, 115.

[3] M. Hanack, R. Polley, *Inorg. Chem.,* 33, **1994**, 3201.

[4] F.H. Moser, A.L. Thomas, *The Phthalocyanines,* CRC, Boca Raton, FL, **1983**; Vols. 1 and 2.

[5] A. Capobianchi, G. Pennesi, A.M. Paoletti, G. Rossi, R. Caminiti, C. Sadun, C. Ercolani, *Inorg. Chem.*, 35, **1996**, 4643-4648.

[6] R. Caminti, M.P. Donzello, C. Ercolani, C. Sadun, *Inorg. Chem.,*38, **1999**, 3027-3029.

[7] A. Capobianchi, A. M. Paoletti, G. Pennesi, G. Rossi, R. Caminti, C. Ercolani, *Inorg. Chem.*, 33, **1994**, 4635.

[8] W. Kobel, M. Hanack, *Inorg. Chem.*, 25, **1986**, 103.

[9] G. Rossi, M. Gardini, G. Pennesi, C. Ercolani, V. L. Goedken, *J. Chem. Soc. Da ton Trans.*, 193, **1989**.

[10] M. Hanack, J. Osio- Barcina, E. Witke, J. Pohmer, *Synthesis*, 211, **1992**.

[11] R. Polley, M. Hanack, *Synthesyis,***1997**, 295.

[12] H. Bertagnolli, A. Weber, W. Corner, T.S. Ertel, U. Reinohl, M. Hanack, M. Hees, R. Polley, *Inorg. Chem.,*36, **1997**, 6397.

[13] J. C. Hsieh, C. J. Liu, Y. H. JU, *Thin Solid Films*, 322, **1988**, 98-103.

[14] J. W. Gardner, M. Z. Iskandarani, B. Bott, *Sensors actuators B*, 9, **1992**, 133.

[15] H. Y. Wang, J. B. Lando, *Langmuir*, 10, **1994**, 790.

[16] A. Generosi, V. Rossi Albertini, G. Rossi, G. Pennesi, R. Caminiti, *J. Phys. Chem. B*, 107 (2), **2003**, 575-579.

[17] A. Generosi, B.Paci, V. Rossi Albertini, P. Perfetti, G. Rossi, A.Capobianchi, A.M. Paoletti, G. Pennesi, R. Caminiti, *Appl. Phys. Lett.,* 86, **2005**, 114106.

[18] V. Rossi Albertini, A. Generosi, B.Paci, P. Perfetti, G. Rossi, A. Capobianchi, A.M. Paoletti, R. Caminiti, *Appl. Phys. Lett.,*82 (22), **2003**, 3868-3870.

[19] A. Generosi, B. Paci, V. Rossi Albertini, P. Perfetti, G. Rossi, A.M. Paoletti, G. Pennesi, R. Caminiti, *Submitted to Applied Physics Letters*, September **2005**.

Conclusions

In this work, an unconventional experimental technique, the Energy Dispersive X-ray Reflectometry, has been the main tool to investigate a series of gas sensing metallo-organic materials (Metallo-phthalocyanines) and their response towards an oxidising gas such as nitrogen dioxide NO_2. This kind of X-ray analysis is well known in the scientific community as a complementary technique to obtain morphological information (thickness and roughness) of layered samples. Because of that, X-ray Reflectometry has traditionally been confined to a very limited range of applications, mostly devoted to the characterization of samples produced with a certain degree of uncertainties.

Nevertheless, the energy dispersive mode enhances the potentialities of this technique, combining the possibilities of the traditional applications (ex-situ measurements), with the in-situ time resolved approach.

Starting from these considerations, we tested the use of this technique as a "*morphological monitor*" for evaluating the response of novel gas sensing materials, in alternative to standard measurements.

Form the point of view of the experimental approach, this represented the first main goal of the work. Therefore we can state that:

- The results reported validate the use of the *in situ* EDXR technique as a powerful non-destructive tool to investigate the response of novel sensing materials (via the observation of their morphological parameters change) providing, at the same time, the general features of the gas-film interaction. This unconventional method - based on the time resolution of the Energy Dispersive X-ray Reflectometry technique- proved to be a novel alternative to standard procedures evaluating the response of gas sensing materials. The conclusions are:

- the *morphological monitoring* is shown to be sensitive to the gas-material interaction and is able to detect the breathing-like behaviour of the sensing films
- the *morphological monitoring* is sensitive to the devices reset treatment
- the *morphological monitoring* is sensitive to the gas concentration in a range comparable to the usual electro-resistive measurements.

- However, while the conventional electro-resistive measurements are only able to give information on whether the gas is interacting with the sensor or not, the Energy Dispersive X-ray Reflectometry proved to be also able to discriminate interaction processes of different nature (in the present case the absorption limited to the film surface and the adsorption involving the material bulk).

The other relevant aspect of this work is the use of metal-phthalocyanines as sensing materials for pollutant gases as NO_2.
Utilising the $TiPc_2$ patented device as a reference standard, it is possible, by comparison, to affirm that Ruthenium Phthalocyanine films fulfils the main requests in order to classify the material as a sensor, as summarized in the following list:

- Sensing ability: the material is sensitive to the atmospheric pollutant NO_2 (both morphologically and electrically)

- Selectivity: the material is stable in ambient conditions and in controlled atmospheres enriched by common gases (N_2). A limitation, typical of all phthalocyanine devices, concerns the presence of sulphides contaminants.

- Stability: the material is stable before and after the exposure to the pollutant, thus preserving the information acquired.

- Reversibility: the material can be easily restored by various chemical or physical treatments (reductive atmosphere, thermal treatments) without loosing its sensing properties, i.e. it is a renewable device.

- Sensitivity: the material is sensitive to concentrations of NO_2 gas fluxes within the detection limits of other similar devices.

- Time response: both morphological and electrical responses are as fast (also at the first exposure to the pollutant) as other similar devices.

However, the research work, did not concern only the technological applications of such materials as the active component of sensing devices. Indeed we were interested also in deepening the knowledge about the basic chemical and physical interactions occurring during the interaction process between the material itself and the pollutant, which turned out to be a very interesting and rich field of investigation.

Since film morphology affects both the adsorption/desorption properties and the sensor’s performances (reversibility, response time, and recovery rates), much work was dedicated in the past to the former aspect, but the latter was not deeply investigated in depth until now. Regarding such basic research, some interesting aspects have been revealed and some novel information obtained both on the reference molecule, $TiPc_2$, and on the$(RuPc)_2$.

Titanium Bis-phthalocyanine- NO_2 interaction

- The film undergoes a "breathing like" expansion as the gas diffuses inside the bulk in a single step reaction, whose thickness kinetic can be described by a Boltzmann sigmoidal curve.

- The response of the surface roughness showed an unexpected anomalous behavior. The $\sigma(t)$ curve exhibits a peak, i.e. after a normal initial rise, it reaches a maximum value and, then, begins to decrease until a final constant value is reached. This effect was attributed to a re-arrangement of the layer formed by the NO_2 – $Ti(Pc)_2$ molecules interacting at the film surface, passing through an intermediate phase characterized by an increased roughness. The study provides experimental evidence for a structural surface rearrangement in $Ti(Pc)_2$ films induced by interaction with NO_2 molecules.

- The chemical reactions occurring during the sensing process are responsible of the increase of conductivity that, in turn, is associated to the expansion of the materials structure: the conductivity peak corresponds to the maximum speed of the diffusion process.

Ruthenium Phthalocyanine- NO_2 interaction

- The gas absorption process develops in two stages:
  1. a surface adsorption process.
  2. a bulk absorption process.

- The bulk absorption process is reversible upon thermal reset of the samples: it is attributed to the diffusion of gas molecules in the film bulk.

- The surface adsorption process is irreversible: it is attributed to the interaction between the Ruthenium metal and the NO_2 molecules and is inhibited by thermal pre-treatment of the films.

- The conductivity change occurring when $(RuPc)_2$ films come in contact with NO_2 molecules, is dependent on the gas concentration. This fact excludes the attribution of the gas sensing process to the surface reaction and confirms the morphological hypothesis of the sensing activity being related to the bulk diffusion. Further investigations are required in order to establish a correlation between the film thickness, the gas concentration and the electrical response.

Appendix

Processing of Reflectivity data

- STEP 1: Data processing

Reflectivity data are collected as ASCI files from the acquisition ADCAM-MAESTRO software MCA.

At first the data are converted as a function of the scattering parameter using the formula:

q (x′) = Channels (x) *T* K* sinθ. T being a numerical value to convert from channels to energies depending on the shaping mode (fine gain and corse gain) of the MCA software, and K = 1.0136 = constant.

At this point, the raw data can be plotted as shown in figure 1 (a) but the shape of the profile must be corrected normalizing towards the primary beam. Indeed, the reflectivity profile of raw data plotted as a function of the scattering parameter is shown together with the white beam. In figure 1(b), the same reflectivity profile is plotted after the correction for the white spectra.

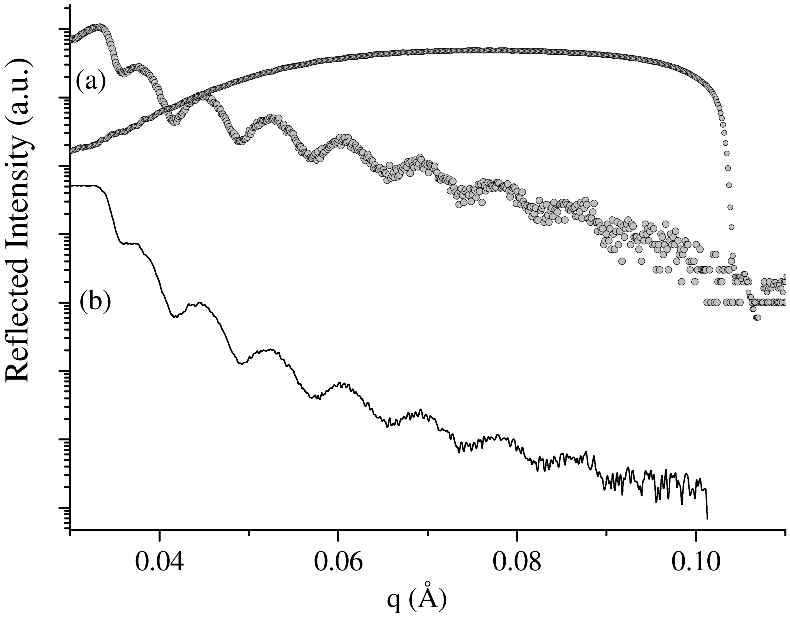

Figure 1. (a) The raw reflectivity spectra and the white primary beam are plotted as a function of the scattering parameter. (b) The same pattern after the normalization procedure.

Further corrections towards adsorption and diffused scattering are not required in case of these laboratory measurements.

As discussed in the section devoted to the theory of X-ray Reflectivity, the absorption contribution is always negligible. Indeed the diffuse scattering is usually taken into account when these measurements are performed using synchrotron radiation.

In fact, when such a powerful source is used, the intensity range of the reflectivity profile is much enhanced and usually from the edge till the last oscillation, 8-10 order of magnitude are explored. In this case, the contribution of the diffused scattering can't be ignored. However, when a laboratory measurement is performed the intensity ranges only 4 to 6 order of magnitudes and the diffuse contribution does not interfere.

In figure 2(a) the profile of a raw reflectivity spectra is plotted before(line) and after (dots) the normalization for the diffuse scattering, figure 2(b). As visible, despite the contribution of the diffuse signal, the two reflectivity profiles are perfectly overlapping, and, as previously mentioned, the contribution of the diffuse background becomes relevant only at the high order Kiessig fringes, which are not collectable using a laboratory instrumentation.

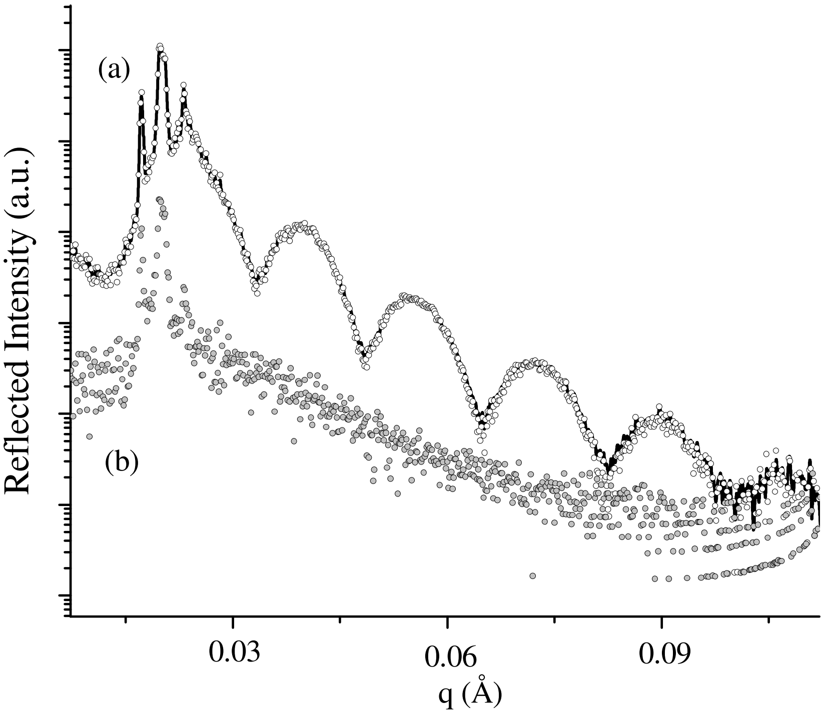

Figure 2. *(a) A raw reflectivity pattern before (line) and after (dots) the correction for the diffused scattering (b). The two patterns are perfectly overlapping.*

- STEP 2: Fitting procedure

The Parratt model describes the intensity of a radiation reflected by a thin film and separated from the substrate, on which it is deposited, by a sharp interface. The iterative matrix model has been calculated in case of a film onto a substrate, being the matrix a square 2x2.

The result was developed as a function of the scattering wave number being the reflectometry technique performed in the Energy Dispersive Mode, instead of the more common angular dispersive one.

The result is the following:

$$\mathbf{|R|^2=\{1-2[(Real\ (R_l^{*}R_r-R_lR_r)exp(-2kd)]/[1+exp(\ -4kd)-2Reale\ (R_lR_r)exp(-2kd)]\}}$$

where: $R_l = (k_0 - k)/ (k_0 + k)$ is the Fresnel film reflectivity, $R_r = (k - k_s)/ (k + k_s)$ is the Fresnel substrate reflectivity, $k_0 = q/2$ being the radiation wave number in air and d is the film average thickness.

The quantities k_f and k_s are the radiation wavenumbers in the film and in the substrate respectively, which depend strongly on k_0:

$$\mathbf{k_f = (k_0^2 - 4\pi\rho)^{1/2}} \text{ and } \mathbf{k_s = (k_0^2 - 4\pi\rho_s)^{1/2}}$$

When the surface or interface is not sharp, the reflected intensity is modified by the Nevot-Croce factor. In our case, the roughness of the monocrystalline Si substrate was neglected, and the film surface roughness only was taken into account in the fitting procedure, the general reflectivity expression thus becoming:

$$\mathbf{|R|^2 = \{|R_l|^2|exp(-2\ kk_0\sigma^2)|+|\ R_r|^2-2Re[R_lR_r\ exp(-2\ kk_0\sigma^2)exp(2ikd)]\ /}$$
$$\mathbf{1+|R_l|^2|\ R_r|^2|exp(-2\ kk_0\sigma^2)|-\ 2Re[R_lR_r\ exp(-2\ kk_0\sigma^2)exp(2ikd)]\};}$$

This expression, corresponding to the Parratt Model developed in case of a film upon a flat substrate and explicated towards the wave numbers instead of the more common scattering angle, was introduced into a data processing programme: Origin 6.1. Accordingly to the code required by the data analysis programme, the fitting expression become:

```
arg_a=abs(x^2-a);
arg_b=abs(x^2-b);
A1=x-sqrt(arg_a);
B1=x+sqrt(arg_a);
C1=sqrt(arg_a)+sqrt(arg_b);
D1=sqrt(arg_a)-sqrt(arg_b);
E=2*d*sqrt(arg_a);
```

```
F=2*x*s^2*sqrt(arg_a);
NUM=A1^2*C1^2*exp(-2*F)+B1^2*D1^2-2*a*(b-a)*cos(E)*exp(-F);
DEN=B1^2*C1^2+A1^2*D1^2*exp(-2*F)-2*a*(b-a)*cos(E)*exp(-F);
y=m*(NUM/DEN)*exp(-4*x^2*s^2).
```

Indeed, five free parameters were used in the fit, one to normalize the intensities due to different counting times (m), the others corresponding to the morphological parameters of interest:

a: scattering length density of the substrate *4π
b: scattering length density of the film*4π
d: average thickness of the film
s: surface roughness of the film

In figure 3, an example of reflectivity pattern (dots) is plotted together with its fit (line) and the fitting parameters which where deduced.

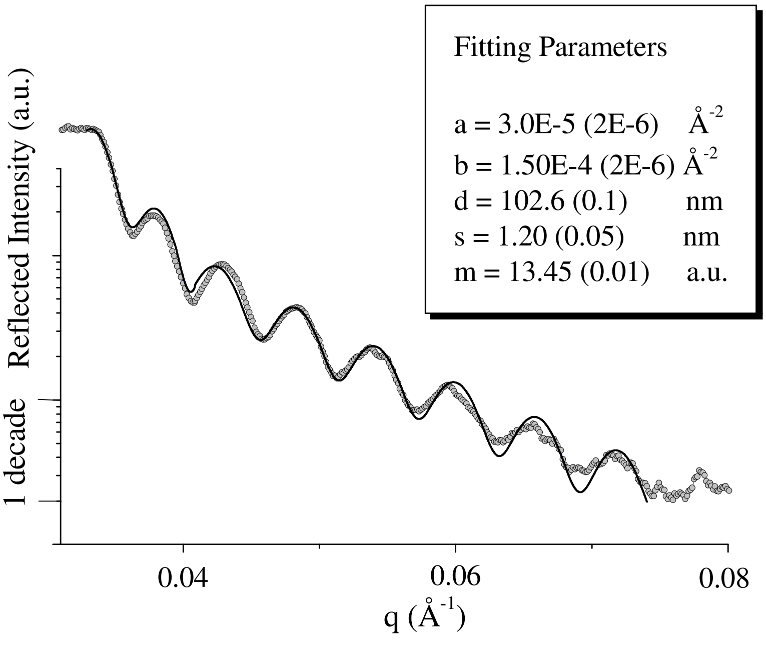

Figure 3. A reflectivity pattern (dots) and its fit (line) are plotted as a function of the scattering parameter. In the inset the numerical values of the fitting parameters are reported.